Fall 2016

Potential Impacts of Climate Change on Photochemistry of Zostera Marina L.

Billur Celebi
Old Dominion University

POTENTIAL IMPACTS OF CLIMATE CHANGE ON PHOTOCHEMISTRY OF *ZOSTERA MARINA* L.

by

Billur Celebi
B.S. June 2004, Middle East Technical University, Turkey
M.Sc. April 2007, Middle East Technical University, Turkey

A Dissertation Submitted to the Faculty of
Old Dominion University in Partial Fulfillment of the
Requirements for the Degree of

DOCTOR OF PHILOSPHY

OCEANOGRAPHY

OLD DOMINION UNIVERSITY
December 2016

Approved by:

Richard C. Zimmerman (Director)

Victoria J. Hill (Member)

Alexander Bochdansky (Member)

Mark J. Butler IV (Member)

ABSTRACT

POTENTIAL IMPACTS OF CLIMATE CHANGE ON PHOTOCHEMISTRY OF *ZOSTERA MARINA* L.

Billur Celebi
Old Dominion University, 2016
Director: Dr. Richard C. Zimmerman

Seagrasses account for approximately 10% of the ocean's total carbon storage, although photosynthesis of seagrasses is carbon limited at today's oceanic pH. Therefore, increasing atmospheric CO_2 concentration, which results in ocean acidification/carbonation, is predicted to have a positive impact on seagrass productivity. Previous studies have confirmed the positive influence of increasing CO_2 on photosynthesis and survival of the temperate eelgrass *Zostera marina* L., but the acclimation of photoprotective mechanisms in this context has not been characterized. This study aimed to quantify the long-term impacts of ocean acidification on photochemical control mechanisms that promote photosynthesis while simultaneously protecting eelgrass from photodamage. Eelgrass were grown in controlled outdoor aquarium tanks at different aqueous CO_2 concentrations ranging from ~50 to ~2100 µM from May 2013 to October 2014, and compared for differences in optical properties and photochemistry. Even with daily and seasonal variations of temperature and light, CO_2 enrichment consistently increased plant size, leaf thickness and chlorophyll use efficiency, and decreased pigment content and the package effect while maintaining similar light harvesting efficiency. These CO_2 responses resembled high light acclimation suggesting a common photosynthetic sensory function, such as redox regulation, controls long-term acclimation of leaf morphology. Laboratory incubations resolved this mutual regulation of redox state via carbon and light availability, by measuring O_2 production, total CO_2 uptake and fluorescence of the acclimated leaves. The morphological acclimations due to CO_2 enrichment were facilitated by improved

photosynthetic capacity. Increasing CO_2 availability, relative to oxygen concentrations, maximized chlorophyll specific photosynthesis to its physiological limits at pH 6.2 by minimizing photorespiration, and increased the light requirement to saturate photosynthesis. The instantaneous increase of photosynthesis up to 8 fold reduced the role of alternative electron pathways and non-photochemical quenching for photoprotection, therefore increasing quantum yield of oxygen production. These findings explained how seagrasses resist photodamage in shallow high light environments, while maintaining long daily period of light-saturated photosynthesis to compensate carbon limitation and sustain growth. The quasi-mechanistic models generated by this study provide a pathway for including the photoprotection and photoacclimation processes in understanding the dynamic response of seagrasses to fluctuating coastal environments and climate change.

This dissertation is dedicated to Murat and Carmel.

ACKNOWLEDGEMENTS

I would like to thank my dissertation committee members: Dr. Richard C. Zimmerman, Dr. Victoria J. Hill, Dr. Alexander Bochdansky, and Dr. Mark J. Butler IV, for their endless guidance and patience. I extend my appreciation to my guidance committee members: Dr. Richard C. Zimmerman, Dr. Alexander Bochdansky, and Dr. Eileen E. Hofmann, for their valuable guidance throughout my doctoral candidacy experience.

I will be forever indebted to my mentor Dr. Richard C. Zimmerman for this degree and more importantly for enriching my academic vision. I feel so lucky to have met him as my role model for how to be a dedicated scientist, an inspiring instructor and an advisor generously sharing time and knowledge.

All members of Bio-optical Research group have become like a family to me throughout the good and difficult days and nights, in the lab and at the field. I am thankful to David Ruble for always willing to help me in designing and building experimental devices, to Dr. Victoria J. Hill for finding realistic and practical solutions whenever I felt frustrated. I greatly valued our brainstorming sessions with Meredith McPherson and Malee Jinuntuya about and beyond science. I am thankful to Tiffany Cedeno and Carmen Zayas for helping me sampling.

I owe special thanks to Dr. Susan Park, Dr. Troy Hartley and Janet Krenn not only providing a fellowship but also welcoming me to the network of Virginia Sea Grant family for the rest of my academic career. I am thankful to Dr. Fred Dobbs and Jenifer Alonzo for teaching me the important skills of scientific communication. I thank to Chris Witherspoon, Karen P. Burns and Jovonne Vrechek for training me in science outreach and introducing me to the young curious generation of marine scientist via the Mentoring Young Scientists Program.

All my dear ODU friends I have met throughout my stay here in Norfolk, I appreciate your understanding and will miss your friendship that made PhD life enjoyable. Especially to

Alexandra, Jose, Luna, Wrinkles, Red and Lale: thank you for looking after Carmel and me with inexpressible kindness.

I am so thankful to my parents for their love and their encouragement to follow my dreams, to my best friend and husband Murat for his limitless patience, love and support. And, my beloved doggy Carmel, I am so grateful to you being in my life during this long journey.

I thank the Department of Ocean, Earth and Atmospheric Sciences at Old Dominion University for the support through the Dominion Scholarship and for teaching opportunities. Part of this research was carried out at the Virginia Aquarium and Marine Science Center, for which I would like to thank W. Mark Swingle and aquarium staff for running and maintaining our research facility. This research was funded by grants from Virginia Sea Grant/NOAA Graduate Research Fellowship (Award NA10OAR4170085), National Science Foundation (Award OCE-1061823) and Virginia Aquarium and Marine Science Center.

TABLE OF CONTENTS

Page

LIST OF TABLES

Table Page

LIST OF FIGURES

Figure Page

CHAPTER I

INTRODUCTION

Background

Climate change, and its acceleration by anthropogenic activity, alters the biogeochemistry of seawater which forces organisms and ecosystems to acclimate and/or adapt to these new conditions. Photosynthesis is one of the important processes impacted by the changes in ocean biogeochemistry due to eutrophication, ocean acidification and warming. The rate of this important energy conversion process is dependent mostly on light, temperature and inorganic nutrients including CO_2. While eutrophication increases available nutrients, it stimulates the growth of nuisance algae that decrease light penetration into the bottom, transferring the productivity of coastal ecosystems from the benthos to the pelagic and leading to corresponding trophic cascades (Burkholder et al., 2007). Alternatively, warming and ocean acidification alter the chemical distribution of dissolved inorganic carbon (DIC) in the water. The uptake of increasing atmospheric CO_2 by oceans lowers ocean pH and increases carbon-limited photosynthetic rates of some aquatic organisms (Doney et al., 2009b).

Numerous studies have examined the impact of global warming and increasing CO_2 concentration on the physiology and ecology of terrestrial plants (Woodward, 2002). In comparison, long term impacts of the simultaneous effects of warming and ocean acidification on marine primary producers are less well understood. Many calcifying organisms are affected negatively by ocean acidification (Doney et al., 2009b) but photosynthetic rates of phytoplankton show variable responses to increasing CO_2 concentration (Doney et al., 2009a). In contrast, photosynthetic rates of a variety of seagrass species examined for short time period seem to benefit from ocean acidification (Durako, 1993; Invers et al., 2001; Jiang et al., 2010), which implies their photosynthesis is carbon limited in the modern ocean (Beer and Koch, 1996;

Zimmerman et al., 1997). The few long term studies linked the positive influence of [CO_2] to overall growth parameters such as shoot, root and seed production rates of eelgrass (Zimmerman et al., 1997; Palacios and Zimmerman, 2007). Whether seagrasses will be real winners in the future hot climate requires additional information on the simultaneous impacts of [CO_2], light and temperature on physiological acclimation and growth rates that can ultimately be scaled to population level responses (Short and Neckles, 1999; Touchette and Burkholder, 2000).

Seagrasses have adapted to the marine environment through morphological and physiological changes from their terrestrial monocotyledon origins (Larkum et al., 2006b). Some of these adaptations play key roles in their differential photosynthetic responses from other aquatic photosynthetic organisms. Seagrasses originated 75 to 100 MYA in a high CO_2 atmosphere, which contrasts with today's conditions in coastal environments, and nutrient rich flooded sediments (Den Hartog, 1979; Hemminga and Duarte, 2000). Eutrophication of shallow coastal environments causes photosynthetic competitors, namely algae, to bloom (Burkholder et al., 2007). Algae have also more efficient mechanisms for uptake of inorganic carbon (Aizawa and Miyachi, 1986; Raven and Johnston, 1991). The high density of algae alters both the quantity and quality of photosynthetically active radiation (PAR) reaching the seagrass canopy (Cummings and Zimmerman, 2003; Ralph et al., 2007; Vaudrey et al., 2010). The availability of light may also be reduced by suspended non-algal particles (Zimmerman et al., 2015). There are many in-situ studies confirming the strong correlation between the light availability and abundance of seagrasses (Zimmerman et al., 1991; Zimmerman, 2006; Krause-Jensen et al., 2011). Therefore over long term the growth and depth distribution of seagrasses is often light limited (Duarte, 1991).

Attainment of net positive growth rates, either in terms of shoot density or above and below-ground biomass, depend on the metabolic carbon balance and the availability of organic carbon

reserves to support growth and proliferation. The size of the internal sugar pool is directly related to net carbon assimilation which relies on the ratio of photosynthesis to respiration (*P*:*R*). Rates of these biochemical processes depend, to a first order, on the physiological status of the tissue (e.g., age, pigment concentration, enzyme concentration etc.) and then on the environmental conditions such as the substrate concentration (CO_2 for photosynthesis, O_2 for respiration), temperature and light. Therefore, seasonal changes in growth rates result from the combination of daily - even hourly - physiological constraints on C-uptake and storage, N-assimilation and photochemistry of individual leaves (Boston et al., 1989).

Experimental manipulations revealed that the instantaneous rate of seagrass photosynthesis is carbon limited in modern ocean pH ranges (Zimmerman et al., 1997; Invers et al., 2001). The C-limitation is related to the rate of CO_2 supply for the dark reaction of photosynthesis catalyzed by Ribulose-1,5-bisphosphate carboxylase oxygenase (Rubisco). However, Rubisco catalyzes both the carboxylation and oxygenation of ribulose-1,5-bisphosphate in a competitive reaction process that depends on the relative concentrations of CO_2 and O_2. The oxygenase reaction reduces the net photosynthetic capacity of many plants. In terrestrial plants, carboxylation exceeds oxygenation by about 4:1 at ambient levels of [CO_2] and [O_2] but the ratio is only 2:1 to 3:1 for aquatic species (Raven, 1984). Increasing atmospheric CO_2 should thus increase the effective CO_2:O_2 ratio in a way that increasingly favors carboxylation over oxidation, potentially increasing the net photosynthetic potential of many plants, including aquatic autotrophs.

CO_2 is one of the three forms (CO_2, HCO_3^- and CO_3^{-2}) of dissolved inorganic carbon (DIC) in seawater (Emerson and Hedges, 2008; Doney et al., 2009b). At modern ocean pH levels, the concentration of dissolved CO_2 is only 1% of total DIC, yet it is the only form of DIC Rubisco reacts with. Accumulation of CO_2 from seawater by eukaryotic marine phytoplankton and marine angiosperms is limited by the diffusion rate and dehydration kinetics of bicarbonate to

CO_2 (Reinfelder, 2011). Dissolved CO_2 enters the cell through simple diffusion whose rates depend on the flow, temperature and concentration gradient in the boundary layer along the leaf surface. Various plants, many algae, and photosynthetic bacteria have evolved mechanisms that increase the flux of CO_2 to Rubisco, including C_4 carbon fixation, crassulacean acid metabolism (CAM), and the ability to take up other inorganic forms of carbon (Boston et al., 1989). The biophysics and biochemistry of uptake dependent carbon concentrating mechanisms (CCMs) vary within and among the dominant groups of eukaryotic marine phytoplankton (Reinfelder, 2011). CCMs may include the activity of external and/or intracellular carbonic anhydrases (CA) (responsible for interconversion of HCO_3^- and CO_2), HCO_3^- transport, and possibly a C4-like carbon pump although conclusive proof for this pathway in aquatic autotrophs remains elusive (Badger and Price, 1994). In general, the efficiency of CCMs is low for coccolithophores, moderate for dinoflagellates and high for diatoms. For algae, the expression of CCMs can be regulated by environmental factors (Beer, 1996; Beardall and Giordano, 2002), including photon flux and the availability of dissolved CO_2 in the surrounding medium. Compared to marina algae, seagrasses have much lower CCM activity (Raven et al., 2002; Raven et al., 2011).

Low activity of CCMs causes the photosynthesis of seagrasses to be carbon-limited (Björk et al., 1997; Touchette and Burkholder, 2000). Consequently, their photosynthesis saturates at relatively low irradiances (E_k). However, achieving maximum photosynthesis rates (P_{max}) at low irradiances is often interpreted as a characteristic of shade adapted plants (Larkum 2006). This kind of interpretation of *P* vs. *E* curve would categorize seagrasses as shade adapted plants. Yet, experiments by Zimmerman et al.(1997) showed that the P_{max} of eelgrass can be increased under high [CO_2] without affecting the efficiency of light-limited photosynthesis (α), so that their E_k value increases instantaneously with P_{max}. True shade adaptation typically involves an increase in photosynthetic efficiency under low light conditions (steeper initial slope, α) but not

necessarily a change in P_{max}. Thus, the low E_k values of seagrasses are a result of carbon limited photosynthesis rather than shade acclimation.

Because carbon limitation severely restricts instantaneous photosynthetic capacity (i.e. P_{max}), even in the brightest light environments, seagrasses require long average daily period of irradiance-saturated photosynthesis (H_{sat}) to maintain positive carbon balance ($\int_0^{24hr} P{:}R \geq 1$), limiting them to shallow water environments with high irradiances. These high light environments should make seagrass leaves vulnerable to photoinhibition, i.e. the irreversible photooxidative destruction of the photosynthetic apparatus, throughout much of the day when photosynthesis is light saturated but CO_2-limited. Yet, C-limited seagrasses thrive in high light environments without experiencing significant photodamage. This adaptation might signify active roles of photoprotective mechanisms in seagrasses which still have not been well characterized. Known photoprotective mechanisms in seagrasses include short term energy dissipation through the xanthophyll cycle (Ralph et al., 2002) and photoacclimation by adjustment of light harvesting pigment concentrations (Cummings and Zimmerman, 2003). During the xanthophyll cycle the epoxide groups from xanthophylls (e.g. violaxanthin, antheraxanthin, diadinoxanthin) are enzymatically removed to create so-called de-epoxidised xanthophylls (e.g. diatoxanthin, zeaxanthin). These reactions play a key role in dissipating captured solar energy within light harvesting antenna proteins by non-photochemical quenching; therefore reducing the flow of excited electrons to the photosynthetic reaction centers (Demmig-Adams et al., 2004). Non-photochemical quenching (NPQ; either through the xanthophyll cycle or fluorescence) is one of the main ways of protecting against photoinhibition in most plant systems. Therefore, understanding physiological feedback mechanisms and environmental factors controlling CCM activity, light requirements and photoprotection can help to identify this important physiological regulation.

Beside the diverse influence of photosynthetic routes, the *P:R* ratio is also altered by changing respiration rates. There are two types of respiration: 1) mitochondrial dark respiration which generates chemical energy for cellular metabolism and 2) photorespiration, which is light dependent, occurs in the chloroplast and peroxisome, and represents a 'drain' on photosynthetic energy production with no apparent physiological benefit. In most studies comparing *P:R* ratios, the respiration term accounts only for dark respiration because photorespiration rate is inseparably integrated into the light-dependent photosynthesis rate measurements. Like all plants, dark respiration of seagrasses increases with increasing temperature and O_2 concentration (Downton et al., 1976; Zimmerman et al., 1989; Hemminga and Duarte, 2000). Indeed, respiration rates respond more dramatically to temperature than light-saturated but carbon-limited photosynthetic rates (Q_{10} of respiration ≥ Q_{10} of photosynthesis; at pH ≈ 8.1). This imbalanced metabolic response is at least partially why eelgrass (*Zostera marina* L.) is predicted to do poorly as the climate warms (Evans et al., 1986; Moore and Jarvis, 2008; Moore et al., 2012) but projected CO_2 increase may offset some of the negative effects of temperature stress by stimulating photosynthesis (Zimmerman et al., 2015; Zimmerman et al., 2016). However, in addition to increasing dark respiration rates, high O_2 concentrations directly limit photosynthetic rates under carbon limitation by inducing photorespiration (Raven, 1991; Ogren, 2003).

Photorespiration is due to the oxygenase activity of Rubisco, whose end products are phosphoglycolate and 3-phosphoglycerate (Douce and Heldt, 2004). Phosphoglycolate is recycled through a sequence of reactions within the peroxisome and mitochondria, yielding glycine and serine, which are eventually converted to CO_2 and 3-phosphoglycerate that can reenter the Calvin cycle. These reactions in the glycollate pathway consume both $NADH_2$ and ATP, thereby decreasing the yield of photosynthetic energy available to the plant. Since

photorespiration consumes energy and reduces the glucose formation rate without a clear metabolic benefit, it appears to be a puzzling process (Maurino and Peterhansel, 2010).

Given that O_2 competes reversibly with CO_2 for the same active site of Rubisco, increasing the CO_2:O_2 ratio will enhance carbon fixation and therefore reduce carbon limitation. This dual function of the Rubisco may result in zero net carbon fixation of healthy leaves under high light conditions when the ratio of CO_2:O_2 reaches a threshold at which oxygenation overcomes carboxylation (Caemmerer and Quick, 2004). Atmospheric concentrations of CO_2 and O_2 have changed repeatedly throughout Earth's history, and many plants have evolved CCMs that improve photosynthetic performance under low CO_2 availability (Raven et al., 2008; Raven et al., 2011). Therefore, ocean acidification may play a particularly important role in down regulating photorespiration and significantly improving photosynthetic performance of seagrasses.

To date, most studies of seagrass metabolism report gross photosynthesis as the sum of net photosynthesis and dark respiration, and therefore do not account separately for the photorespiration hidden in the net photosynthesis measured in the light. Indeed it is difficult to measure real gross photosynthesis of C3 plants separately from photorespiration during light measurements of photosynthetic rates (Sharkey, 1988). Seagrasses are C3 plants (Beer and Wetzel, 1982) and there is evidence that they perform photorespiration (Beer, 1989) but not enough is known about this potentially important process to quantify its significance in terms of overall photosynthetic performance. It is, in fact, possible that photorespiration may serve a photoprotective mechanism to maintain electron transport during periods of light saturated (i.e. carbon limited) photosynthesis (Ort and Baker, 2002). There is also recent evidence that photorespiration might play a role in nitrate assimilation (Rachmilevitch et al., 2004) and influence multiple signaling pathways by contributing to cellular redox homeostasis (Foyer et al., 2009).

A mechanistic understanding of both carbon concentrating and photoprotective mechanisms of seagrasses may reveal how they survive in high light environments in a low CO_2 world, and their response to a changing climate. This study aims 1) to investigate the photo-protective mechanisms of the temperate eelgrass (*Zostera marina* L.) and assess their relative importance while simulating future climate conditions and 2) to clarify the link between the environmental control of photosynthesis and regulation of carbon metabolism.

Objectives of the study

The regulation of photosynthesis in seagrasses seems to be contradictory: although photosynthesis is severely carbon limited at high irradiances, seagrasses require high light for growth. This apparent conflict should make seagrass photosystems extremely vulnerable to photoinhibitory damage, but this is apparently not the case. This study will attempt to resolve the puzzle of limitation of photosynthesis in eelgrass with respect to light, temperature and CO_2 availability and translate that understanding to the dynamics of metabolic carbon balance that determines the ecological success of seagrasses in nature. The work will address the following specific questions:

Chapter II: Long term regulation of light harvesting in Eelgrass, *Zostera marina* L., in response to ocean carbonation

- Does leaf pigment composition change with increasing CO_2?
- Does CO_2 alter the response of photosynthetic machinery to light and temperature?
- What are the consequences of increasing CO_2 for light capture efficiency?

Chapter III: Photorespiration in Eelgrass (*Zostera marina* L.): a photoprotection mechanism for survival in a CO_2-limited world

- (How much) Do photosynthesis, photorespiration and fluorescence and/or xanthophyll cycle increase with increasing light and CO_2?

- Do the photoprotective mechanisms alter the *P:R* ratio?
- Do the photoprotective mechanisms vary among leaves adapted to grow under different environmental conditions?

Chapter IV: Regulation of photosynthetic control in eelgrass in response to changing photorespiratory conditions due to ocean acidification

- Do increasing temperature and CO_2/O_2 ratio alter the ratio of photorespiration to photosynthesis?
- Does the seawater CO_2/O_2 ratio regulate the DIC uptake, oxygen production and non-photochemical quenching in eelgrass?

Significance

Changing environmental conditions can alter the recovery and stress responses of coastal ecosystems. Seagrasses play an important role in coastal biogeochemical cycles and merit the attention of managers and scientists under global change scenarios. Their population growth and productivity may differ from their photosynthetic counterparts, namely marine algae, due to their evolutionary adaptations. Quantification and a mechanistic understanding of their photobiology and physiological processes is needed to predict their responses in future climatic conditions. Major drivers of change in marine environments are warming and acidification. This research project focusing on both aspects of the changes simultaneously will enable us to predict the physiological and ecological benefits and costs of climate change on eelgrass populations in the Chesapeake Bay region where they are at the southern limit of their geographical distribution along the Atlantic coast.

CHAPTER II

LONG TERM REGULATION OF LIGHT HARVESTING IN EELGRASS, *ZOSTERA MARINA* L., IN RESPONSE TO OCEAN CARBONATION

Introduction

Although photosynthetic organisms are fundamentally dependent on solar energy, light induces stress when the ratio of photon flux to photosynthesis is high, which can occur either with increasing incident light or decreasing photosynthesis in response to decreased temperature and/or low CO_2 (Demmig-Adams and Adams, 1992). Whenever light energy absorption exceeds the photochemical utilization of that energy through photosynthesis, the excess energy must be dissipated through photoprotective mechanisms, such as thermal dissipation and alternative electron flow, to prevent damage to the photosynthetic unit. These flexible and fast-responding photoprotective mechanisms allow plants to cope with fluctuating light environments (short term acclimation, <1 hr), but on a longer time scale sustained environmental changes trigger acclimation responses that modify the photosynthetic machinery via changes in gene expression and protein synthesis (Eberhard et al., 2008). Acclimation to high light includes increasing the density of photosynthetic units, electron transport carriers and Rubisco (Walters, 2005), which may increase the capacity of alternative electron transport reactions in which electron acceptors other than CO_2 become important, such as O_2 leading to photorespiration and/or the Mehler reaction (Niyogi, 2000). Nitrate reduction also uses electrons from photosystems as well, although not at high rates. All these pathways increase the trans-thylakoid pH gradient within the chloroplast that triggers thermal energy dissipation via the xanthophyll cycle (Demmig-Adams and Adams, 1992). For this reason, high light acclimated plants typically have larger pools of xanthophyll cycle components (i.e., more

carotenoids) to dissipate excess energy for protection. For example, sun adapted crop plants use about 25% of absorbed light for photosynthesis, 19% for photorespiration and the remaining 56% of the absorbed light energy is dissipated by non-photochemical processes (Demmig-Adams and Adams, 1992). In contrast, shade-acclimated leaves experience photodamage at lower light levels than sun-acclimated plants because of low capacity of electron transport and non-photochemical energy dissipation.

Relative to other marine photosynthetic organisms, seagrasses have high light requirements for survival (Duarte, 1991; Lee et al., 2007). The paradigm of light limited distribution is acknowledged by many authors studying the impacts of environmental parameters on seagrass survival in natural conditions as well as in mesocosm studies (Dennison and Alberte, 1982; Dennison, 1987; Duarte, 1991; Alcoverro et al., 1999). Unlike marine algae and phytoplankton, seagrasses possess fully functional roots and rhizomes that depend on leaf photosynthesis for reduced carbon (Smith et al., 1988; Zimmerman et al., 1989). This additional 10% metabolic demand (Zimmerman et al., 2015) requires either high maximum photosynthetic capacity or an extended period of light-saturated photosynthesis at lower maximum capacity. Light, as the primarily driver of photosynthesis, therefore becomes, an important controlling factor for growth, even when photosynthetic capacity is limited by CO_2 availability. Instantaneous increase in photosynthesis with increasing CO_2 (Zimmerman et al., 1997; Invers et al., 2001) shows that the seagrass photosynthesis, especially in eelgrass, typically operates well below its physiological capacity, requiring long periods of saturating light level to satisfy the metabolic demand of above and belowground biomass, especially under heat stress (McPherson et.al. 2015, Zimmerman et.al. 2015). This requirement for long daily periods of light saturated photosynthesis, resulting in high light requirements for seagrass survival, limits the distribution of seagrasses to shallow depths.

In contrast, the optical properties of seagrass leaves make them nearly as efficient as algae in terms of light harvesting (Cummings and Zimmerman, 2003), with numerous morphological adaptations to harvest light energy effectively in submerged aquatic environments and acclimate to variable light conditions (Kirk, 1994). Structural adaptations include pigmentation of the epidermal layer only, while the inner mesophyll layer is populated by non-pigmented cells. These non-pigmented cells surround the lacunar space that is important for leaf buoyancy and O_2 transfer to belowground tissues. Therefore, any increase in leaf thickness associated with non-pigmented layers might play an important role for turgor pressure and buoyancy adjustments under variable salinity conditions while not contributing to light harvesting. Adjustments of light harvesting usually occur via the changes of pigment concentrations and/or their ratios (Falkowski and Raven, 2007). Accessory carotenoid pigments present in seagrasses serve photoprotection purposes via the xanthophyll cycle (Ralph et al., 2002). Seagrasses show a typical photoacclimation response of increasing pigment concentration under light limitation (Cummings and Zimmerman, 2003), similar to unicellular algae and macrophytes, but the effectiveness of this strategy is limited by the package effect (Kirk, 1994). Previous studies about the package effect in seagrasses highlighted the importance of increasing pigment content on the optical cross section, a measure of chlorophyll use efficiency, yet having relatively constant light harvesting efficiencies in their native light environment (Cummings and Zimmerman, 2003; Enríquez, 2005).

Seagrasses are highly affected by changes in environmental conditions that vary on both temporal and spatial scales (Orth et al., 2006a; Koch et al., 2009). In addition to natural fluctuations, seagrass ecosystems must acclimate/adapt to long-term changes induced by the anthropogenic activities such as eutrophication, climate warming and ocean acidification. Eutrophication reduces the light quantity and quality in the water column, and alters sediment biogeochemistry in ways that can limit seagrass growth (Burkholder et al., 2007). Although

climate warming resulting from anthropogenic increases in atmospheric CO_2 is projected to negatively affect seagrasses, particularly those growing near their equatorial distribution limits (Moore and Jarvis, 2008; Moore et al., 2012), increasing CO_2 availability resulting from ocean acidification/carbonation (the other CO_2 effect) may help offset the negative impact of increasing temperature by increasing light-saturated photosynthetic capacity of seagrasses (Palacios and Zimmerman, 2007; Koch et al., 2013; Zimmerman et al., 2016). Since high light requirements of sesagrasses result from the carbon limitation of photosynthesis rather than a limitation in photon capture efficiency, increasing photosynthesis due to ocean acidification/carbonation may impact light harvesting mechanisms. This photoacclimation and its consequences to the overall performance of seagrasses are unresolved. The purpose of this study was to assess the long-term photoacclimation of eelgrass leaves to ocean acidification via adjustments of pigment content and its consequences on leaf optical properties. The specific objectives were to 1) examine the combined effects of CO_2, light and temperature on the light harvesting efficiency, 2) link the changes in light harvesting to the photosynthetic capacity and eventually to the plant performance in terms of growth and survival, and 3) compare the performance under the same environmental conditions between long-term (15 months) CO_2 acclimated eelgrass plants and short-term (3 months) acclimated plants to evaluate the significance of plant's history in acclimation strategies.

Materials and Methods

The experimental facility

This experiment was conducted using an outdoor aquatic climate research facility (ACRF) on the shore of Owls Creek at the Virginia Aquarium, Virginia Beach VA, USA (Figure 1).

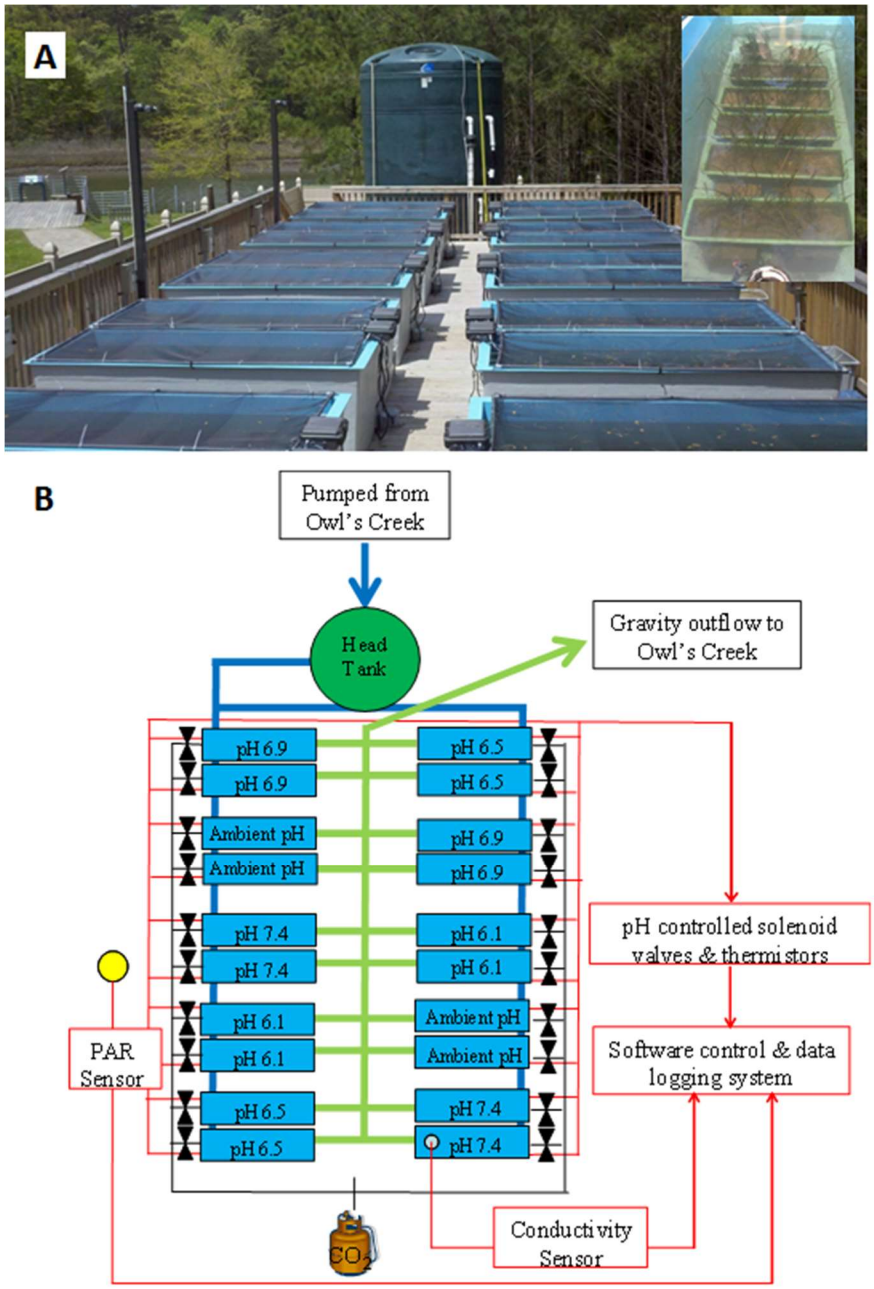

Figure 1. The Climate Change Experimental Facility at the Virginia Aquarium and Marine Science Center showing: 20 aquaria with window screens and sensor control units, water head tank circulating seawater from Owls Creek and CO_2 source from storage tank. Small photo in (A) shows trays with transplanted seagrass in each aquaria.

Owls creek is a small polyhaline estuary located near the southern limit of eelgrass distribution on the Virginia coast just south of the Chesapeake Bay. Salinity fluctuates from 20 to 30 (PSS) as a function of tidal exchange with the adjacent waters of the Mid-Atlantic Bight and local storm runoff from the small coastal watershed (Sisson et al., 2010). Concentrations of dissolved inorganic nutrients (N ≅ 10 μM, P ≅ 1 μM) are consistently higher than the concentrations required to saturate eelgrass growth based on previous work by Zimmerman et al. (1987).

Raw water from Owls Creek was pumped continuously into a 70 m^3 head tank and gravity-fed into the bottom of 20 fiberglass open top aquaria (3 m^3 each) at one end of each aquarium. An overflow standpipe at the opposite end of each aquarium provided drainage and kept the water depth at 1 m. The continuous flow system provided a volume turnover rate of 10 day^{-1} in each aquarium. All aquaria were covered with a single layer of neutral density plastic window screen that reduced the incident irradiance by 40% to simulate their natural environment and protect the leaves from photodamage. These screens were removed during February and March 2014 to prevent snow accumulation. All aquaria were bubbled with compressed air delivered through 2 m lengths of Pentair Bio-Weave diffuser hose to enhance turbulent mixing and prevent boundary layer limitation of leaf metabolism.

Beverage-grade CO_2 was injected from a cryogenic storage tank into the diffuser hoses through solenoid valves operated by pH controllers (Eutech Alpha pH 190) poised at a gradient of pH values (4 aquaria at each pH) ranging from ambient (no CO_2 addition, pH ≅ 7.7, $[CO_{2(aq)}] \cong 50$ μM) to pH 6.0 ($[CO_{2(aq)}] \cong 2100$ μM). pH electrodes were calibrated weekly using NBS buffers. The alkalinity of water samples collected periodically from the aquaria was determined by automatic titration (Gieskes and Rogers, 1973) and regressed against salinity (r^2=0.86) to provide a continuous record of alkalinity from measured salinity. Speciation of dissolved inorganic carbon for each aquarium was calculated from measured values of temperature, pH, and salinity/alkalinity using CO2SYS (van Heuven et al., 2011) and the NBS pH scale; CO_2

constants: K1, K2 from Mehrbach et al. (1973) refit by Dickson and Millero,(1987); KSO_4 source from Dickson (1990) and total boron source from Uppstrom (1974). Although pH values below 7.5 exceed the range of ocean acidification predicted by the IPCC through the end of the 21st century, estuarine systems experience a much wider, and more temporally variable range in pH/CO_2 than the open ocean, incorporating much of the experimental range used here (Duarte et al., 2013; Waldbusser and Salisbury, 2014; Ruesink et al., 2015). Further, this range provides a useful gradient in CO_2 availability required to determine functional responses (slopes & intercepts) necessary for predicting the future performance of eelgrass in a high CO_2 world.

The aquaria were exposed to daily and seasonal fluctuations of ambient temperature, irradiance and salinity. The temperature was measured in each aquarium using Omega 44005 precision thermistors and custom voltage divider circuits calibrated to a precision of 0.1° C. Sunlight was measured as photosynthetically active radiation (PAR, in air) using a factory-calibrated LI-COR LI190sb plane irradiance sensor (μmol photons m^{-2} s^{-1}) placed 3 m above the aquaria. Salinity was measured using a factory calibrated SeaBird SBE-37 MicroCAT placed in one of the aquaria. All instrument readings were averaged for 1 minute and recorded at 10-minute intervals using a National Instruments data acquisition system controlled by custom software written in LabView running under Windows XP. Aquaria, electronic sensors and plants were cleaned weekly to control biofilm accumulation.

The instantaneous irradiance measures were integrated to calculate the in-air and shade corrected (40% reduction) daily total flux (mol quanta m^{-2} d^{-1}). Additionally, the daily H_{sat} period, representing the number of hours per day when instantaneous irradiance exceeded the photosynthesis-saturating irradiance (E_k) values of 200 and 400 μmol quanta m^{-2} s^{-1}, was calculated. These E_k values were chosen based on photosynthesis versus E_{PAR} response curves of eelgrass leaves grown in ambient and CO_2 enriched tanks.

Source Population

Eelgrass shoots, with intact roots and rhizomes, were collected by SCUBA divers using hand tools in May 2013 from a restored eelgrass meadow in South Bay, a coastal lagoon near the southern tip of the DelMarVa (USA) Peninsula (Orth et al., 2006b). Shoots were transferred the same day to the Aquarium Facility in coolers filled with seawater. Approximately 50 vegetative shoots with intact roots and rhizomes were carefully transplanted into plastic trays, filled with sediment collected from Elizabeth River, VA. Five trays were placed into each aquarium randomly. All aquaria were kept at ambient pH (no CO_2 addition) for 1 month to permit the recovery of shoots from transplantation shock, and to compare transplant performance across the aquaria. CO_2 enrichment of the experimental aquaria was initiated in June 2013 and maintained through October 2014 (18 months covering two summer growth periods). Additional eelgrass shoots were collected from the same location in April 2014. For each tank, 2 separate trays of these new plants (i.e. 2nd-year transplants) were added next to the acclimated shoots from 2013 (i.e. 1st-year transplants). These shoots were immediately exposed to CO_2 enrichment.

Leaf optical properties (LOPs)

For the analysis of leaf optical properties, one 2nd youngest leaf per tank from both 1st year and 2nd-year transplants were collected monthly. Approximately 5 cm long segments, cut 1 cm above the basal meristem, were cleaned of epiphytes by wiping with a laboratory tissue. Lengths and widths of each segment were measured using a digital caliper. Fresh weights were measured using an analytical balance. Area specific leaf density was calculated as the ratio of mass to leaf area (mg cm^{-2}, Table 1). Spectral absorbance [$D(\lambda)$] and reflectance [$\rho(\lambda)$] of intact leaf segments within the range 350-750 nm were measured in Shimadzu UV 2101PC scanning spectrophotometer fitted with an integrating sphere:

$$A(750) = \left[1 - 10^{-D(750)} \right] - \rho(750) \quad (1)$$

Photosynthetic leaf absorptances [$A_L(\lambda)$] were calculated by subtracting the non-photosynthetic absorptances at 750 nm [$A(750)$] (Kirk, 1994).

$$A_L(\lambda) = [\, 1 - 10^{-D(\lambda)} \,] - \rho(\lambda) - A(750) \quad (2)$$

The photosynthetic absorptances were then used to calculate the leaf-specific photosynthetic absorption coefficients [$a_L(\lambda)$] and the optical cross sections [$a^*_L(\lambda)$].

$$a_L(\lambda) = -\ln [\, 1 - A_L(\lambda) \,] \quad (3)$$

$$a^*_L(\lambda) = a_L(\lambda) / [\text{Chl } a] \quad (4)$$

Photosynthetic and photoprotective pigments were extracted by homogenizing the leaf segments in a glass tissue grinder with ice-cold 80% acetone. Concentrations of chlorophyll *a* (Chl-*a*), chlorophyll *b* (Chl-*b*) and total carotenoids (TCar) were calculated using the extinction coefficients of Lichtenthaler and Wellburn (1983), except for the first month of sampling. In May 2013, only photosynthetic pigments were extracted using 90% acetone and calculated using the extinction coefficients of Jeffrey and Humphrey (1975).

Table 1. List of symbols, their definition and dimensions. Parenthetic notation (λ) denotes wavelength dependence of the variable.

Symbol	Definition	Dimensions
FW	Fresh Weight	mg
LA	Leaf Area	cm^2
Chl-*a*	Chlorophyll *a*	μg cm^{-2} or mg g^{-1} FW
Chl-*b*	Chlorophyll *b*	μg cm^{-2} or mg g^{-1} FW
TChl	Total Chlorophyll	μg cm^{-2} or mg g^{-1} FW
TCar	Total Carotenoid	μg cm^{-2} or mg g^{-1} FW
$A_L(\lambda)$	Leaf absorptance	Dimensionless
$D(\lambda)$	Leaf absorbance	Dimensionless
$\rho(\lambda)$	Leaf reflectance	Dimensionless
$a_L(\lambda)$	leaf-specific absorption coefficient	Dimensionless
$a_L^*(\lambda)$	Optical cross-section	m^2 g^{-1} Chl-*a*
λ	Wavelength	nm

Statistical analysis

Statistical analyses were performed with IBM SPSS Statistics 22, MATLAB R2014b and SigmaPlot 12.5 software packages. Environmental data sampled at high frequency were converted to daily, monthly and total (18 month) averages to match the sampling frequency of leaf optical properties for cross-correlation analyses. The effects of CO_2 enrichment were analyzed by a repeated measures general linear model (SPSS) with time as the fixed factor (within subjects) and pH as the covariate (between subjects). For the comparison of long-term trends, pH was considered as the main covariate because the levels of this parameter were maintained constant throughout the 18 months. Aquaria were considered repeated subjects because leaf samples were collected from each aquarium every month. Degrees of freedom were adjusted using the Greenhouse-Geisser Epsilon correction whenever error covariance matrices failed the sphericity assumption. Additionally, the effect of CO_2 on each leaf optical measure within each time level (month) was quantified by linear regression with respect to log [CO_2]. These coefficient estimates for each month (i.e. monthly slopes) were compared using tests of within-subjects contrasts and categorized into 3 groups (high, mean and low) based on the deviation from a mean slope calculated for the overall CO_2 effect.

The simultaneous interacting effects of environmental parameters were analyzed using multiple linear regression models. Leaf properties were regressed against environmental parameters averaged over the 2-week period preceding the sampling date, as 5 cm leaf segments used for measurements represented on average three to seven days old tissues during warm and cold seasons, respectively (based on monthly growth rates of leaves, sensu Zimmerman et al. (2016)). This integrated time analysis accounted for the response time of the leaf properties and determined the relative significance of each environmental factor to drive the observed acclimations. For each LOP, first a general multiple linear regression was performed against to all three environmental predictors, where data from all pH treatments were

aggregated. Additionally, for each pH treatment, separate multiple linear regressions using the backward stepwise method were performed to differentiate the dominant environmental predictors among the different treatments. Within each pH treatment, however, maintaining aquarium pH at constant values resulted in some temporal variation in [CO_2] due to the dependency of CO_2 solubility on temperature, as well as salinity. Therefore, during these treatment specific multiple linear regression analysis, the collinearity statistics between CO_2 and temperature were evaluated with precaution if the variance inflation factor (VIF) index of collinearity statistics exceeded the threshold value of 2 (Help IBM SPSS Statistics). VIF quantifies the severity of multicollinearity in an ordinary least squares regression analysis.

Finally, the responses of long-term acclimated plants (1st-year transplants) were compared to short term acclimated plants (2nd-year transplants) using a mixed linear model where the fixed factors were transplantation and time, and pH as a covariate.

Results

Variability in environmental parameters

Aquarium pH averaged at 7.5 during the initial transplant recovery period prior to the onset of CO_2 enrichment in June 2013 (Figure 2 A). From June 2013 to October 2014, the daily average pH of the enriched treatments were consistent at 6.1±0.02, 6.5±0.04, 6.9±0.03, and 7.4±0.04, confirming no overlap between the treatment levels. The pH level of ambient treatments, which were not enriched with CO_2, showed daily and seasonal variability representing the natural fluctuations in Owls creek due to both biological activity and weather related events. In these aquaria, the pH ranged between 7.4 and 8.1 with an average of 7.7±0.05 over 18 months. In contrast, aqueous CO_2 concentrations in all treatments varied simultaneously throughout the experimental period due to seasonal variability in salinity and temperature, though without an overlap among the treatments (Figure 2 B). The overall average

$CO_{2(aq)}$ for the different treatments were 55 ± 6, 107 ± 17, 371 ± 32, 823 ± 80 and 2121 ± 118 μmol CO_2 kg^{-1} SW during the enrichment period. $[CO_{2(aq)}]$ was higher during the cold winter months in enriched aquaria, because decreasing temperature increases the solubility of CO_2 at a constant pH. In contrast, $[CO_{2(aq)}]$ was lower in the ambient aquaria during winter due to increased pH of the source water, from decreased respiratory activity in Owls creek ecosystem.

Salinity was the same in all aquaria and influenced both by the oceanic tidal flux into the creek and freshwater drainage from the surrounding watershed (Figure 2 C). Average salinity was 24 (PSS) during the experiment, with brief periods as low as 10 (PSS) during heavy rainfall events. Overall, monthly salinity averages were consistently higher than 20 (PSS), which is in agreement with the salinity zones eelgrass are distributed in the Chesapeake Bay (Batiuk et al., 2000; Orth et al., 2010) and within the wide salinity tolerance range (6-35 pps) of this species globally (den Hartog, 1970; Hellblom and Björk, 1999).

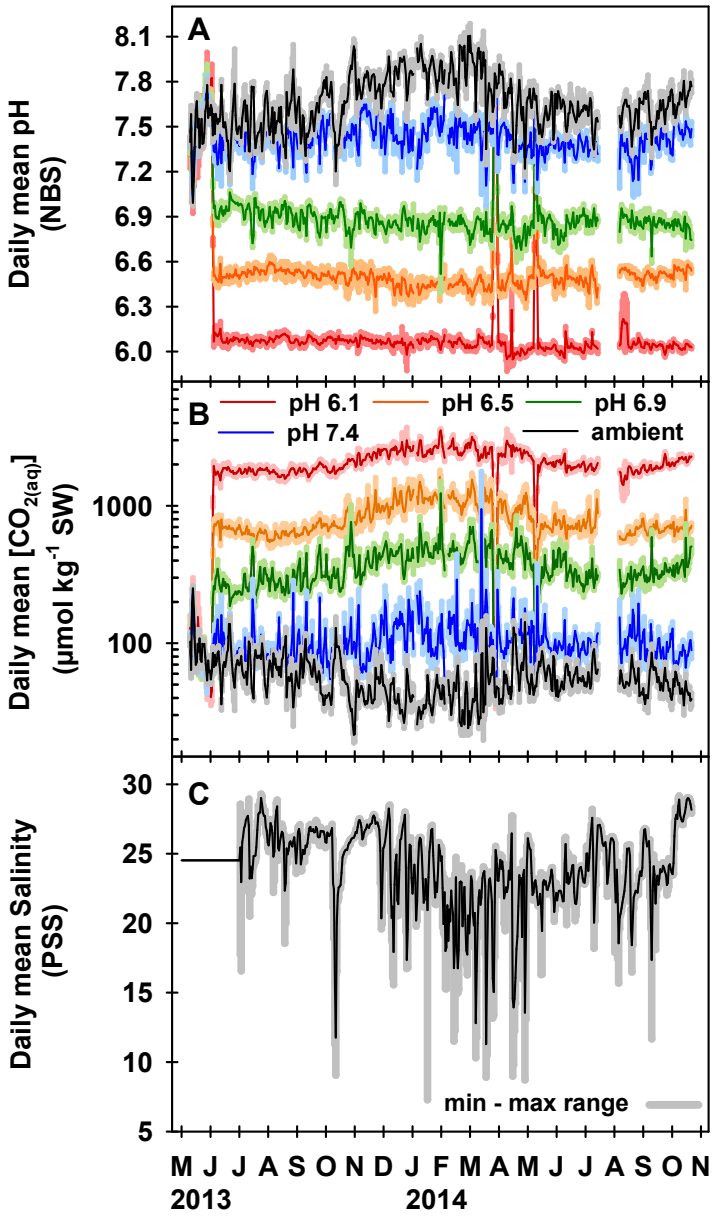

Figure 2. Environmental conditions during the experiment. In (A) and (B) solid lines represent the average of daily mean values of 4 aquaria for each treatment while shaded area indicates the SE. The CO_2 enrichment started in June 2013 after the transplant recovery period. In (C) shaded area indicates maximum and minimum values. Continuous salinity recording started in July 2013, prior to that average salinity value was used for CO2SYS calculations.

Both temperature and downwelling surface irradiance showed seasonal trends as well as daily patterns (Figure 3). The seasonal time lag between temperature and light was estimated by cross-correlation. The changes in light level preceded the temperature changes by 43 days ($r = 0.7$). Highest irradiances were observed during June in both years while the temperature was highest in July and August. The seasonal amplitude of daily-integrated irradiances the eelgrasses experienced varied from 6 to 24 mol quanta m^{-2} d^{-1}, with randomly scattered cloud effects (Figure 3 A). The daily H_{sat} period based on E_k of 200 μmol quanta m^{-2} s^{-1} was consistently higher than 4 h d^{-1} reaching up to 9 h d^{-1} in summer months, which was important to compare the duration of photoprotection needed each day. When E_k, was increased up to 400 μmol quanta m^{-2} s^{-1} based on results presented in Chapter 3 and by McPherson et al. (2015), which showed E_k and P_{max} increased with increasing CO_2, then the H_{sat} period decreased below 4 h between October and February. Shorter duration of H_{sat} to sustain the same daily total photosynthesis (where Daily $P = H_{sat} * P_{max}$) resulted from the higher maximum photosynthesis rates (P_{max}) due to increased CO_2 availability. During these months, temperature decreased from 15°C to 2°C (Figure 3 B), the lowest temperature recorded during the experiment. Temperature ranged from 2°C in winter up to 30°C in summer. The numbers of days with seawater temperature exceeding 25°C at least a 1 h per day were 97 d and 124 d, for 2013 and 2014, respectively. Long-term exposure to temperatures above the optimum 25°C induces a stress response in eelgrass, thus the heat stress period lasted 27 days longer during the summer of 2014. The temperature was consistently lower than 25°C from October 2013 until May 2014.

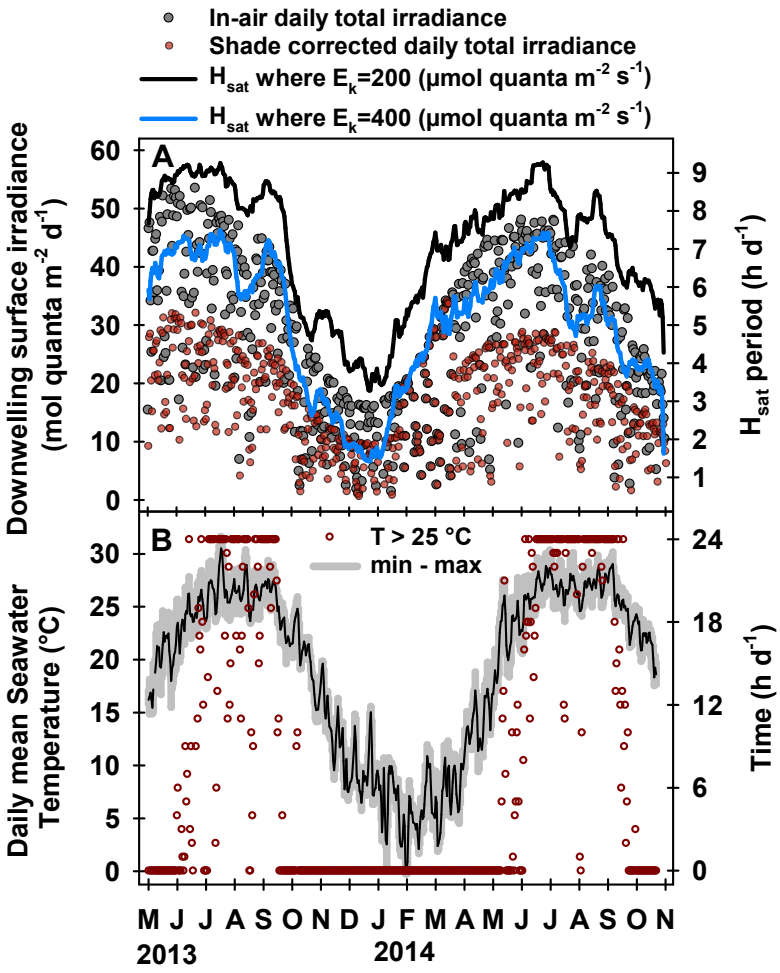

Figure 3. Environmental conditions during the experiment. (A) Solid lines (on the secondary y-axis) show the hours (H_{sat}) each day the instantaneous light level exceeded the light level required to saturate photosynthesis (E_k). (B) Symbols (on the secondary y-axis) show the hours each day the temperature was above 25°C.

Responses to CO_2 Enrichment

Plant size, a measure of the one-sided area of all leaves per shoot, increased linearly with log [CO_2] after 2 months growth in the experimental aquaria (Figure 4 A). This CO_2 response, expressed as monthly slopes of plant size vs. log[CO_2], remained consistently positive after July 2013. The largest plant sizes in all treatments (warm colors) were observed in fall 2013 and early summer 2014, which were also the months with highest response to CO_2 enrichment as indicated by higher slope values. These slopes in fall 2013 and summer 2014 corresponded to 4 and 3 fold differences in plant size, respectively, between the highest CO_2 enriched (i.e pH 6.1) and ambient treatments. In addition to more leaf area per shoot, the area specific leaf density (mg FW cm^{-2}) increased logarithmically with CO_2 treatment (Table 2). The area-specific leaf density increased in all treatments during the hot months of both years (Figure 4 B, heat map) when the response to CO_2 enrichment was enhanced as well. The rate of logarithmic increase in area specific leaf density with available CO_2 ranged from as low as 2 to maximum of 10 mg FW cm^{-2} $(\log CO_2)^{-1}$, with an overall average of 7 (solid line). The positive CO_2 effect was only negligible in 2 months, one being during the initial acclimation period to aquarium environment as expected (circle symbols). The change in area specific leaf density had important consequences when pigment concentrations were normalized either to biomass for interpretation of metabolic acclimation or to area for interpretation of light harvesting acclimation. All pigment measures, except Chl *a:b,* responded to CO_2 enrichment significantly (Table 2). Both area- and biomass-specific pigment concentrations decreased as CO_2 availability increased, indicated by consistent significant negative monthly slope values after the acclimation period (Figure 5 and Figure 6). After 3 months of CO_2 enrichment, the biomass-specific total Chlorophyll (*a* + *b*) content of high CO_2 treatments decreased to 35% of ambient treatment, even though they were exposed to the same light environment (Figure 5 A). This difference in chlorophyll content among CO_2 treatments was less pronounced when normalized

to leaf area, being as low as 55% of ambient treatments' values (Figure 5 B). In addition to stable CO_2 response, chlorophyll content of all treatments increased during winter and decreased during summer months, resembling a classic high light photoacclimation, and were more obvious for biomass specific changes. Chl *a*:*b* ratios also responded to seasonal changes in temperature and light but not to CO_2 enrichment (Figure 5 C). Similar to chlorophyll content, the negative CO_2 response of total carotenoids, indicated by consistently significant negative monthly slopes, was more enhanced for biomass specific concentrations (Figure 6 A) than area specific estimates (Figure 6 B) (i.e. 60% vs. 40% reduction from ambient values). However, total carotenoid content decreased less with increasing CO_2 such that TCar:TChl ratios increased with increasing CO_2, particularly during the winter of 2014 (Figure 6 C).

Table 2. General linear model repeated measures summary table. Abbreviations are defined in Table 1.

Measure	Source	Tests of effects	Type III Sum of Squares		df	Mean Square	F	Sig.
FW/LA	pH_{avg}	between subjects		227.51	1.0	227.51	292.6	<0.001
	Error			14.00	18.0	0.78		
	Time	within subjects		1311.3	14.0	93.66	5.36	<0.001
	Time * pH_{avg}	Sphericity Assumed		890.74	14.0	63.62	3.64	<0.001
	Error (Time)	Mauchly's Test Sig.	0.30	4404.1	252.0	17.48		
Chl-a/FW	pH_{avg}	between subjects		0.76	1.0	0.76	143.0	<0.001
	Error			0.10	18.0	0.01		
	Time	within subjects		1.62	14.0	0.12	2.89	<0.001
	Time * pH_{avg}	Sphericity Assumed		1.44	14.0	0.10	2.57	0.002
	Error (Time)	Mauchly's Test Sig.	0.19	10.11	252.0	0.04		
Chl-a/LA	pH_{avg}	between subjects		88.42	1.0	88.42	112.5	<0.001
	Error			14.15	18.0	0.79		
	Time	within subjects		482.23	6.2	77.51	3.87	0.001
	Time * pH_{avg}	Greenhouse-Geisser		417.98	6.2	67.18	3.36	0.004
	Error (Time)	Mauchly's Test Sig.	0.01	2241.6	112.0	20.02		
TChl/FW	pH_{avg}	between subjects		1.26	1.0	1.26	144.4	<0.001
	Error			0.16	18.0	0.01		
	Time	within subjects		2.85	14.0	0.20	2.98	<0.001
	Time * pH_{avg}	Sphericity Assumed		2.39	14.0	0.17	2.50	0.002
	Error (Time)	Mauchly's Test Sig.	0.10	17.24	252.0	0.07		
TChl/LA	pH_{avg}	between subjects		149.56	1.0	149.56	114.8	<0.001
	Error			23.45	18.0	1.30		
	Time	within subjects		905.63	5.9	153.38	3.99	0.001
	Time * pH_{avg}	Greenhouse-Geisser		771.88	5.9	130.72	3.40	0.004
	Error (Time)	Mauchly's Test Sig.	0.02	4089.5	106.3	38.48		
Chl a:b	pH_{avg}	between subjects		0.01	1.0	0.01	1.28	0.273
	Error			0.18	18.0	0.01		
	Time	within subjects		4.08	4.6	0.88	2.67	0.031
	Time * pH_{avg}	Greenhouse-Geisser		4.35	4.6	0.94	2.85	0.023
	Error (Time)	Mauchly's Test Sig.	0.00	27.49	83.4	0.33		

Table 2. *continued*

Measure	Source	Tests of effects	Type III Sum of Squares		df	Mean Square	F	Sig.
Tcar/FW	pH_{avg}	between subjects		0.08	1.0	0.08	138.7	<0.001
	Error			0.01	18.0	0.00		
	Time	within subjects		0.08	13.0	0.01	1.58	0.093
	Time * pH_{avg}	Sphericity Assumed		0.08	13.0	0.01	1.61	0.083
	Error (Time)	Mauchly's Test Sig.	0.24	0.86	234.0	0.00		
Tcar/LA	pH_{avg}	between subjects		8.04	1.0	8.04	83.55	<0.001
	Error			1.73	18.0	0.10		
	Time	within subjects		21.18	13.0	1.63	2.08	0.016
	Time * pH_{avg}	Sphericity Assumed		19.46	13.0	1.50	1.91	0.030
	Error (Time)	Mauchly's Test Sig.	0.15	183.31	234.0	0.78		
Tcar:TChl	pH_{avg}	between subjects		0.00	1.0	0.00	15.83	<0.001
	Error			0.00	18.0	0.00		
	Time	within subjects		0.03	4.1	0.01	3.79	0.007
	Time * pH_{avg}	Greenhouse-Geisser		0.02	4.1	0.01	3.14	0.018
	Error (Time)	Mauchly's Test Sig.	0.00	0.12	74.5	0.00		
a*(430)	pH_{avg}	between subjects		38.87	1.0	38.87	123.1	<0.001
	Error			5.68	18.0	0.32		
	Time	within subjects		297.84	14.0	21.27	6.02	<0.001
	Time * pH_{avg}	Sphericity Assumed		209.60	14.0	14.97	4.24	<0.001
	Error (Time)	Mauchly's Test Sig.	0.06	890.81	252.0	3.53		

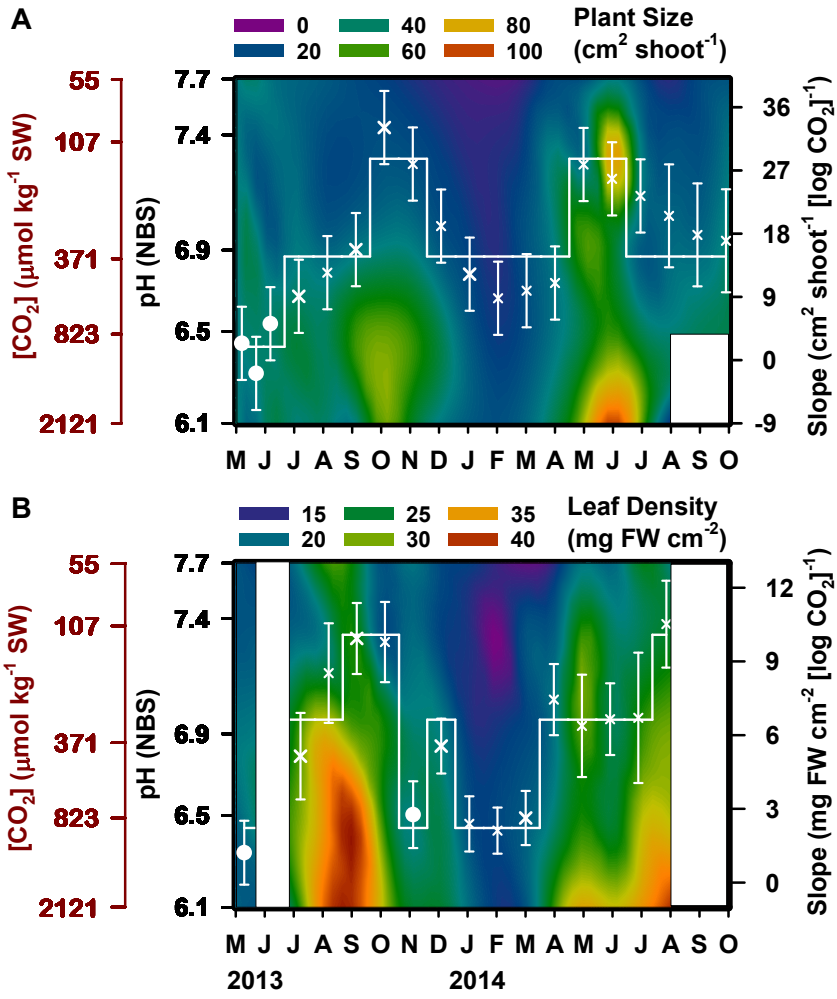

Figure 4. Heat maps of (A) plant size and (B) area specific leaf density as a function of pH (primary left axis) and corresponding average $[CO_{2(aq)}]$ (secondary left axis) throughout time. White symbols on each plot represent the slope of the response variable vs. log $[CO_{2(aq)}]$ derived from linear regression analysis (right axis), the statistical significance of the slope is indicated with ×. Error bars represent ± 1 S.E. of the regression slope. Horizontal lines indicate slopes that were determined to be statistically identical by within-subject contrasts analysis.

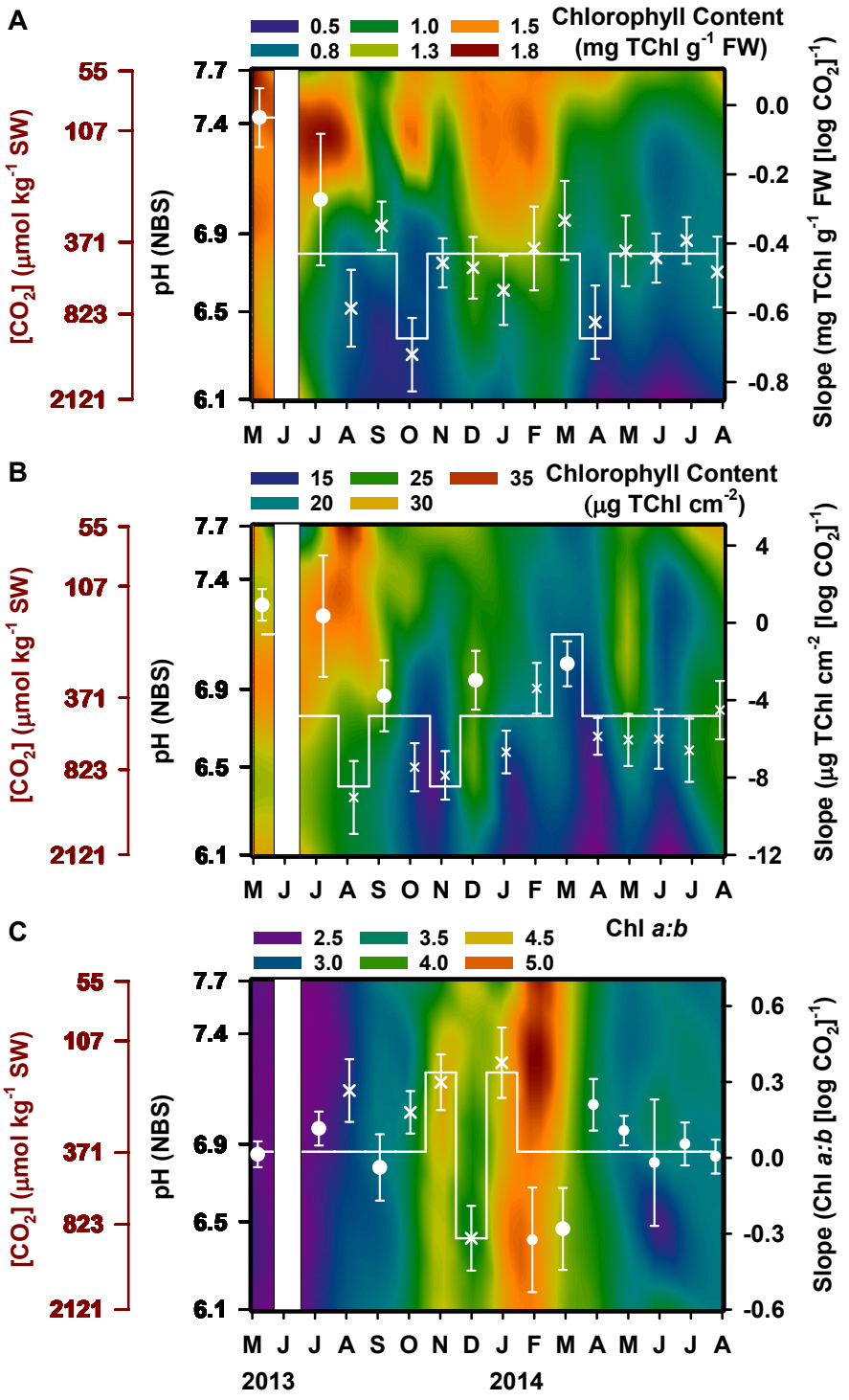

Figure 5. Heat maps of photosynthetic pigments per biomass (A) , per leaf area (B) and their ratios (C) as a function of pH (primary left axis) and corresponding average [$CO_{2(aq)}$] (secondary left axis) throughout time. White symbols on each plot represent the slope of the

Figure 5. *continued*

response variable vs. log [$CO_{2(aq)}$] derived from linear regression analysis (right axis), the statistical significance of the slopes is indicated with $\times$. Error bars represent ± 1 S.E. of the regression slope. Horizontal lines indicate slopes that were determined to be statistically identical by within-subject contrasts analysis.

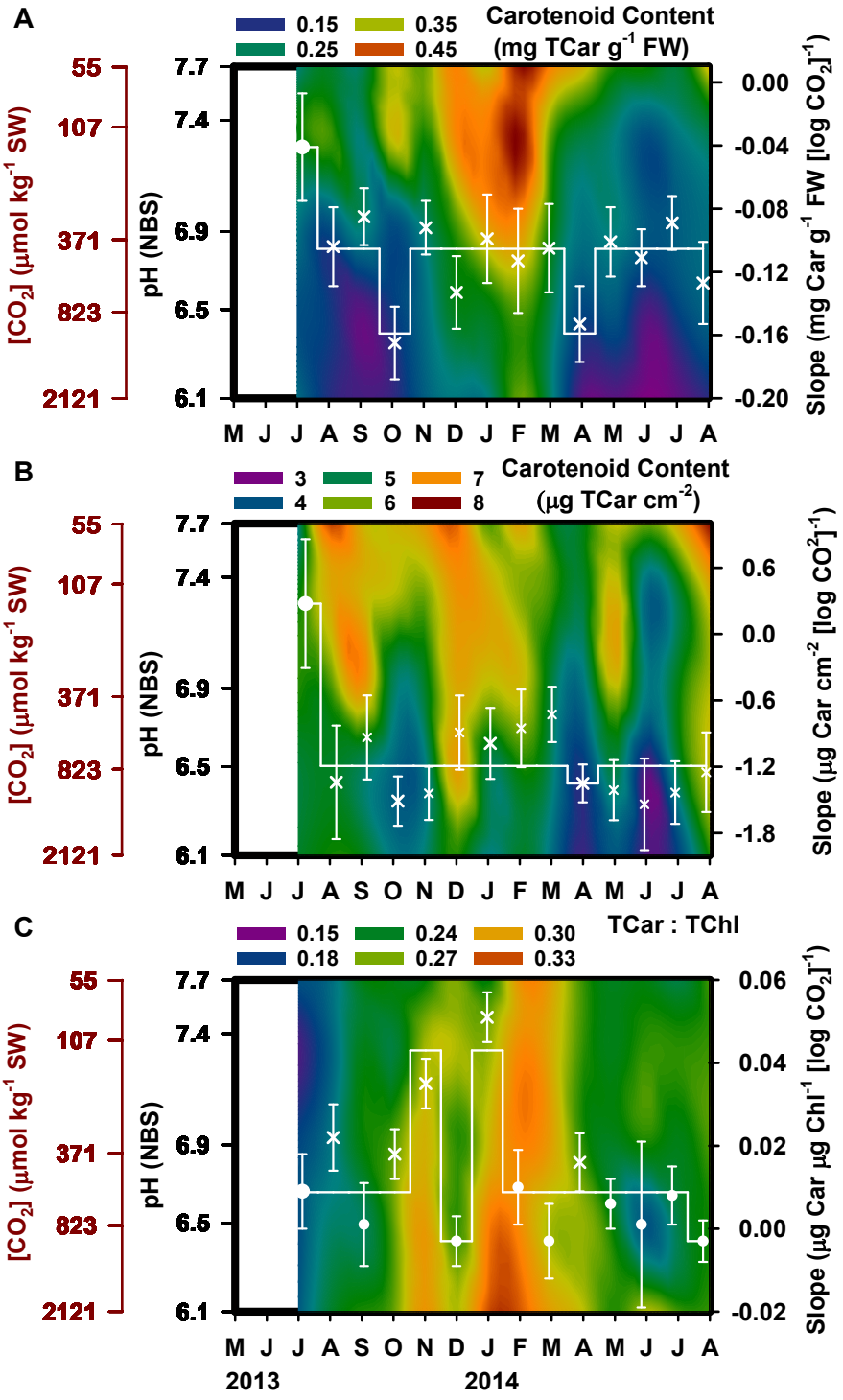

Figure 6. Heat maps of photoprotective pigments per biomass (A) , per leaf area (B) and their ratios to photosynthetic pigments (C) as a function of pH (primary left axis) and corresponding average [$CO_{2(aq)}$] (secondary left axis) throughout time. White symbols on each

Figure 6. *continued*

plot represent the slope of the response variable vs. log [$CO_{2(aq)}$] derived from linear regression analysis (right axis), the statistical significance of the slopes is indicated with $\times$. Error bars represent ± 1 S.E. of the regression slope. Horizontal lines indicate slopes that were determined to be statistically identical by within-subject contrasts analysis.

The changes in pigment content both with CO_2 and seasonally impacted the spectral leaf absorptances unequally (Figure 7 A). While absorptances in the green region (i.e. at 550nm) differed more among the CO_2 treatments than seasons, absorptances within the blue region (i.e. 430-460nm), where absorption maxima of chlorophylls co-occur with carotenoids, varied more dominantly with seasons – almost 20% increase from August 2013 (highest PAR level) to December 2013 (lowest PAR level). The significant differences in chlorophyll content across the CO_2 gradient, combined with differences in leaf absorptances, dramatically impacted the optical cross-section [$a_L^*(\lambda)$] of intact leaves (Figure 7 B), which is a measure of chlorophyll use efficiency. Because the highest variability in the spectral optical cross section across treatments was observed within the Soret region (400 to 450 nm) primarily responsible for driving photosynthesis, $a_L^*(430)$ was chosen to represent the response of optical cross section to CO_2 enrichment through time (Figure 7 C). In all seasons, after the initial acclimation period, CO_2 enrichment increased $a_L^*(430)$ significantly, implying increased chlorophyll use efficiency due to reduced package effect when photosynthesis is not carbon limited.

Under the same range of environmental conditions, the range of area-specific leaf density of high CO_2 acclimated plants was greater than in the ambient treatments, 5-fold vs 3-fold (Figure 8 A). However, the allocation of biomass towards photosynthetic pigments was higher in the ambient treatments than the high CO_2 treatments, even though leaf chlorophyll content increased in all treatments with increasing tissue biomass per unit area. The combination of increased tissue biomass per area, but with less pigment overall suggested an increase in the volume of non-photosynthetic tissues within the leaves grown under high CO_2. This 5-fold increase in area specific leaf density was accompanied by an 8% decrease in the absorptance at 677nm (Figure 8 B). The negative effect of leaf thickness on absorptance did not differ among the CO_2 treatments. The optical cross section [$a^*_L(\lambda)$] was not significantly affected by area specific leaf density but increased consistently with CO_2 treatment (Figure 8 C, Table 3).

The differences in $a^*_L(\lambda)$ across treatments were, however, dependent on the area specific chlorophyll content (Figure 9 A). The exponential decrease in optical cross section with more pigment per leaf area, regardless of leaf thickness, indicated the self-shading effect was caused by increasing pigment concentrations within the photosynthetic cells of surface epidermal layer. The package effect is defined by the nonlinear asymptotic relationship between leaf absorption and leaf chlorophyll, which should be linear (Beer's Law) in the absence of package effect (Figure 9 B-D). The onset of chlorophyll self-shading occurred at low pigment concentrations in the blue (440nm) and red (677nm) regions, 2.78 and 5.26 μg cm^{-2}, respectively. However, the low absorption in green region (550nm) required 14.3 μg Chl cm^{-2} to reach optical saturation. Whereas the chlorophyll concentrations of ambient treatments were higher than this threshold value all the time throughout the experiment, leaves in high CO_2 treatments fluctuated around this threshold value.

Seasonal Responses Induced by Light and Temperature

Area specific leaf density increased with both increasing CO_2 but more significantly with increasing temperature (indicated by higher standardized coefficients) (Table 3 and in Appendix Table 18). Within each of the CO_2 treatments, temperature was the most significant environmental predictor of area specific leaf density, whereas light and CO_2 variability had no significant effect within high CO_2 treatments (Figure 10 A, Table 4). Area specific chlorophyll content showed negative relationship more strongly with CO_2 than with light, but positive relationship with temperature (Figure 10 B, Table 3). The response of chlorophyll content to temperature was reversed when expressed per biomass (Table 3) suggesting the dilution of pigment fraction within the increased biomass accumulation in summer, most likely because of increasing leaf thickness with non-photosynthetic tissues.

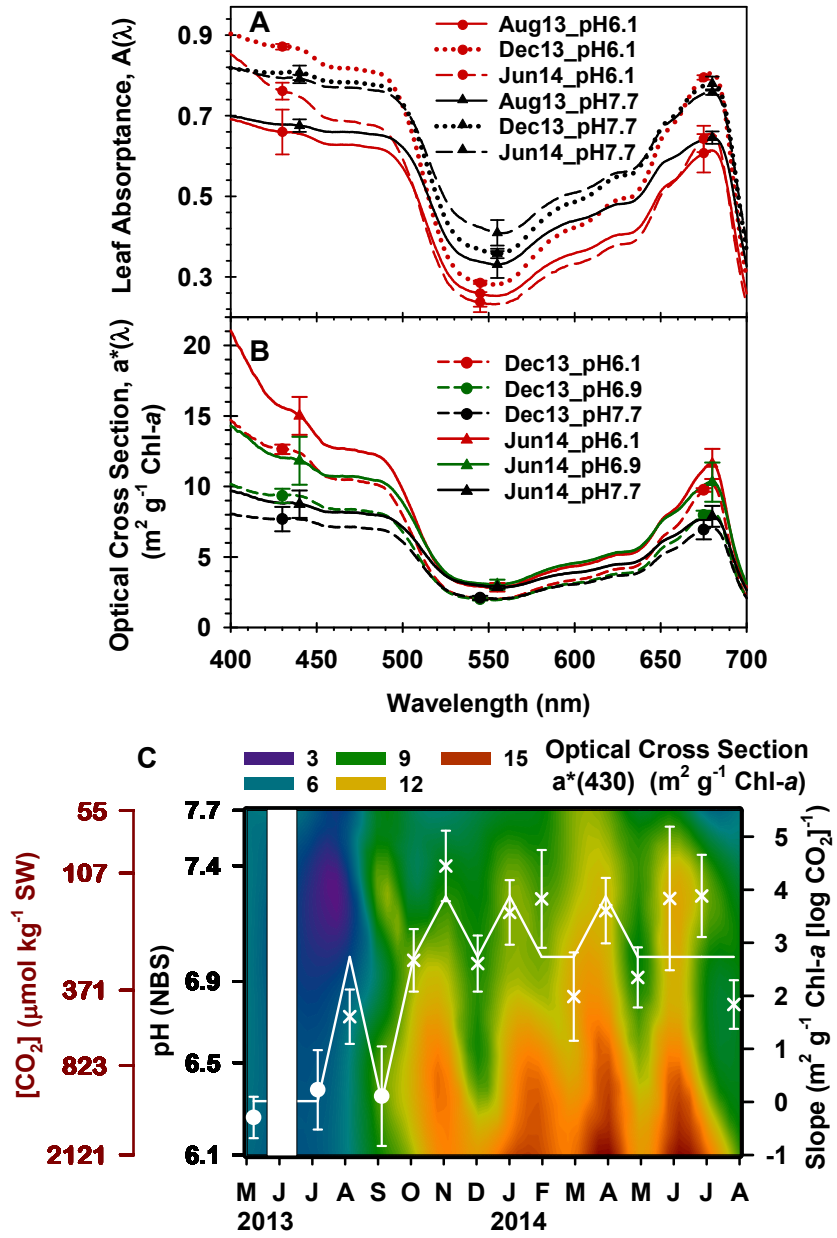

Figure 7. Spectral average leaf absorptance (A) and average optical cross section (B) for different CO_2 treatments during August 2013 (highest PAR level, [µmol photons m^{-2} s^{-1}]), June 2014 (highest daily total PAR, [mol photons m^{-2} d^{-1}]) and December 2014 (lowest PAR and lowest daily total PAR). Error bars represent ±S.E. (C) Heat map of optical cross section (analyzed only for a single wavelength, at 430nm) as a function of pH (primary left axis) and corresponding average [$CO_{2(aq)}$] (secondary left axis) throughout time.

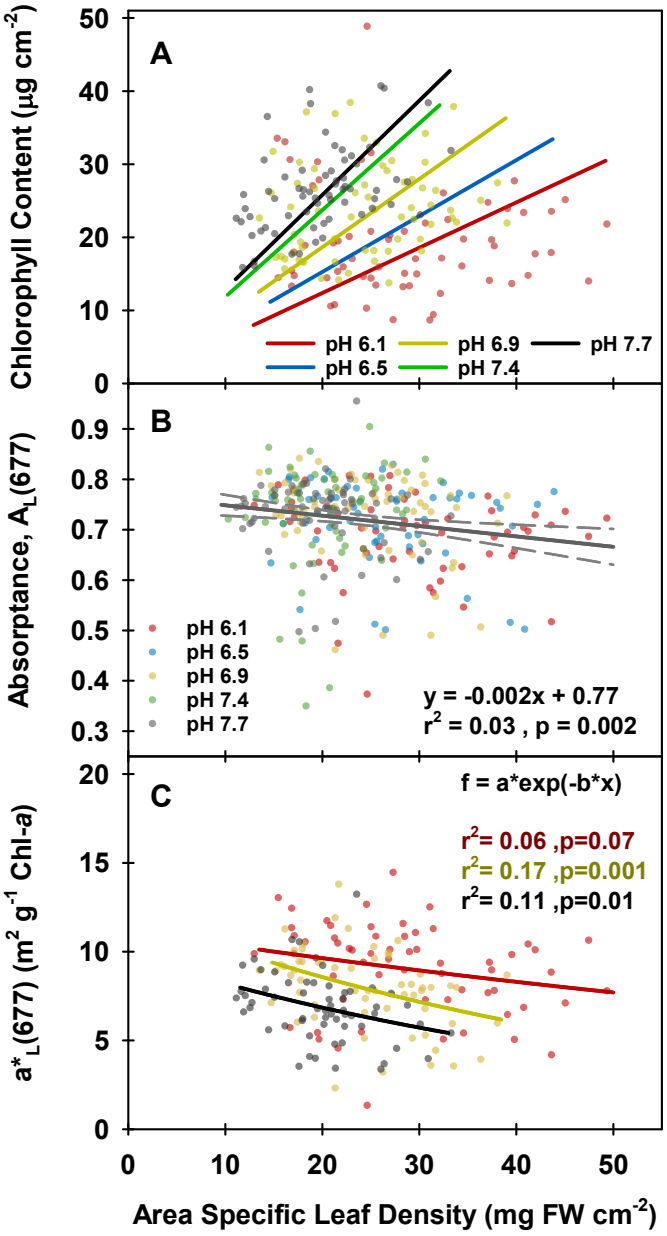

Figure 8. Effects of CO_2 enrichment on Chlorophyll content (A), Leaf Absorptance at 677 nm (B) and optical cross section at 677 nm (C) as a function of the area specific leaf density. Colors represent different CO_2 treatments. For graphical clarity, only data points from three CO_2 treatments were plotted in (A) and (C).

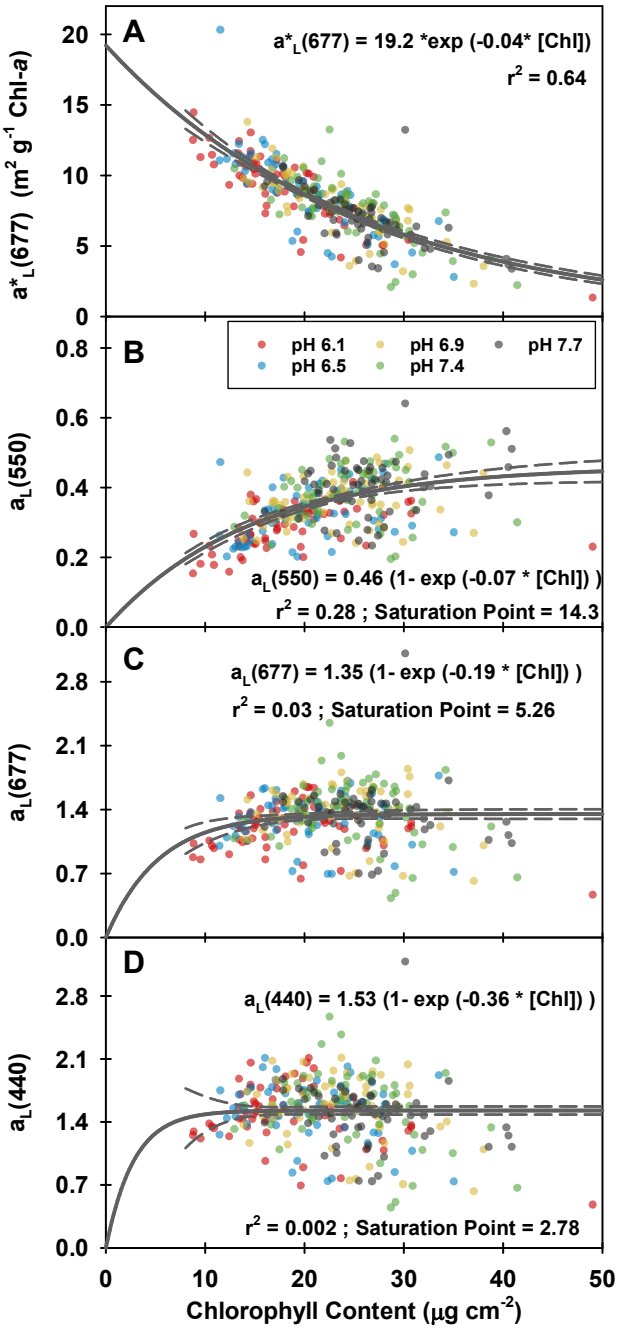

Figure 9. Optical cross section, $a^*_L(\lambda)$, at 677 nm (A) and Leaf specific absorption coefficient, $a_L(\lambda)$, at 550 nm (B), 677 nm (C) and 440 nm (D) as a function of photosynthetic pigment content for all leaves across CO_2 treatments (represented by different colors) and months. Solid lines represent nonlinear regression analysis with 95% CI (dashed lines).

Analysis of CO_2 treatments individually highlighted that the regulating environmental factor of area specific chlorophyll content depended on the CO_2 environment (Table 4). Chlorophyll content of ambient plants responded positively to increasing temperature and negatively to increasing light, whereas the seasonal variability of [CO_2] at such a low CO_2 environment had no significant impact (Figure 10 B). High CO_2 acclimated plants (i.e. pH 6.1, 6.5 and 6.9 aquaria), however, did not change their chlorophyll content significantly with changing light or temperature but responded to the seasonal CO_2 variability in their high CO_2 environment (Figure 10 B, Table 4). Similar to the chlorophyll response, the main driver of negative carotenoid response across the treatments was [CO_2] (Table 3). Increasing light played a secondary role in decreasing carotenoid content. The temperature effect was significant in low CO_2 treatments and was not observed under CO_2 saturated environments (Figure 10 C, Table 4).

CO_2 enrichment did not change the Chl *a*:*b* ratio significantly (Table 3). Chl *a*:*b* decreased profoundly with increasing temperature than with increasing light (Figure 11 A). Optical cross section increased with CO_2 but decreased with temperature indicating a strong package effect in low CO_2 high temperature environment (Figure 11 B). Leaf absorptance (at 677nm), which was negatively correlated with area specific density (i.e. leaf thickness) (Table 3), decreased equally significant with increasing light and temperature. Despite the overall negative effect, CO_2 was the least significant predictor of leaf absorptance (Figure 11 C).

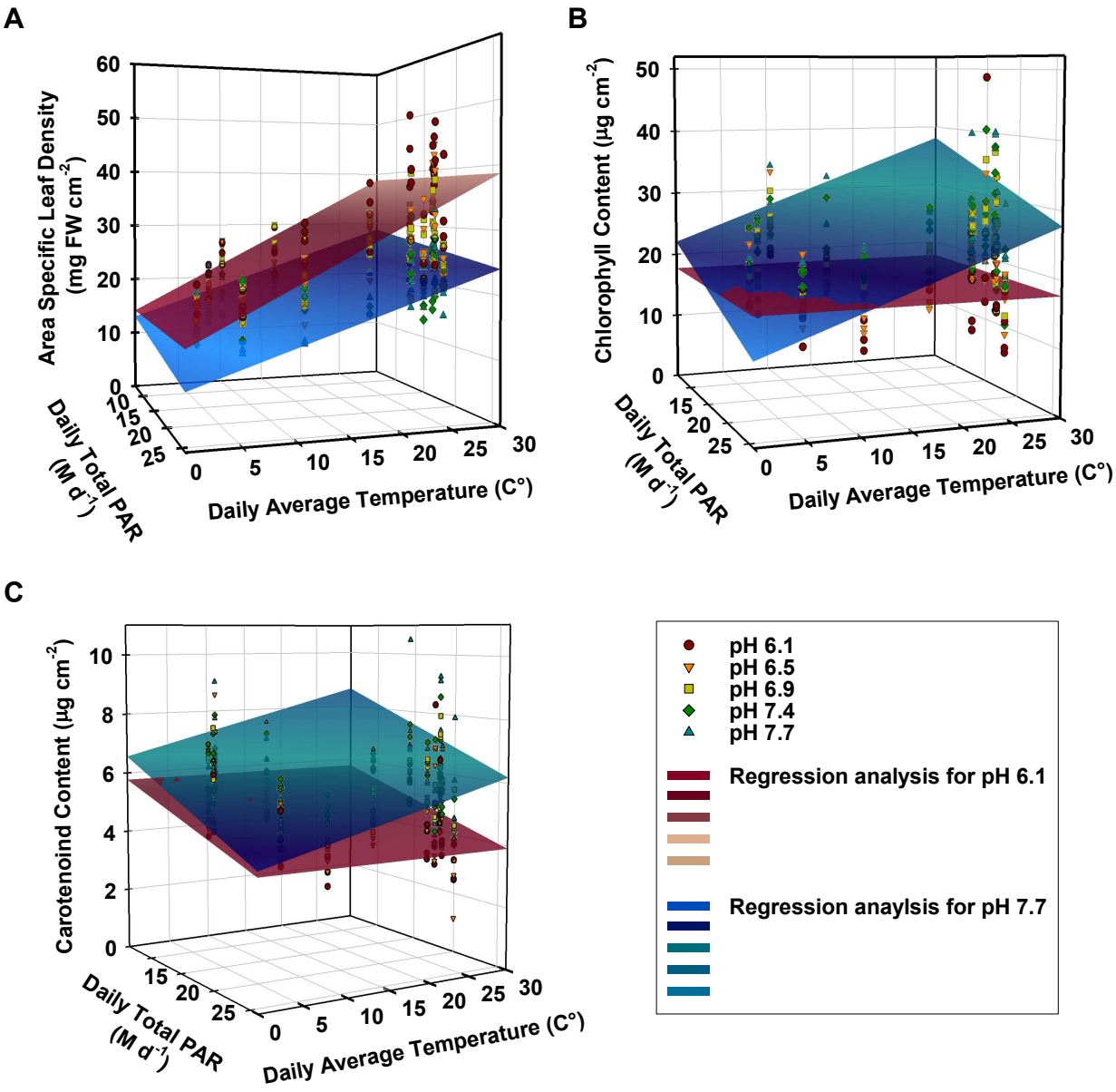

Figure 10. Interactive effects of temperature and daily total irradiance (PAR) on area specific leaf density (A), on chlorophyll content (B) and on carotenoid content (C). All data from time-series are shown with symbols and color coded for specific CO_2 treatments. Three-dimensional planes were modeled by multiple linear regression analysis.

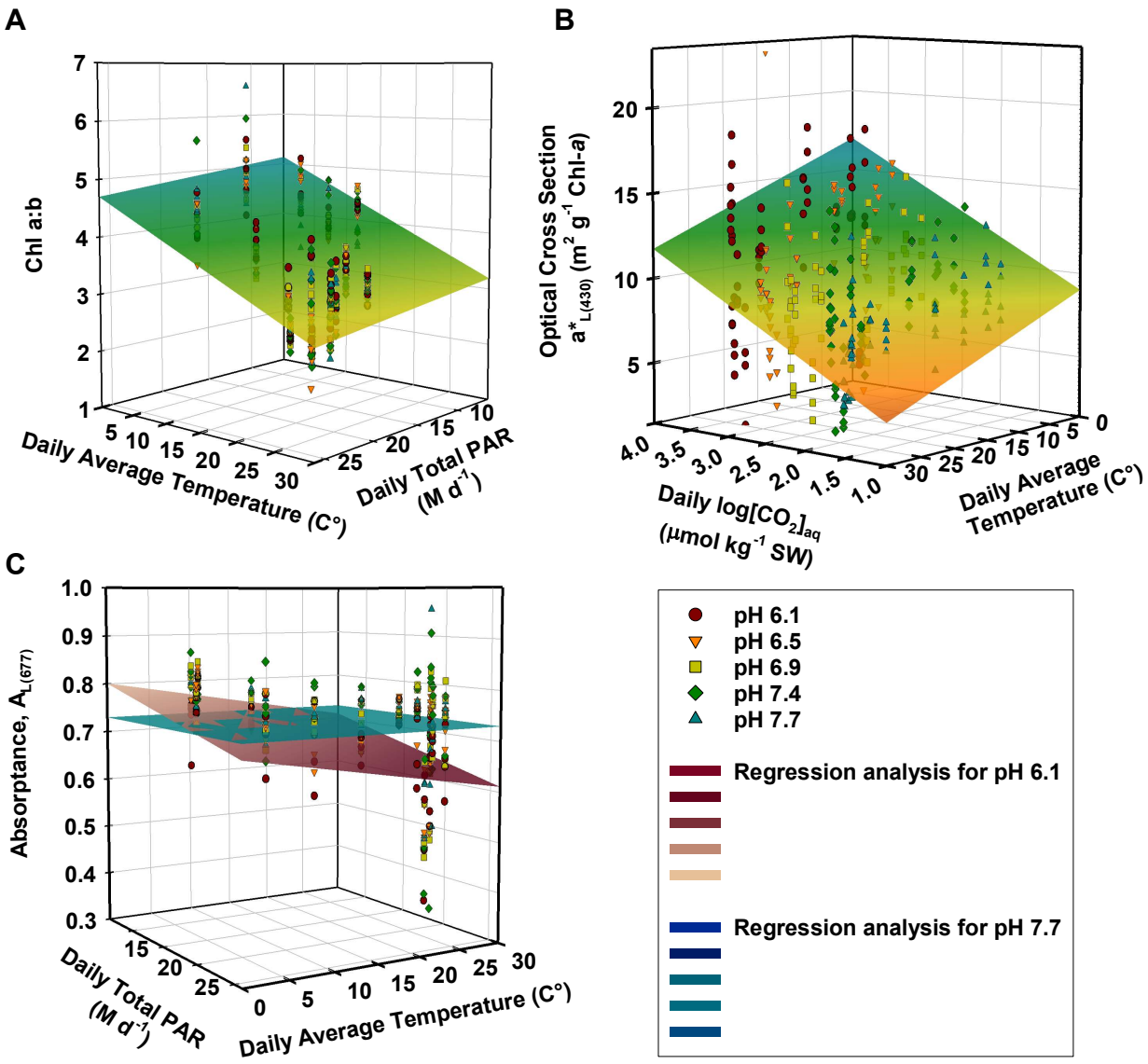

Figure 11. Interactive effects of CO_2, temperature and daily total irradiance (PAR) on chlorophyll a:b ratio (A), on optical cross section (B) and on absorptance (C). All data from time-series are shown with symbols and color coded for specific CO_2 treatments. Three-dimensional planes were modeled by multiple linear regression analysis.

Table 3. Summary of linear regression comparisons with their relative importance coefficients. * indicate significance at p<0.005 level. Abbreviations are defined in Table 1.

Standardized Coefficients (significance)	Multiple Linear Regression (3 predictors)			a. Simple Linear Regression (1 predictor) b. Multiple Linear Regression (2 predictors)	
Dependent variable:	Daily Average log[CO_2]	Daily Average Temp	Daily Total PAR	FW per LA (mg cm^{-2})	Total Chl per LA (µg cm^{-2})
FW per LA (mg cm^{-2})	0.456*	0.731*	-0.103 (p=0.039)		pH dependent [a]
Total Chl per LA (µg cm^{-2})	-0.467*	0.397*	-0.184*		
Total Chl per FW (mg g^{-1})	-0.591*	-0.329*	-0.005 (p=0.929)		
Total Car per LA (µg cm^{-2})	-0.487*	0.148 (p=0.024)	-0.342*		
Chl a:b	0.035 (p=0.332)	-0.697*	-0.154*	a -0.418*	
Tcar:TChl	0.180*	-0.544*	-0.119 (p=0.044)	-0.325*	
A550 (%)	-0.517*	0.146 (p=0.029)	-0.170 (p=0.011)	b -0.206*	0.479*
A677 (%)	-0.151*	-0.236*	-0.209*	-0.173*	-0.099 (p=0.084)
a^*_L430 (m^2 g^{-1} Chl-*a*)	0.448*	-0.417*	0.124 (p=0.052)	-0.018 (p=0.565)	-0.834*
a^*_L677 (m^2 g^{-1} Chl-*a*)	0.351*	-0.443*	0.123 (p=0.065)	-0.086 (p=0.014)	-0.795*

Table 4. Multiple linear regression model results for effects of environmental parameters on leaf optical properties specific for each pH treatment. (exc.: defined by the stepping method criteria parameters were excluded from the model if the significance level of their F values >0.10)

Backward stepwise linear regression (#: collinearity statistics VIF>2.0)		pH 6.1		pH 6.5		pH 6.9		pH 7.4		pH 7.7	
		Beta	Sig.	Beta	Sig.	Beta	Sig.	Beta	Sig.	Beta	Sig.
FW per LA (mg/cm^2)	Daily Average log[CO_2]	exc.		exc.		exc.		0.311	0.026	exc.	
	Daily Total PAR	exc.		exc.		exc.		exc.		-.239	0.068
	Daily Average Temp	0.764	<0.001	0.741	<0.001	0.743	<0.001	0.879	<0.001	0.832	<0.001
Total Chl per LA (µg Chl/cm^2)	Daily Average log[CO_2]	-.375	0.004	-.351	0.008	-0.475	<0.001	exc.		exc.	
	Daily Total PAR	exc.		exc.		exc.		exc.		-.489	0.001
	Daily Average Temp	exc.		exc.		exc.		0.378	0.004	0.796	<0.001
Total Car per LA (µg Cx/cm^2)	Daily Average log[CO_2]	-.356	0.020	exc.		exc.		0.497	0.049#	exc.	
	Daily Total PAR	-.450	0.004	-.293	0.028	exc.		-0.822	0.001#	-0.509	0.003
	Daily Average Temp	exc.		exc.		exc.		0.765	0.021#	0.449	0.008
Chl a:b	Daily Average log[CO_2]	0.581	<0.001	exc.		0.346	0.021#	exc.		-0.239	0.022
	Daily Total PAR	-0.291	0.006	-0.251	0.009	-0.225	0.029#	exc.		exc.	
	Daily Average Temp	exc.		-0.672	<0.001	-0.358	0.031#	-0.814	<0.001	-0.652	<0.001
A677 (%)	Daily Average log[CO_2]	exc.		exc.		0.523	<0.001	0.225	0.086	-0.575	<0.001
	Daily Total PAR	-0.314	0.045	exc.		exc.		-0.264	0.045	exc.	
	Daily Average Temp	-0.265	0.089	-0.354	0.007	exc.		exc.		exc.	
a^*_L430 (m^2/g Chl-*a*)	Daily Average log[CO2]	0.562	<0.001	0.416	0.001	0.610	<0.001	exc.		-0.485	0.003
	Daily Total PAR	exc.		exc.		exc.		exc.		0.603	<0.001
	Daily Average Temp	exc.		exc.		exc.		-0.304	0.023	-0.514	0.001

Response Time of Leaf Properties to CO_2 Enrichment

CO_2 enrichment of the second set of eelgrass transplants, freshly collected from the same field location in the spring of 2014, together with eelgrass plants exposed to CO_2 enrichment since spring of 2013 showed the differences in response time of leaf properties to [CO_2]. Within 4 months under the same environmental conditions specific growth rate, area specific chlorophyll content, Chl *a*:*b* ratio and a_L*(430) of 2014 transplants converged with those of 2013 transplants in all treatments (Table 5). These fast responding measures can be good indicator parameters to be measured even during short-term experiments. However, the area specific leaf density, plant size and area specific carotenoid content of 2014 transplants differed significantly from the long-term acclimated 2013 transplants (Figure 12). The differences were observed in high CO_2 treatments meaning these properties have longer response time to CO_2 enrichment. Therefore, the minimal experimental duration required to detect the impact of CO_2 enrichment depends on the response variable monitored as the impact indicator. In ambient treatments, during the hot summer of 2014, plants that overwintered in their natural ecosystem (2014 transplants) performed similarly to plants grown in the aquaria (2013 transplants). The area specific leaf density and plant size of long term acclimated eelgrass plants were consistently higher than 2014 transplants in CO_2 enriched treatments despite the extended heat stress period in 2014 summer. The CO_2 acclimation took longer for these two parameters, which may emphasize the requirement for long-lasting metabolic adjustments, than for pigment and optical properties, which are likely to be plastic within a leaf for light capture efficiency and redox regulation.

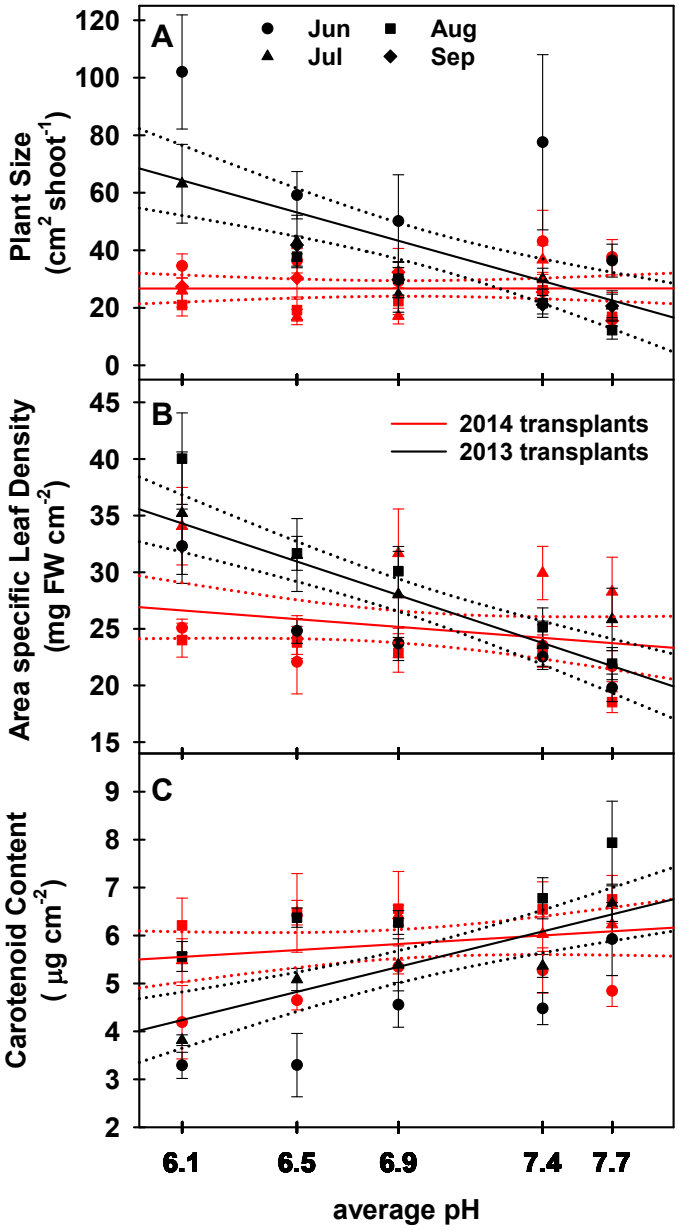

Figure 12. Validation of acclimation response time to CO_2 enrichment via comparison of 1st year (2013) and 2nd year (2014) transplants during summer 2014.

Table 5. Mixed linear model results for comparison of leaf optical properties between long- term acclimated and short-term acclimated eelgrass leaves.

Measure	Total Chl per LA (µg cm^{-2})	Total Car per LA (µg cm^{-2})	Chl a:b	FW per LA (mg cm^{-2})	a*430 (m^2 g^{-1} Chl-*a*)	Plant Size (cm^2 $shoot^{-1}$)	Specific growth rate (d^{-1})
Source	Sig.	Sig.	Sig.	Sig.	Sig.	Sig.	Sig.
Intercept	0.164	0.824	<0.001*	<0.001*	<0.001*	<0.001*	0.001*
Transplantation	0.074	0.003*	0.153	<0.001*	0.160	<0.001*	0.348
Time	0.077	0.254	0.608	0.278	0.004*	0.855	0.295
pH_{avg}	<0.001*	<0.001*	0.121	<0.001*	<0.001*	0.001*	0.740
Transplantation * Time	0.801	0.860	0.678	0.557	0.854	0.759	0.306
Transplantation * pH_{avg}	0.128	0.004*	0.147	<0.001*	0.234	0.001*	0.326
Time * pH_{avg}	0.325	0.731	0.707	0.292	0.017*	0.861	0.414
Transplantation * Time * pH_{avg}	0.793	0.943	0.760	0.749	0.843	0.843	0.290

Discussion

CO_2 enrichment increased both biomass yield (i.e. biomass per leaf area) and the size of eelgrass plants (i.e. leaf area per shoot), likely because of increased photosynthetic capacity (Chapter 3). However, eelgrass leaves decreased their pigment content when given high aqueous CO_2 even though the light environment was identical across all treatments. Although pigment adjustments are typically interpreted as a response to light availability (Demmig-Adams and Adams, 1992; Ralph et al., 2002), the down-regulation of pigment content in eelgrass leaves in response to increased [CO_2] suggested that availability of this primary substrate for the dark reactions of photosynthesis plays a critical role in balancing redox state in the chloroplast, which regulates long term LHC expression (Backhausen and Scheibe, 1999; Pfannschmidt, 2003; Hanke et al., 2009; Huner et al., 2012). Redox feedback mechanisms are under the control of the oxidation state of plastoquinone in the thylakoid membrane that depends on the continuity of the electron transport under various limiting conditions (Pfannschmidt, 2003; Pfannschmidt and Yang, 2012). Therefore, the photosynthetic machinery performs an important sensory function, in addition to energy capture, which further explains the interdependent regulation of pigment composition and optical properties of eelgrass leaves by CO_2, temperature and light.

Physiological optimization of photosynthesis requires a balance between the photochemical processes (photon energy capture, electron transport) and biochemical processes (temperature/substrate-dependent enzymatic reactions)(Pfannschmidt and Yang, 2012). The enzymatic reactions of Rubisco, i.e. photosynthesis and photorespiration, are both sensitive to increasing temperature but antagonistically respond to increasing CO_2. Relative to photosynthesis, however, recycling of CO_2 and Calvin-Benson Cycle intermediates through photorespiration increases the energy requirement from the light reactions that can be generated via absorbing more photons (Jones et al., 2012). The requirement of more photon

absorption due to increasing photorespiration with increasing temperature might explain the increasing area-specific chlorophyll content of eelgrass leaves with increasing temperature in carbon limited ambient treatments. This idea coincided with decreasing quantum efficiency of eelgrass leaves under photorespiratory conditions (Chapter 4). In contrast, growth in a high CO_2 environments would increase photosynthetic rates and reduce the need of alternative electron pathways, such as photorespiration, for photoprotective purposes, which would explain the observed negative relationship between chlorophyll content and CO_2 in eelgrass.

Similarly, increasing photosynthetic capacity of high CO_2 acclimated plants, as observed in Chapter 3, could have decreased the need for photoprotection by carotenoids. De-epoxidation of carotenoids in the xanthophyll cycle with increasing light is fast (in minutes), while epoxidation recovery when light decreases is slow (in hours), especially under additional stress (Demmig-Adams and Adams III, 1996). Therefore, a larger pool of carotenoids in low CO_2 acclimated plants may allow using the NPQ dissipation pathway more effectively to reduce photo-oxidative damage, given that these plants are exposed to photosynthetic saturating light levels more than 9 hrs day^{-1} during summer in addition to heat stress due to carbon limitation of photosynthesis. A supporting finding for this argument has been observed in Chapter 3 where plants in ambient treatments regulated their NPQ more dynamically in response to increasing light and CO_2.

Although reducing pigment concentration as a response to CO_2 enrichment did increase the optical cross section of leaves, hence the chlorophyll use efficiency, it also reduced the leaf absorptances, more in green (A550) than red (A680). However, this reduction in photon capturing efficiency in the red seemed to be correlated more with the increasing area specific leaf density. Assuming the absolute (i.e. volumetric) density of the leaves remained unchanged to aid the leaf buoyancy, the increases in area specific density reported here were likely related to the increasing leaf thickness. This result agrees with minimized absorption per unit weight for thick aquatic plants while they maximize light absorption per surface (Agustí et al., 1994).

Microphotographs of leaf cross-sections taken in September 2013 (provided in Appendix Figure 32 as a courtesy of Dr. Fred Dobbs) also revealed differences in leaf thickness between CO_2 enriched and ambient treatments, coinciding with the maximal increase of area specific density as a function of [CO_2]. However, increased thickness of the non-pigmented mesophyll and lacunar space would not alter the light capture efficiency per unit chlorophyll, since photosynthetic pigments of seagrasses are found only in epidermal layers. Restricting photosynthetic pigments to the epidermis in aquatic plants, such as in seagrasses, may be required for gas exchange (Zimmerman, 2006) but likely enhances the package effect relative to terrestrial plant leaves in which pigments are distributed through several vertical layers of mesophyll cells. Due to constraints of leaf anatomy, the light harvesting acclimation operates at the areal scale for aquatic plants while metabolic acclimation, especially respiration, is expressed in terms of biomass (Vogelman et al.; Walters, 2005). Therefore, the magnitude of the decrease in pigment content per biomass does not truly represent the extent of changes in light-harvesting capabilities in eelgrass.

In all seasons H_{sat} values of all aquaria, were higher than the required minimum to maintain positive carbon balance (4 hrs in winter and 9 hrs in summer) (Zimmerman et al., 2015). These H_{sat} estimates indicated the eelgrass plants in this study had more than enough light to saturate photosynthesis for most of the day and can be considered as high light grown plants. However, in the ambient CO_2 treatments, the high light environment was insufficient to maximize growth and to protect eelgrass from heat stress (Zimmerman et al., 2016), even though photosynthetic pigment concentrations were higher than in plants exposed to elevated CO_2. Despite reduced light harvesting capacity, plants grown under high CO_2 conditions used solar energy more efficiently for photosynthesis - rather than for NPQ or alternative electron transport pathways such as photorespiration (Chapter 4), increased biomass accumulation per leaf area and plant size, thus allowing the plants to store enough carbon resources to support higher respiration

under heat stress. Therefore, the survival, and inevitably the depth distribution, of eelgrass rely on photon use efficiency rather than photon capture efficiency in today's carbon limited coastal ecosystems. Any environmental signal causing perturbation in photosynthesis thus will trigger acclimation, and a regulatory strategy based on photosynthesis itself will allow the plant to compensate various stress conditions with similar mechanisms (Anderson et al., 1995). Such a strategy would also explain why the elevated CO_2 response of leaf optical properties resembled high light response. The optical cross-section $a_L^*(\lambda)$, accepted as a measure of photoacclimation in changing light environments (Cummings and Zimmerman, 2003), responded to increasing CO_2 as if the light was increased, meaning the underlying mechanisms of this acclimation is regulated by a common photosynthetic control mechanism, such as the redox state in the chloroplast.

Although the outdoor design of this experiment provided important natural variability in a number of environmental drives that is often absent from laboratory experiments (Andersson et al., 2015), light and temperature were not fully independent of each other -having a correlation coefficient of 0.65. However, the 43 days lag between the two factors, considering the sampled tissues were less than 2 weeks old, and the removal of shades during February and March 2014 probably reduced the variance inflation factor (VIF) index of collinearity statistics in multiple linear regression analyses. The low VIF index in this study assured the multiple linear regression models with CO_2, temperature and light as predictors to be a significant explanatory fit. The wide CO_2 range across the treatments under a wide range of light and temperature environments quantitatively estimated the general linear response of leaves to the long-term trend of ocean carbonation. Furthermore, the treatment specific regression analyses indicated that the relative importance of environmental parameters (temperature, CO_2 and light) controlling the leaf properties differed under various CO_2 scenarios, thereby highlighting the thresholds for different acclimation strategies.

Photosynthetic acclimation is a dynamic process operating at various timescales. This study lasting for 18 months, allowed the annual rhythm of eelgrass performance to be examined under a gradient of CO_2 concentrations superimposed upon natural fluctuations of environmental parameters. Acclimation of area specific leaf density and plant size of eelgrass had a long response time, as well as acclimation of root:shoot ratio (Zimmerman et al., 2016). Long-term developmental processes responding to changes in growth conditions, such as changing leaf anatomy and root/shoot ratios, have been observed to take weeks to months to occur (Longstaff and Dennison, 1999; Walters, 2005; Lee et al., 2007). In contrast, adjustments of photosynthetic machinery operate on much shorter timescales (Demmig-Adams and Adams, 1992), as evidenced by the agreement of photosynthetic pigment composition of transplants from both years when exposed to same environmental conditions regardless of their growth history. It has been suggested plants previous growth history and the natural limits of the species' acclimation range may play a role in acclimation ability and its detection (Yin and Johnson, 2000; Walters, 2005). The similarities and differences of various parameters observed in this study among the different transplants draw attention to the timescale of CO_2 acclimation to justify the length of the experiments to measure acclimation mechanisms, an important outcome for experimental design.

In summary, this experiment demonstrated that the regulation of pigment composition and light harvesting in eelgrass not only responds to varying light environment but was also affected by the availability of the photosynthetic substrate CO_2. Increasing chlorophyll use efficiency and decreasing role of the photoprotection in high CO_2 acclimated plants indicated utilization of absorbed light energy efficiently for photosynthetic carbon assimilation might be the key for long-term regulation of leaf morphology. Further experiments to address the rates of photochemical pathways in such acclimated plants with respect to changes in CO_2, light and temperature would help to understand the rate limiting physiological processes in redox

regulation that trigger acclimation responses. Even so, being able to persist for almost 100 million years in highly dynamic coastal systems combined with long-term climate trends highlights both the plasticity and the strong acclimation capacity of seagrass populations. In addition to understanding the underlying mechanisms for their competitive survival in a dynamic system, this study allowed quantifying the long-term regulation of light harvesting in response to ocean carbonation to predict the extent of seagrasses in future climatic conditions.

CHAPTER III

PHOTORESPIRATION IN EELGRASS (*ZOSTERA MARINA* L.): A PHOTOPROTECTION MECHANISM FOR SURVIVAL IN A CO_2-LIMITED WORLD

Introduction

Photosynthesis and photorespiration are competing processes due to the bi-functionality of ribulose 1,5-biphosphate carboxylase/oxygenase (Rubisco) (Spreitzer and Salvucci, 2002). During photorespiration the oxygenation reaction of Rubisco consumes Calvin Cycle substrates by combining them with O_2, thereby reducing photosynthetic carbon fixation (Raghavendra, 2000). This photorespiratory oxygenation reaction results in the formation of glycolate (Ogren, 2003), which is processed into glycerate via a series of reactions in chloroplast, mitochondrion and peroxisome (Ogren, 1984). The glycine decarboxylation step of these reactions generates CO_2. Since the oxygenation reaction of Rubisco decreases the productivity of C_3 plants, it has often been viewed as an inefficient legacy of evolution that might be engineered out of terrestrial plants in a quest for increased productivity (Andrews and Lorimer, 1978; Somerville, 2001; Xin et al., 2015). Recent work, however, suggests that Rubisco's CO_2/O_2 specificity in different species may be near-optimally adapted to their gaseous environment (Tcherkez et al., 2006). More importantly, especially for carbon-limited seagrasses, photorespiration may serve as an important metabolic "clutch" to protect the photochemical pathway at high irradiance (Heber and Krause, 1980; Osmond, 1981; Osmond et al., 1997; Igamberdiev et al., 2001). At high irradiances, when Calvin Benson cycle is C- limited, continuation of light reactions results in excess reducing power and energy leading to oxidative stress (Voss et al., 2013). Photorespiration helps to maintain optimal redox state and minimize the accumulation of reactive oxygen species (ROS) by dissipating these excess reducing equivalents (NADPH) as

well as energy (ATP), despite producing H_2O_2 (Foyer et al., 2009). By recycling the photorespired CO_2, photorespiration may also facilitate carbon assimilation in CO_2 limited environments, thereby minimizing photosynthetic inefficiencies resulting from C-limitation (Busch et al., 2013; Xin et al., 2015). Additionally photorespiration plays an important role within the regulatory network of other metabolic pathways (Xin et al., 2015); such as nitrate assimilation (Rachmilevitch et al., 2004), phosphorus recycling (Ellsworth et al., 2015) and stress responses (Voss et al., 2013).

In terrestrial systems, alternative carbon concentrating mechanisms (CCMs) such as CAM and C_4 pathways reduce the potential photorespiration by increasing the CO_2 availability relative to the interfering O_2 around the Rubisco (Bauwe, 2011; Bowes, 2011). As a result maximum conversion efficiency of solar energy to biomass increased from 4.6 % to 6 % (Zhu et al., 2008). Photorespiration was considered to operate at lower levels in aquatic systems as a result of other carbon concentrating mechanisms; such as the use of HCO_3^- as a source of dissolved inorganic carbon (DIC) through active or enzyme facilitated uptake or dehydration (Bidwell and McLachlan, 1985; Beardall, 1989; Bowes and Salvucci, 1989; Madsen and Sand-Jensen, 1991; Frost-Christensen and Sand-Jensen, 1992; Madsen et al., 1993). In today's oceanic water (pH ~8.2), 89% of the DIC is in form of HCO_3^- and only 0.5% exists as dissolved CO_2 (Zeebe, 2012). However, not all aquatic C_3 plants have similar efficiencies to use both forms for photosynthesis (Raven and Beardall, 2003; Raven et al., 2011; Raven and Beardall, 2014). Additionally, CO_2 acquisition by simple diffusion through the leaf surface is more difficult for submerged plants due to the 10,000-fold lower diffusion rates of gases in a liquid environment relative to air (Borum et al., 2006). Consequently, for aquatic C_3 plants that do not use CCMs effectively, such as seagrasses, carbon limitation likely increases the photorespiratory function of Rubisco (Tolbert et al., 1976; Touchette and Burkholder, 2000).

Seagrasses are flowering marine plants that originated approximately 100 Mya from terrestrial ancestors (Larkum et al., 2006b), when the atmospheric and oceanic CO_2 concentrations were much higher than today's values (Zeebe, 2012). The resulting higher CO_2/O_2 ratios probably stimulated photosynthesis and minimized photorespiration in C_3 plants during their early evolutionary history (Kuypers et al., 1999). Although seagrasses are C_3 plants, their adaptation to a submerged environment has produced important anatomical differences from terrestrial C_3 angiosperms. (Touchette and Burkholder, 2000; Larkum et al., 2006a). They have no stomatal openings as gas exchange occurs across the leaf surface by diffusion, which uncouples the carbon limitation from water limitation. Seagrasses also have a lacunal system with arenchema extending from the roots to the leaves that facilitates the transport of O_2 to the roots buried in permanently flooded anoxic sediments, and allows transport of CO_2 from the roots to leaves, providing an alternative carbon source (Madsen and Sand-Jensen, 1991). Although Rubisco activity in seagrasses is lower than the typical activities in freshwater emergent angiosperms and marine red algae, it is comparable to those observed in marine green and brown macroalgae (Beer et al., 1991). On the other hand, seagrasses are typically less efficient in utilizing HCO_3^- than macroalgae (Beer et al., 1991). Simulations of nearshore seawater DIC distribution during the Cretaceous period have predicted that photosynthetic rates of seagrasses would have been similar to macroalgae (Beer and Koch, 1996). However, in today's oceans, seagrass photosynthesis is generally considered to be carbon limited (Durako, 1993; Beer and Koch, 1996; Zimmerman et al., 1997; Invers et al., 2001).

Carbon limited photosynthesis also restricts seagrasses to shallow, high light environments, where low daytime CO_2:O_2 ratios in the water column may increase seagrass vulnerability to photorespiration (Buapet et al., 2013). In earlier studies, photosynthesis was shown to be inhibited by increasing O_2 concentration, resulting in higher concentrations of glycolate pathway

intermediates, and confirmed the photorespiration in marine plants and macrophytes (Hough, 1974; Black et al., 1976; Burris et al., 1976; Downton et al., 1976; Hough and Wetzel, 1977; Andrews and Abel, 1979). The decreasing O_2 evolution rates relative to electron transfer rates measured by PAM fluorometry at high irradiances in *Zostera marina* and *Halophila stipulacea* also suggested a role for photorespiration in these seagrass species (Beer et al., 1998). However we still do not understand how climate warming and ocean acidification/carbonation will affect photorespiration and photoprotection in seagrasses (Koch et al., 2013).

Long-term CO_2 enrichment experiments simulating the ocean acidification/carbonation have provided quantitative information of the positive responses of growth, carbon balance, survival and reproductive output in eelgrass (Palacios and Zimmerman, 2007; Zimmerman et al., 2016). Surprisingly during the most recent one of these studies, the regulation of pigment content with increasing CO_2 resembled the photoacclimation response to high light environment that pointed to the importance of redox acclimation in eelgrass (Chapter 2). Therefore, the objectives of this study were to estimate the importance of photorespiration in the marine angiosperm *Zostera marina* L. (eelgrass) under today's oceanic carbon concentrations and explore the potential response to ocean acidification/carbonation by 1) quantifying the photochemical rates under different light and CO_2 availability by using eelgrass grown in a high light low CO_2 environment; and 2) comparing how the relative contribution of different photochemical pathways in eelgrass changed under the same experimental conditions, once they have been acclimated to a high CO_2 environment.

Materials and Methods

The experimental facility and sampling from pH treatments

Eelgrass shoots used in this study were grown in an outdoor climate change experimental facility at the Virginia Aquarium and Marine Science Center, VA. The details of experimental

design and control of manipulations for this long term project were described in Chapter 2 and by Zimmerman et al. (2016). To summarize briefly, eelgrass plants, collected in May 2013 from the South Bay sub-tidal population in Eastern Shore, VA, USA, were transplanted into 20 fiberglass open top aquarium tanks. These aquaria were continuously enriched with CO_2 gas from June 2013 to October 2014 to attain treatment levels ranging from pH 6 to ambient (pH ~7.7), with 0.5 pH intervals between the treatments. As discussed in detail by Zimmerman et al. (2016), plant performance was monitored monthly while environmental parameters, which varied daily and seasonally, were recorded hourly.

For the purpose of this study, eelgrass plants from these pH treatments were used to measure the changes in photosynthetic response of leaves after 13 months of acclimation to the high CO_2 environment. During July 2014, freshly collected 2nd youngest leaves from pH 6.1, pH 6.9 and ambient pH treatments were brought to ODU, Norfolk, VA, for laboratory measurements of photochemistry under fully controlled incubation conditions. During the course of the measurements, the daily seawater temperature in aquaria ranged from 25 to 28°C; allowing all the incubation measurements described here to be conducted at the optimal temperature of 25°C without inducing a heat shock. The daily total surface irradiance ranged from 10 to 29 mol photons m^{-2} d^{-1}; corresponding to more than 6 h of photosynthetically saturating irradiance levels (>200 µmol photons m^{-2} s^{-1}) per day, allowing to designate the leaves used in the incubation measurements as high light acclimated. (Further environmental data were summarized in Chapter 2).

Incubation measurements of leaf photochemistry

Photosynthesis and respiration rates were measured polarographically with an oxygen electrode in water-jacketed glass incubation chambers (Appendix Figure 33 , 5ml volume, Rank Bros., Cambridge, UK). Simultaneous to O_2 evolution, leaf variable fluorescence was monitored

using a Pulse Amplitude Modulated (PAM) fluorometer (Mini PAM, Walz, Germany). Incubation water pH (a proxy for dissolved inorganic carbon (DIC) concentration) was measured using an epoxy mini-electrode and pH meter (Cole-Parmer) calibrated with NBS buffers. For this purpose, the lid of the chamber was modified to hold the miniature fiberoptics of the PAM device and the pH electrode in close proximity to the leaf surface. A magnetic stirrer provided turbulent flow to prevent boundary layer limitation of gas exchange across the leaf surface. Continuous analog signals from the three sensors were recorded using custom software written with LabView (2009 edition, National Instruments). Voltage data were post processed into metabolic rates using MATLAB R2014 (The MathWorks Inc.). A halogen (ELH) incandescent projector bulb (e.g. Kodak slide projector) provided photosynthetically active radiation (PAR). The intensity of PAR was adjusted with neutral density filters and calibrated daily with a QSL scalar radiometer (Biospherical Instruments Inc.).

Assuming alkalinity, temperature and salinity are known, ocean carbonation process via enriching the seawater with CO_2 can be continuously controlled by monitoring the pH in both aquaria and incubation chamber. Therefore, the levels of pH in aquaria (Growth pH, rounded to the nearest whole number) and in incubation chamber (Measurement pH) were used as proxies for CO_2 manipulation, a direct substrate for seagrass photosynthesis. Separate leaves, grown at three different pH treatments (GpH: 6, 7 and ambient (~8)), were used to measure the light response at three target pH levels (MpH: 6, 7 and 8); which allowed independent replications within and among the photosynthesis versus irradiance (*P* vs. *E*) curves. The seawater pH in the incubation chamber was adjusted by bubbling CO_2 and/or O_2-N_2 mixture prior to the measurement, while keeping [O_2] at air saturation level. Seawater temperature was kept constant at 25°C by a circulating water bath. Leaves were cleaned of epiphytes and kept in the dark before the incubation measurements. A three cm long piece of leaf tissue, cut approximately one cm above the meristem, was consecutively used during a 10 min dark (i.e.

dark respiration) and a 10 min light (i.e. net photosynthesis) measurement. After incubations, pigment content and optical properties of the leaf tissues (Table 6) were measured as described in Chapter 2.

The seawater used during all incubations was collected in April 2014 from Owl's Creek, a tidal estuary next to the aquarium facility in Virginia Beach, VA just south of the Chesapeake Bay that exchanges water with the Atlantic Ocean. This seawater stock, with salinity of 24 (PSS), was filtered through 0.2µm Nucleopore membrane filters and stored under refrigeration in dark bottles. After incubations, aliquots of seawater were taken from the chamber for alkalinity titrations using an automated potentiometric titrator (Metroohm). Based on temperature, salinity, alkalinity and pH of the seawater during the incubations, concentrations of DIC species (Table 7) were calculated using CO2SYS (Ver. 2.1; Lewis and Wallace 2012).

Table 6. List of symbols, their definitions and dimensions. Parenthetic notation (λ) denotes wavelength dependence of the variable.

Symbol	Definition	Dimensions
Chl-*a*	Chlorophyll *a*	µg
Chl-*b*	Chlorophyll *b*	µg
TChl	Total Chlorophyll	µg
TCar	Total Carotenoid	µg
FW	Fresh Weight	mg
LA	Leaf Area	cm^2
$A_L(\lambda)$	Leaf absorptance	Dimensionless
$D(\lambda)$	Leaf absorbance	Dimensionless
$R(\lambda)$	Leaf reflectance	Dimensionless
$a_L^*(\lambda)$	Optical cross-section	m^2 g^{-1} Chl-*a*
λ	Wavelength	nm
PAR	Photosynthetically active radiation	µmol photons s^{-1} m^{-2}
PUR	Photosynthetically usable radiation	µmol photons s^{-1} m^{-2}
E	Incident irradiance	µmol photons s^{-1} m^{-2}
Ek	Photosynthesis-saturating irradiance	µmol photons s^{-1} m^{-2}
Pg	Gross photosynthesis	
Pnet	Net photosynthesis	
P_T	True photosynthesis	
P_R	Photorespiration	
R_D	Dark respiration	
α	Photosynthetic efficiency at light-limited region of PE curve	µmol O_2 μmol^{-1} photons
Φ_{O2}	Quantum yield of oxygen evolution	µmol O_2 μmol^{-1} photons
Fm, Fm’	Maximal fluorescence from dark and light adapted leaf	Dimensionless

Table 6. *continued*

Symbol	Definition	Dimensions
F0, F0’	Minimal fluorescence from dark and light adapted leaf	Dimensionless
Fv	Variable fluorescence	Dimensionless
Φ_{PSII}	Effective Quantum yield of fluorescence ([Fm’ - F’] / Fm’)	Dimensionless
ETR	Electron transport rate	μmol electrons s^{-1} m^{-2}
NPQ	Nonphotochemical quenching ([Fm - Fm’] / Fm’)	Dimensionless

Table 7. Distribution of dissolved inorganic carbon and dissolved oxygen concentrations in seawater during the incubation measurements of net photosynthesis at different light levels, including dark respiration measurements. All measurements were done at 25°C using seawater with salinity of 24 ppt.

		At the start of light measurements			At the start of dark measurements		
	Target pH	Growth pH 6	Growth pH 7	Growth pH 8	Growth pH 6	Growth pH 7	Growth pH 8
Sample Size	6	7	7	5	7	7	5
	7	6	6	6	6	6	6
	8	5	5	5	5	5	5
Average pH	6	6.09 ± 0.01	6.08 ± 0.01	6.05 ± 0.01	6.09 ± 0.01	6.08 ± 0.01	6.04 ± 0.01
	7	6.91 ± 0.01	6.85 ± 0.02	6.87 ± 0.02	6.91 ± 0.01	6.84 ± 0.02	6.86 ± 0.02
	8	7.94 ± 0.05	7.95 ± 0.01	7.94 ± 0.02	8.00 ± 0.04	7.98 ± 0.01	7.98 ± 0.02
Average [TCO_2] (µmol/L)	6	3712.4 ± 27.9	3131.3 ± 17.9	3255.8 ± 48.4	3726.8 ± 27.2	3153.2 ± 19.5	3277.1 ± 48.9
	7	2217.9 ± 8.8	1874.3 ± 11.5	1861.1 ± 9.9	2216.6 ± 9.9	1875.9 ± 10.2	1865.5 ± 11.3
	8	1857.0 ± 15.2	1533.8 ± 3.2	1535.3 ± 4.9	1837.2 ± 14.2	1525.5 ± 3.5	1526.4 ± 4.7
Average [HCO^-_3] (µmol/L)	6	1963.2 ± 0.1	1623.7 ± 0.0	1624.0 ± 0.1	1963.3 ± 0.1	1623.8 ± 0.0	1624.0 ± 0.1
	7	1943.2 ± 0.7	1609.6 ± 0.7	1608.8 ± 0.7	1943.1 ± 0.7	1609.7 ± 0.6	1609.0 ± 0.7
	8	1742.3 ± 20.5	1442.2 ± 4.4	1444.2 ± 6.8	1714.4 ± 20.0	1430.6 ± 4.9	1431.9 ± 6.6

Table 7. *continued*

		At the start of light measurements			At the start of dark measurements		
	Target pH	Growth pH 6	Growth pH 7	Growth pH 8	Growth pH 6	Growth pH 7	Growth pH 8
Average [CO_2] (µmol/L)	6	1747.7 ± 27.8	1506.4 ± 17.9	1630.8 ± 48.3	1762.1 ± 27.1	1528.3 ± 19.5	1652.0 ± 48.8
	7	265.3 ± 8.4	258.2 ± 11.1	245.6 ± 9.5	264.1 ± 9.5	259.8 ± 9.8	249.8 ± 10.9
	8	22.8 ± 3.2	18.2 ± 0.5	18.6 ± 0.9	19.4 ± 2.4	16.9 ± 0.5	17.1 ± 0.8
Average [O_2] (µmol/L)	6	209.5 ± 3.1	215.0 ± 3.5	215.9 ± 2.0	212.6 ± 2.3	214.6 ± 3.0	216.0 ± 2.0
	7	214.6 ± 3.0	218.4 ± 4.3	217.5 ± 3.1	215.7 ± 3.4	219.4 ± 3.3	216.3 ± 1.7
	8	206.4 ± 2.4	215.8 ± 2.4	211.8 ± 2.7	212.2 ± 3.3	218.7 ± 1.6	215.4 ± 2.8

Determination of photochemical rates

Table 6 summarizes a list of parameters, their symbols and units used in the following calculations. Oxygen evolution rates of each tissue were separately normalized to fresh weight, leaf area and total pigment concentration to account for the phenotypic differences resulting from acclimation to different growth conditions. Photosynthetic parameters of *P* vs *E*. curves were estimated from these rates by fitting the cumulative one-hit Poisson model pioneered for photosynthesis by Webb et al. (1974):

$$P_{net} = P_g - R_D \quad (5)$$

$$P_{net} = [\, P_E * (1 - e^{-E/E_k}) \,] - R_D \quad (6)$$

where P_{net} was the measured net photosynthesis rate and R_D was the measured dark respiration rate, from which the gross photosynthesis P_g was calculated. P_g was defined as a function of light, where P_E represented the light-saturated gross photosynthesis rate varying with $[CO_2]$ and $[HCO_3^-]$ (sensu McPherson et al. (2015)). E_k was the photosynthesis saturating irradiance. *E* was separately defined as photosynthetically available radiation (PAR $=\sum_{400}^{700} E(\lambda)$) and by photosynthetically utilized radiation (PUR $=\sum_{400}^{700} [E(\lambda)*A(\lambda)]$), where $A(\lambda)$ was the spectral leaf absorptance and integrated the variability of light capture efficiency due to changes in leaf optical properties. Quantum yield of oxygen evolution (Φ_{O2}) at different light levels (in units of mol O_2 mol^{-1} absorbed photon) was calculated by $\Phi_{O2} = P_{g\ (per\ Leaf\ Area)}$ / PUR. Photosynthetic efficiency, which represents the linear slope of photosynthetic response in the light limited region of *P* vs *E* curve, can be described as either a function of PAR (α) or PUR (Φ_{max}) (Behrenfeld et al., 2004), and calculated as $\Phi_{max} = P_{E\ (per\ Leaf\ Area)} / E_{k\ (PUR)}$.

Although Eqn 5 represents the typical method for determining gross photosynthesis from measured values of P_{net} and R_D, this model does not account for light dependent processes that

use O_2 in the chloroplast, i.e. photorespiration. It was assumed that the Mehler Ascorbate Peroxidase pathway does not affect net O_2 exchange even though it may facilitate ATP generation and electron flow (hence might be detected by fluorescence measurements) (Larkum et al., 2006a). Following the principle explained by Raghavendra (2000) gross photosynthesis can be detailed as the difference between true photosynthesis (P_T) and photorespiration (P_R):

$$P_g = P_T - P_R \quad (7)$$

Under CO_2-saturation (i.e at low pH that increases CO_2:O_2 ratio in seawater), P_R would approach a minimum (~ 0), so that P_g will be an approximate estimate of true photosynthetic O_2 production (P_T). In this study, O_2 production rates measured at low pH (i.e. incubation pH6) were assumed to represent the true photosynthesis (P_T) for each growth condition. Therefore, photorespiration was calculated by subtracting the carbon limited gross photosynthesis measured at pH>6 from the gross photosynthesis at pH 6.

$$P_{R\ [pH>6]} = P_{g\ [pH6]} - P_{g\ [pH>6]} \quad (8)$$

$$P_{R[pH>6]} = [\ P_m * (1- e^{-E/\ E_k})\ ]_{[pH6]} - [\ P_E * (1- e^{-E/\ E_k})\ ]_{[pH>6]} \quad (9)$$

Under this assumption, P_g would approach P_E when light and flow are at saturating values, and it will approach the true physiological capacity (P_m) when carbon, light and flow are saturating. In this formulation, the limit of P_m is set by availability of cellular components such as enzyme and pigment concentrations, and may change as a function of growth conditions.

Pulsed Amplitude Modulation (PAM) fluorescence measurements were analyzed following the calculations outlined in Baker (2008). The maximum (F_m) and minimum (F_0) fluorescence emissions were measured in the dark while measuring respiration with a short saturating pulse of light. The maximum variable fluorescence yield ($F_v = F_m - F_0$) is used to quantify the

maximum quantum yield of fluorescence (F_v/F_m), which is a measure of maximum efficiency at which absorbed light by photosystem II (PSII) can be used for photochemistry. During photosynthesis, the maximum (F'_m) and minimum fluorescence (F_t) emissions induced by the short saturating pulse of PAM were measured again, but this time in the light. Based on these emissions under the presence of the actinic background light, the effective quantum yield of PSII (EQY, Φ_{PSII}), was determined as:

$$\Phi_{PSII} = (F'_m - F_t) / F'_m \quad (10)$$

Φ_{PSII} provides an estimate of the quantum yield of linear electron flux through PSII at a given photon flux. This photochemical quenching is one of the competitive pathways that reduces the fluorescence. The other non-radiative energy loss that quenches fluorescence, called Non-Photochemical Quenching (NPQ), results from the dissipation of excess excitation energy as heat via the Xanthophyll cycle. NPQ was estimated as:

$$NPQ = (F_m - F'_m) / F'_m \quad (11)$$

For comparisons among the treatments and incubations, NPQ and Φ_{PSII} at different light levels were fitted to a four parameter logistic curve, which is commonly used for dose response analysis, with the following formula:

$$NPQ = NPQ_{min} + \frac{(NPQ_{max} + NPQ_{min})}{1+(PUR/EC50)^{-Hillslope}} \quad (12)$$

where the Hill slope, also called a slope factor, quantified the steepness of the dose-response curve. EC50 was the PUR level required to provoke a response halfway between the baseline and maximum responses. The threshold for NPQ_{max} was constrained to 10 based on literature values (Kalaji et al., 2014).

The following relationship was used to estimate the electron transport rate (ETR) based on Φ_{PSII} (Figueroa et al., 2003):

$$ETR\ (\mu mol\ electrons\ m^{-2}s^{-1}) = PUR^{*}\ F_{II}{}^{*}\Phi_{PSII} \quad (13)$$

where F_{II} was the fraction of PUR captured by PSII and its light harvesting complexes (LHC). The typical value of F_{II} for Chlorophyta and seagrasses is about 0.5 (Figueroa et al., 2003; Larkum et al., 2006a). Photosynthetic parameters of ETR curves (i.e. ETR_{max}, α_{ETR} and $E_{k\text{-}ETR}$) were calculated by modifying the model of O_2 based *P* vs *E*. curves (Eq. 6):

$$ETR = ETR_{max}{}^{*}\left(1- e^{-E/\,E_k}\right) \quad (14)$$

Linear electron flow through PSII is directly related to photosynthetic oxygen production, therefore the gross photosynthesis based on fluorescence measurements ($P_{g\text{-}ETR}$) were estimated from ETR with the following formula:

$$P_{g\text{-}ETR}\ (\mu mol\ O_2\ m^{-2}s^{-1}) = ETR^{*}\ \tau \quad (15)$$

where τ was the ratio of oxygen evolved per electron generated at PSII. Since four stable charge separations are necessary to generate one mole of O_2 at PSII, τ is equal to 0.25.

Statistical analysis

Effects of growth pH on pigment content and optical properties of leaves were analyzed by one-way Analysis of Variance (ANOVA) followed by the Tukey multiple comparison method when significant overall effects were identified. Effects of growth pH and measurement pH on dark respiration rates, measured with the O_2 evolution method, were analyzed by Analysis of Covariance (ANCOVA).

O_2 evolution and fluorescence models were implemented by using the non-linear regression curve fitting tools in SigmaPlot (Systat Software Inc., Version 13.0). This tool provided the mean estimates of the model parameters with their error estimates and significances. Additionally, analysis of variance for the regression models were presented to account for the goodness of fit of the *P* vs *E* curves for each experimental condition (Appendix Table 19, Table 20, Table 21 and Table 22). Significant effects of measurement pH and growth pH on model parameters were analyzed by ANCOVA, which allowed only using the means of estimates.

Results

Photoacclimation to growth CO_2

Pigment content and leaf optical properties varied significantly among the leaves grown in different pH treatments (Table 8). Both total chlorophyll and carotenoid content decreased with increasing growth [CO_2] but the molar ratio of Total Car:Total Chl remained constant across CO_2 treatments at about 0.27. The optical cross section increased with growth [CO_2], indicating a reduced package effect. However, these leaves packed more biomass per the same unit of surface area, resulting from an increase in the thickness of the unpigmented mesophyll. These phenotypic responses, described in Chapter2, had important consequences for the comparison of photosynthetic efficiencies due to the normalization of metabolic rates to different leaf properties.

Table 8. Pigment content and optical properties of leaves used in photosynthesis measurements. Effects of growth pH on mean concentrations (±SE) were analyzed by one-way ANOVA. Different letters represent significant differences among the growth pH for each parameter compared by Tukey method at $P<0.05$. FW: Fresh Weight, LA: Leaf Area, Chl: Chlorophyll, Car: Carotenoid.

Growth pH	Ambient (~8)	7	6
Sample Size (n)	16	18	18
FW per LA (mg cm^{-2})	25.8 ± 1.33 ^{a}	27.1 ± 0.92 ^{a}	36.0 ± 1.52 ^{b}
Total Chl per LA (µg Chl cm^{-2})	31.2 ± 1.22 ^{a}	27.0 ± 1.20 ^{b}	20.8 ± 0.86 ^{c}
Total Chl per FW (mg Chl g^{-1} FW)	1.25 ± 0.07 ^{a}	1.01 ± 0.05 ^{b}	0.59 ± 0.03 ^{c}
Total Car per LA (µg Cx cm^{-2})	8.16 ± 0.28 ^{a}	7.25 ± 0.25 ^{b}	5.61 ± 0.17 ^{c}
Chl a:b	3.44 ± 0.04 ^{a}	3.73 ± 0.07 ^{b}	3.61 ± 0.04 $^{a, b}$
TCar:TChl	0.26 ± 0.00 ^{a}	0.27 ± 0.00 ^{a}	0.27 ± 0.00 ^{a}
Absorptance at 550nm	0.38 ± 0.01 ^{a}	0.37 ± 0.01 ^{a}	0.29 ± 0.01 ^{b}
Absorptance at 680nm	0.75 ± 0.01 $^{a, b}$	0.75 ± 0.01 ^{a}	0.73 ± 0.01 ^{b}
Optical Cross Section (a^*_{680})	5.90 ± 0.33 ^{a}	6.73 ± 0.29 ^{a}	8.10 ± 0.24 ^{b}

Light response curves of Oxygen flux

Rates of dark respiration, whether normalized to biomass ($R_{D\ (FW)}$) or leaf area ($R_{D\ (LA)}$), were not affected by growth [CO_2] or instantaneous variations of [CO_2] within the incubation chambers, and averaged 5.96 $\pm$ 0.31 μmol O_2 hr^{-1} g^{-1} FW or 0.50 $\pm$ 0.03 μmol O_2 m^{-2} s^{-1}, respectively (Table 9). Dark respiration rates were independent of pH within the range examined here, indicating no negative impact of changing ionic composition on respiration. In contrast net O_2 production rates increased with light and incubation [CO_2] for all plants, regardless of the CO_2 environment in which they were grown (Figure 13).

The biomass specific rate of light-saturated photosynthesis ($P_{E\ (FW)}$) averaged 14.1 µmol O_2 hr^{-1} g^{-1} FW at low incubation [CO_2] for all plants and increased as a function of incubation [CO_2] (Figure 13). However, $P_{E\ (FW)}$ of the plants grown under ambient conditions was twice as sensitive to increasing [CO_2] than plants grown under CO_2 enrichment (Table 10, 86.8 vs 33.5 µmol O_2 hr^{-1} g^{-1} FW at M_{pH} 6 respectively). This difference was associated with 2 fold higher biomass specific pigment content of the ambient plants (Table 8). This indicates the limitation of oxygen evolution of ambient plants at their natural low CO_2 environment is mainly due to photorespiration even though the plants have excess photosynthetic machinery available and efficiently harvesting light.

For all plants, increased incubation [CO_2] also increased the light requirement to saturate photosynthetic oxygen production ($E_{k\ (PAR)}$ and $E_{k\ (PUR)}$); rather than changing the photosynthetic efficiency (α) within the light limited region of *P* versus *E* response curves (Table 10). Overall, photoacclimation of eelgrass leaves to ocean carbonation resulted in increasing $E_{k\ (PUR)}$ values; 17, 44 and 48 µmol absorbed photon s^{-1} m^{-2} for pH8, pH7 and pH6 plants at their growth pH, respectively.

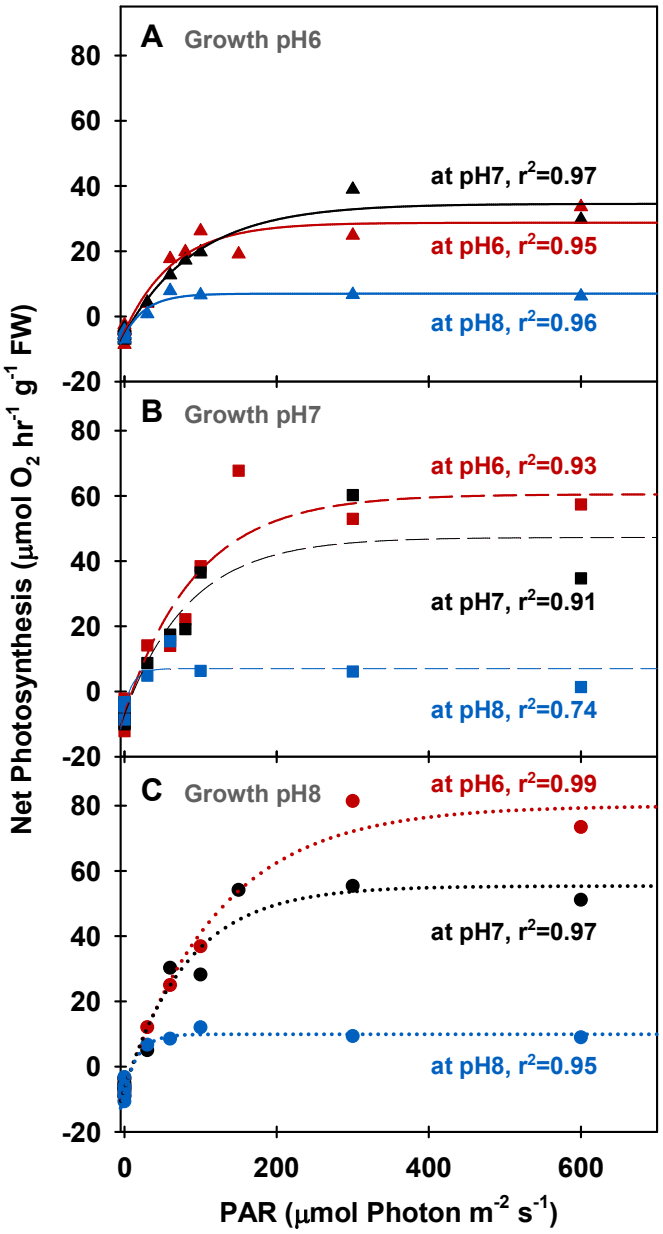

Figure 13. Net Photosynthesis of eelgrass leaves per biomass as a function of irradiance. O_2 production rates were measured at different pH levels (red: pH6, black: pH7 and blue: pH8) using leaves grown at pH6 (A), pH7 (B) and ambient pH (C). Curves were fit using Eq.6.

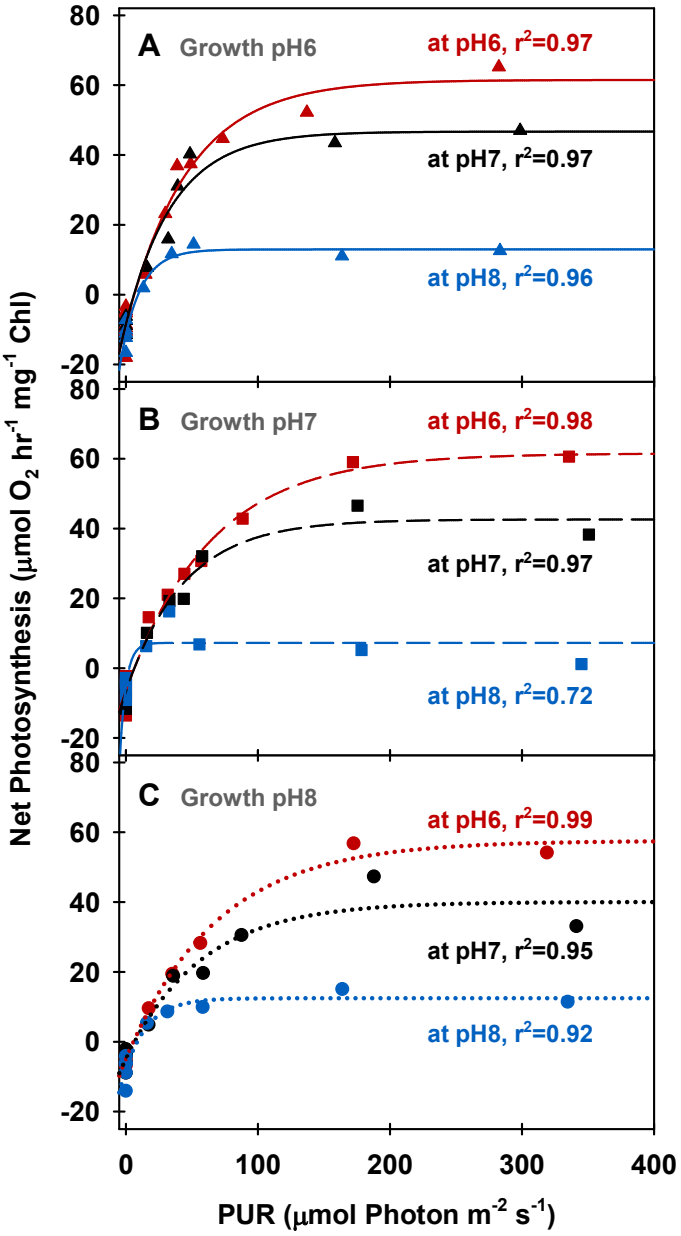

Figure 14. Net Photosynthesis of eelgrass leaves per total Chlorophyll content as a function of absorbed irradiance. O_2 production rates were measured at different pH levels (red: pH6, black: pH7 and blue: pH8) using leaves grown at pH6 (A), pH7 (B) and ambient pH (C). Curves were fit using Eq.6.

Table 9. Dark respiration (R_D) rates measured with O_2 evolution method and estimated by non-linear model fit to *P vs E* curves. Rates are normalized both to Fresh Weight (FW) and Leaf Area. Effects of measurement pH and growth pH on measured R_D were analyzed by ANCOVA.

Growth pH	Measurement pH	Measured Dark Respiration (μmol O_2 hr^{-1} g^{-1} FW)	Modeled Dark Respiration (μmol O_2 hr^{-1} g^{-1} FW)	Modeled Dark Respiration (μmol O_2 s^{-1} m^{-2})
6	6	4.61 ± 0.75	4.73 ± 1.34	0.45 ± 0.10
	7	5.31 ± 0.62	5.50 ± 1.15	0.51 ± 0.08
	8	5.84 ± 0.47	5.90 ± 0.63	0.69 ± 0.07
7	6	6.40 ± 1.14	6.90 ± 3.06	0.51 ± 0.12
	7	6.73 ± 1.20	7.08 ± 3.02	0.53 ± 0.22
	8	5.03 ± 0.91	5.04 ± 1.88	0.37 ± 0.12
Ambient (~8)	6	6.52 ± 0.93	6.83 ± 2.06	0.46 ± 0.07
	7	6.18 ± 0.75	6.71 ± 2.19	0.46 ± 0.14
	8	7.29 ± 1.26	7.29 ± 1.05	0.56 ± 0.10

ANCOVA of Measured R_D	DF	SS	MS	F	P
Growth pH	2	11.551	5.776	1.173	0.318
Measurement pH	1	0.531	0.531	0.108	0.744
Growth pH x Measurement pH	2	10.206	5.103	1.037	0.363
Residual	46	226.435	4.922	--	--
Total	51	255.682	5.013	--	--

Table 10. Model estimates (mean ± SE) of photosynthesis parameters generated by non-linear regression fit to the experimental data using Eq. 6 (N.S. stands for non-significant parameter estimate). Significant effects of measurement pH (M_{pH}) and growth pH (G_{pH}) on mean estimates were analyzed by ANCOVA.

Model Estimates	Growth pH	Measurement pH 6.0	7.0	8.0
P_E (µmol O_2 hr^{-1} mg^{-1} Chl) G_{pH} x M_{pH}: p=0.570 G_{pH}: p=0.583 M_{pH}: p=0.002	6	70.2 ± 4.3	55.2 ± 3.7	24.5 ± 2.1
	7	68.0 ± 3.2	49.3 ± 3.1	12.5 ± 3.1
	8	62.6 ± 2.4	44.9 ± 4.0	20.3 ± 2.4
P_E (µmol O_2 hr^{-1} g^{-1} FW) G_{pH} x M_{pH}: p=0.240 G_{pH}: p=0.185 M_{pH}: p=0.014	6	33.5 ± 2.8	40.0 ± 2.5	12.9 ± 1.1
	7	67.4 ± 7.1	54.3 ± 6.5	12.1 ± 2.9
	8	86.8 ± 4.7	62.1 ± 4.6	17.2 ± 1.7
P_E (µmol O_2 s^{-1} m^{-2}) G_{pH} x M_{pH}: p=0.233 G_{pH}: p=0.199 M_{pH}: p=0.007	6	3.6 ± 0.2	3.5 ± 0.2	1.5 ± 0.1
	7	5.8 ± 0.3	4.3 ± 0.5	0.9 ± 0.2
	8	5.8 ± 0.2	4.3 ± 0.3	1.5 ± 0.2
ETR_{max} (µmol Electron s^{-1} m^{-2}) G_{pH} x M_{pH}: p=0.573 G_{pH}: p=0.482 M_{pH}: p=0.119	6	35.3 ± 0.4	41.0 ± 3.3	22.4 ± 0.5
	7	93.1 ± 2.6	68.3 ± 4.2	32.4 ± 1.1
	8	58.4 ± 5.8	82.2 ± 5.5	22.8 ± 0.7
α_{ETR} (µmol Electron µmol^{-1} absorbed Photon) G_{pH} x M_{pH}: p=0.696 G_{pH}: p=0.735 M_{pH}: p=0.257	6	0.45 ± 0.01	0.50 ± 0.07	0.52 ± 0.03
	7	0.42 ± 0.01	0.48 ± 0.04	0.44 ± 0.04
	8	0.50 ± 0.08	0.46 ± 0.03	0.52 ± 0.04

Table 10. *continued*

Model Estimates	Growth pH	Measurement pH 6.0	7.0	8.0
Φ_{max} (µmol O_2 µmol^{-1} absorbed Photon) G_{pH} x M_{pH}: p=0.263 G_{pH}: p=0.314 M_{pH}: p=0.100	6	0.077 ± 0.01	0.084 ± 0.01	0.107 ± 0.03
	7	0.079 ± 0.01	0.079 ± 0.02	0.14 ± 0.24
	8	0.083 ± 0.01	0.074 ± 0.01	0.081 ± 0.03
E_k (µmol absorbed photon s^{-1} m^{-2}) from 'PG per Chl vs PUR' G_{pH} x M_{pH}: p=0.391 G_{pH}: p=0.348 M_{pH}: p=0.006	6	47.5 ± 7.0	36.4 ± 6.0	14.5 ± 4.9
	7	64.2 ± 7.4	43.9 ± 6.9	4.7 ± 15.8
	8	68.6 ± 7.2	57.1 ± 13.3	17.4 ± 7.1
E_k (µmol photon s^{-1} m^{-2}) from 'PG per FW vs PAR' G_{pH} x M_{pH}: p=0.523 G_{pH}: p=0.501 M_{pH}: p=0.046	6	65.0 ± 14.5	94.7 ± 14.8	28.4 ± 8.6
	7	94.0 ± 24.2	85.3 ± 25.1	11.6 ± 23.5
	8	124.9 ± 18.6	83.9 ± 16.9	18.3 ± 8.7
E_k (µmol absorbed photon s^{-1} m^{-2}) from 'ETR vs PUR' G_{pH} x M_{pH}: p=0.560 G_{pH}: p=0.469 M_{pH}: p=0.117	6	78.5 ± 2.0	82.2 ± 15.6	43.1 ± 2.9
	7	220.1 ± 10.3	142.6 ± 19.0	72.8 ± 7.3
	8	117.5 ± 27.8	180.1 ± 22.9	44.2 ± 3.8

The chlorophyll specific rates of light-saturated photosynthesis ($P_{E\ (Chl)}$) were the same for all plants grown at different CO_2 environments, and increased identically with the incubation [CO_2] (Figure 14). Consequently, the O_2 production efficiency per unit Chlorophyll did not change as a function of the CO_2 environment in which the plants were grown. Therefore, for any plant, the increase of O_2 evolution with incubation [CO_2] was instantaneous at a constant light level (Figure 15, A). Most likely explanation of this instantaneous response would be a reversible and light dependent O_2 consuming process involving the chloroplast, such as photorespiration (P_R), that is reduced/eliminated with increasing [CO_2]. Therefore, for all plants, $P_{E\ (Chl)}$ rates at high incubation [CO_2] (i.e. at $M_{pH}6$) were assumed to be the true physiological capacity ((P_m) i.e. light, carbon and flow saturated photosynthesis) acclimated to their growth environment. Based on this assumption, photorespiration rates were quantified by solving the Eq.9 with the chlorophyll specific gross photosynthesis models (Figure 15, B). Using pigment specific models, rather than biomass or area based models, eliminated the effect of morphological differences among the plants on net oxygen metabolism.

Photorespiration (P_R) increased with light similar to photosynthesis (P); but decreased with increasing incubation [CO_2], as carboxylation became increasingly favored over oxygenation (Figure 15, B). Predicted P_R rates increased rapidly with light to a maximum of 60 to 80% of P_m at low [CO_2] (i.e. $M_{pH}8$) (Figure 15, C). When aqueous [CO_2] was equal to aqueous [O_2] (at $M_{pH}7$, Table 7), maximum P_R rates were only 20% of P_m, which is equivalent to the inherent carboxylation: oxygenation ratio of Rubisco.

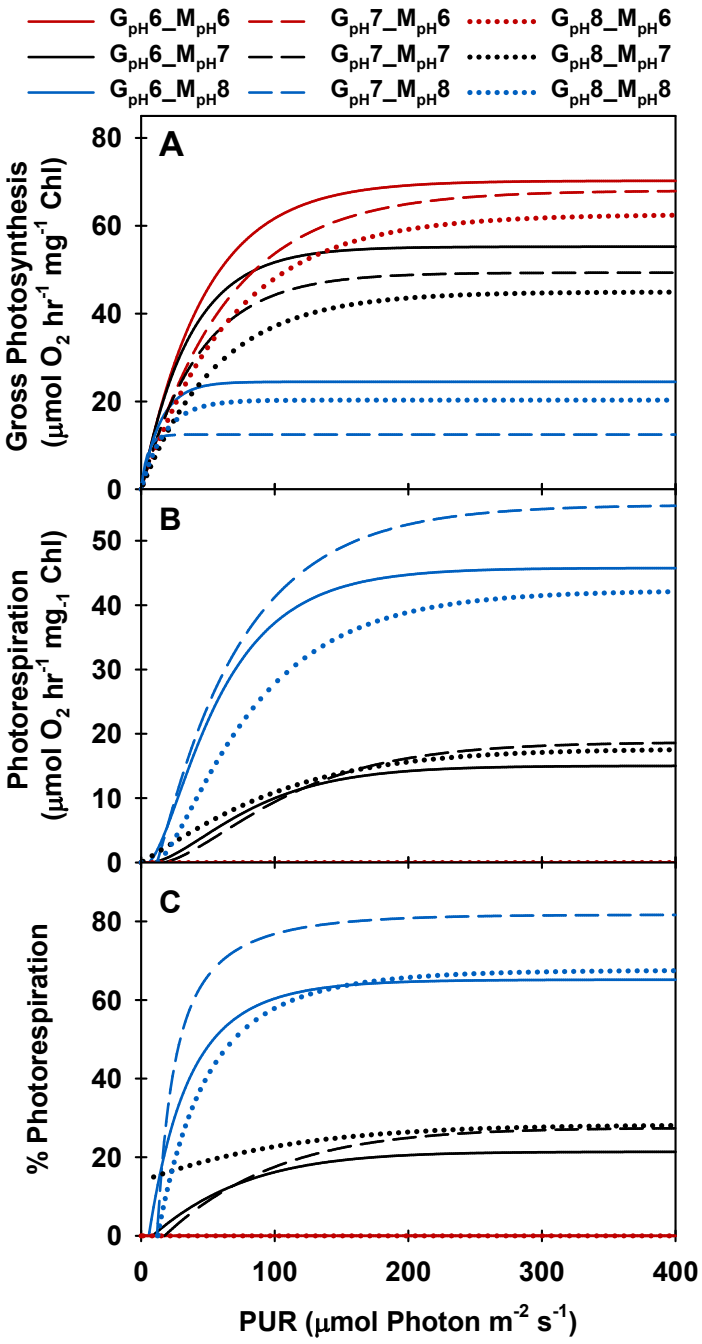

Figure 15. Modeled gross photosynthesis (A) and photorespiration (B and C) of eelgrass leaves as a function of absorbed irradiance. Colors represent different pH levels at which the measurements (M_{pH}) were performed; line styles represent the different pH levels at which the plants were grown (G_{pH}). Photorespiration at M_{pH6} were zero.

All plants reached the lowest Gross Photosynthesis to Dark Respiration ratio (P_g:R_D) of 2 at low incubation [CO_2] when light saturated (Figure 16, A). This ratio increased instantaneously up to 12 for ambient plants ($G_{pH}8$) when saturated with CO_2 in the incubation medium. However, high CO_2 grown plants downregulated their P_E:R_D to an average of 8. This showed the consequence of pigment acclimation on metabolic balance because of growth in high CO_2 environment (Figure 16, grey arrows in B). Having excess pigment content in a carbon-limited environment (as observed in pH8-grown plants) did not improve the P_E:R_D under normal growth conditions even though it allowed the instantaneous 6 fold increase of P_E:R_D when incubation [CO_2] increased. High CO_2 acclimated plants, on the other hand, had 4 fold higher P_E:R_D than ambient plants at their respective growth pH even though decreasing the pigment content by half.

Light response curves of chlorophyll fluorescence

Maximal quantum yields of fluorescence of dark-adapted leaves were above 0.7 regardless of incubation [CO_2], indicating all plants from different pH treatments were healthy during the experiments (Φ_{PSII} at PUR 0 µmol absorbed photon s^{-1} m^{-2}, Figure 17). For all plants, effective quantum yields of fluorescence (Φ_{PSII}) decreased faster with increasing light when the incubation [CO_2] was low ($M_{pH}8$). The decreased photochemical yield resulted from rapid induction of non-photochemical quenching (NPQ) when [CO_2] was limited under light saturation (Figure 18). However, the onset of NPQ in response to light increased with growth CO_2, meaning the NPQ pathway was saturated quickly for high CO_2 acclimated plants at all incubation conditions (Figure 18 A). The rapid saturation of NPQ in response to light was consistent with the decreased carotenoid content of leaves grown under high [CO_2].

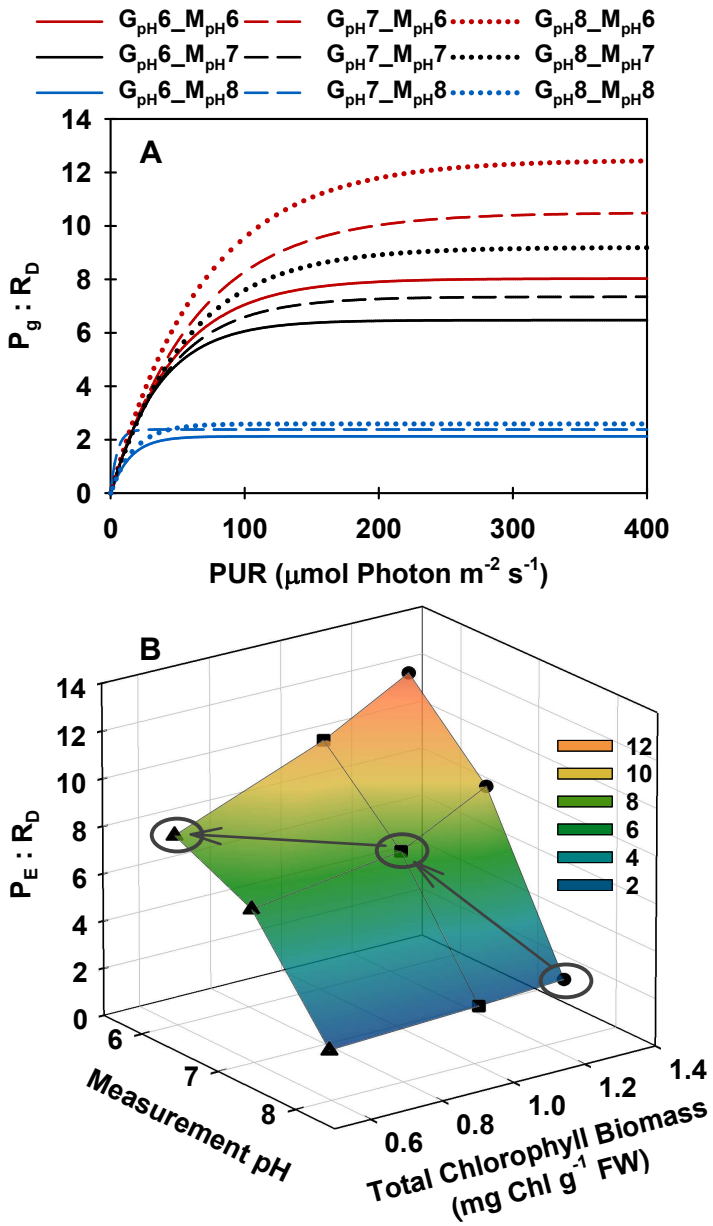

Figure 16. Modeled ratio of gross photosynthesis to dark respiration as a function of absorbed irradiance (A) and as a function of Chlorophyll content at saturating irradiances (B). Colors represent different pH levels at which the measurements (M_{pH}) were performed; line styles (G_{pH}) and symbols (▲at pH6, ■ at pH7, ● at ambient pH) represent the different pH levels at which the plants were grown. (B) Ellipses highlight when plants from different treatments were incubated at their corresponding growth pH. So that, gray arrows show the trajectory of P_E:R_D as a result of phenotypic acclimation to the increasing CO_2 environment.

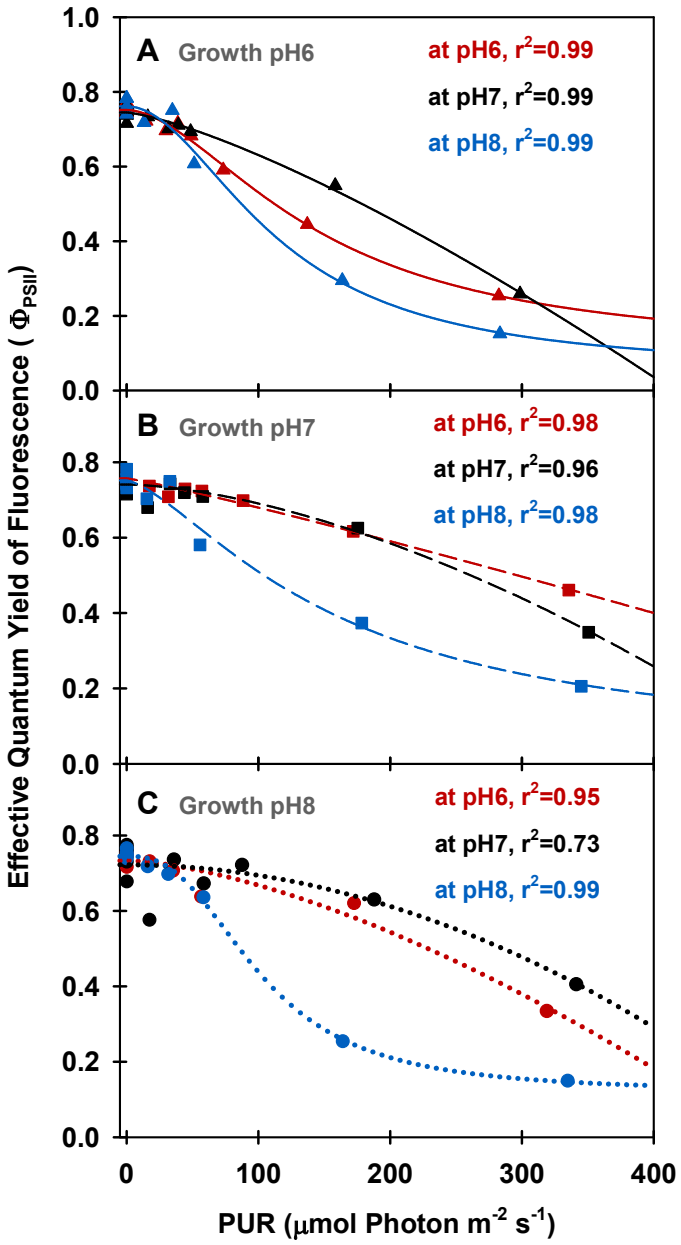

Figure 17. Fluorescence parameters of eelgrass leaves as a function of absorbed irradiance. PAM measurements were performed at different pH levels (red: pH6, black: pH7, blue: pH8) using leaves grown at pH6 (A), pH7 (B) and ambient pH (C). Curves were fit using Eq.12.

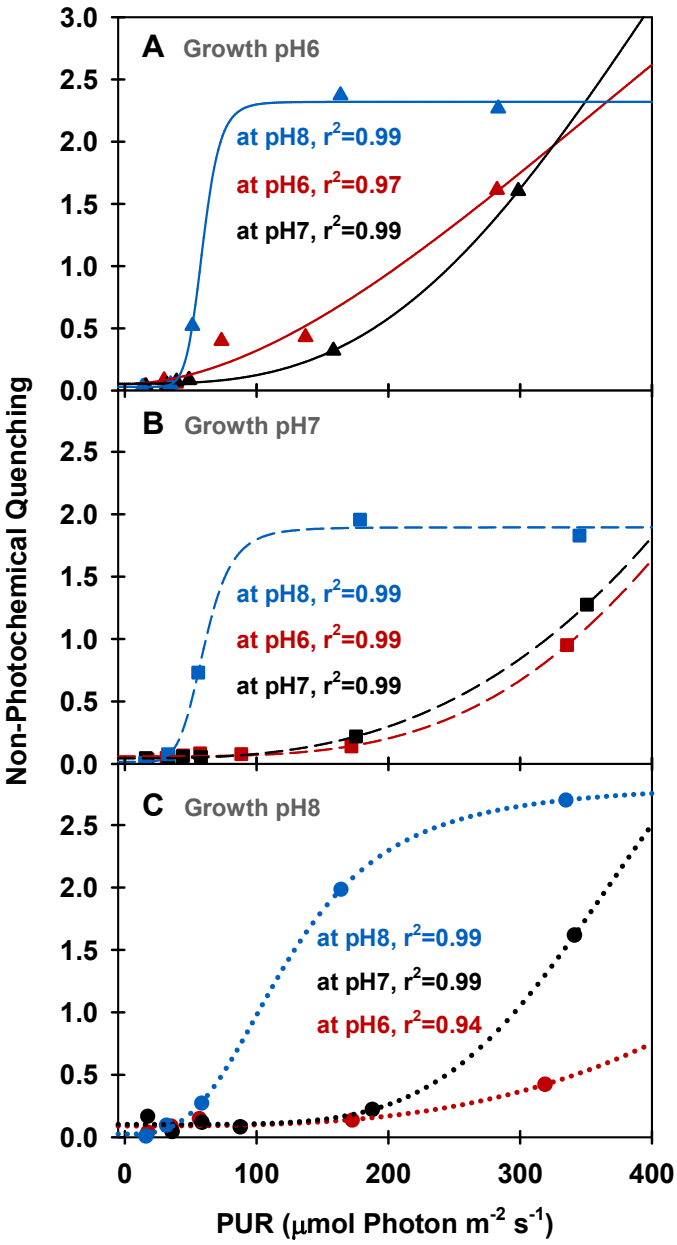

Figure 18. Fluorescence parameters of eelgrass leaves as a function of absorbed irradiance. PAM measurements were performed at different pH levels (red: pH6, black: pH7, blue: pH8) using leaves grown at pH6 (A), pH7 (B) and ambient pH (C). Curves were fit using Eq.12.

At saturating irradiance (350 µmol absorbed photon s^{-1} m^{-2}, Figure 18), NPQ values of ambient plants increased 5 fold with decreasing incubation [CO_2] contrary to high CO_2 acclimated plants ($G_{pH}6$), which reached the same NPQ of 2.5 at this light level regardless of incubation [CO_2]. The dynamic range of NPQ regulation in ambient grown plants in response to instantaneous changes in [CO_2] showed their high tolerance of fluctuating environmental conditions (Figure 18 C); similar to diurnal NPQ cycle capacity of high light acclimated eelgrass leaves to avoid photodamage under fluctuating light environments (Ralph et al., 2002).

The relation between quantum yield of fluorescence (Φ_{PSII}) and quantum yield of oxygen evolution (Φ_{O2}) was nonlinear, and their ratios were closest to the theoretical value of 8 only at low light and high [CO_2] conditions (Figure 19). For this ratio to be higher than 8 either less than half of the photons are directed to PSII (i.e. $F_{II}<0.5$, Eq.13) and/or more than four electrons are processed to evolve one mole of oxygen ($\tau<0.25$, Eq.15). Both of these outcomes highlight deviation from linear electron flow. For ambient plants, Φ_{O2} decreased faster than Φ_{PSII} with increasing light resulting in a drastic increase in Φ_{PSII}:Φ_{O2}, especially at their growth pH 8, which indicated these plants were using alternative electron pathways to keep electron flow running, as detected by PAM method, without producing and/or consuming oxygen in a light dependent respiratory process (i.e. photorespiration).

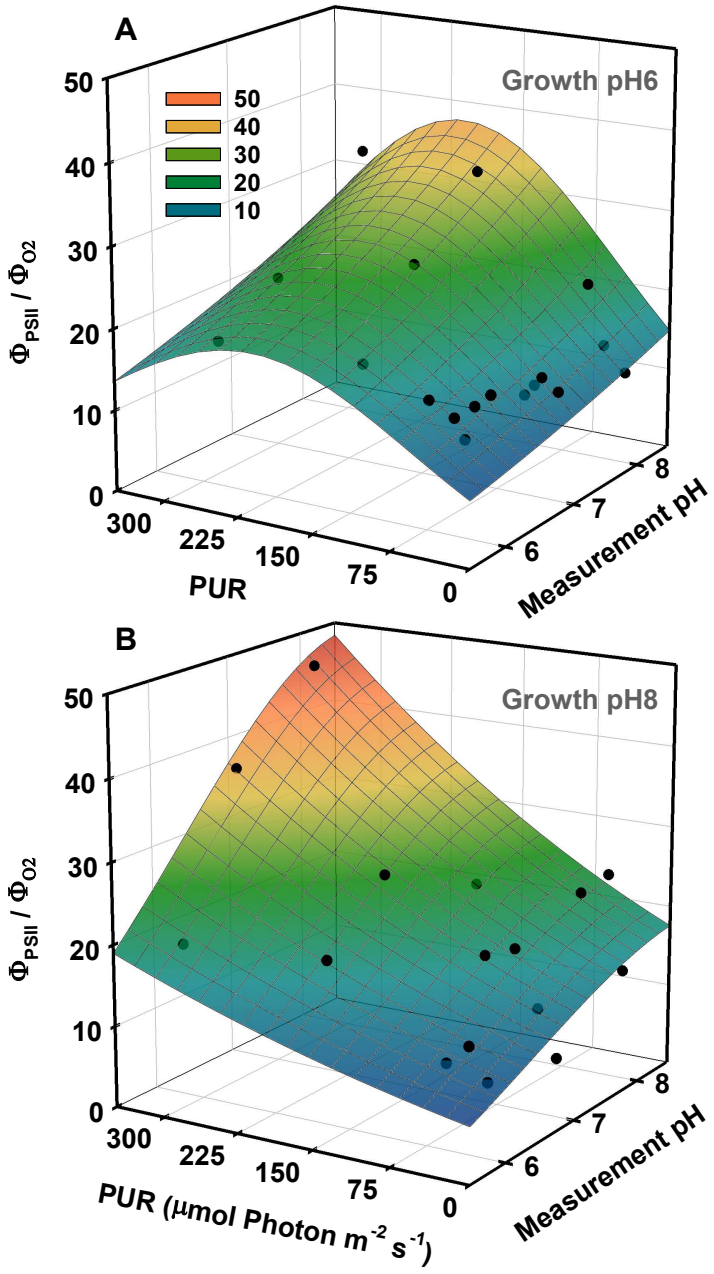

Figure 19. Divergence of quantum yield of fluorescence (Φ_{PSII}) from quantum yield of oxygen (Φ_{O2}) as a function of light and incubation pH. O_2 production and fluorescence were measured simultaneously at different pH levels using eelgrass leaves grown at different CO_2 treatments. Yields were calculated using PUR. Relationship was modeled using Gaussian type non-linear regression fit.

Similar to net photosynthesis rates, electron transport rates (ETR) of all plants increased with light and were lowest at low incubation [CO_2] (i.e. $M_{pH}8$) (Figure 20, Table 10). However, the increase of ETR_{max} with incubation CO_2 was not consistent among the plants due to the non-monotonic trend of EQY with incubation pH (Figure 17). Only ETR_{max} of plants grown at pH7 increased consistently with increasing incubation [CO_2]. For all incubation experiments, PUR levels to saturate ETR ($E_{k\text{-}ETR}$) were consistently higher than the E_k values required to saturate O_2 production (Table 10). For all plants, estimated gross photosynthesis based on ETR were also higher than the gross photosynthesis measured by the O_2 evolution method (Figure 21). However, this overestimation was not consistent among plants grown at different CO_2 environments. The $P_{E\ (LA)}$ to ETR_{max} ratio was around 0.1 for pH6 and pH8 plants when incubated at pH6 and pH8, instead of the theoretical value (τ) of 0.25 (Table 10).

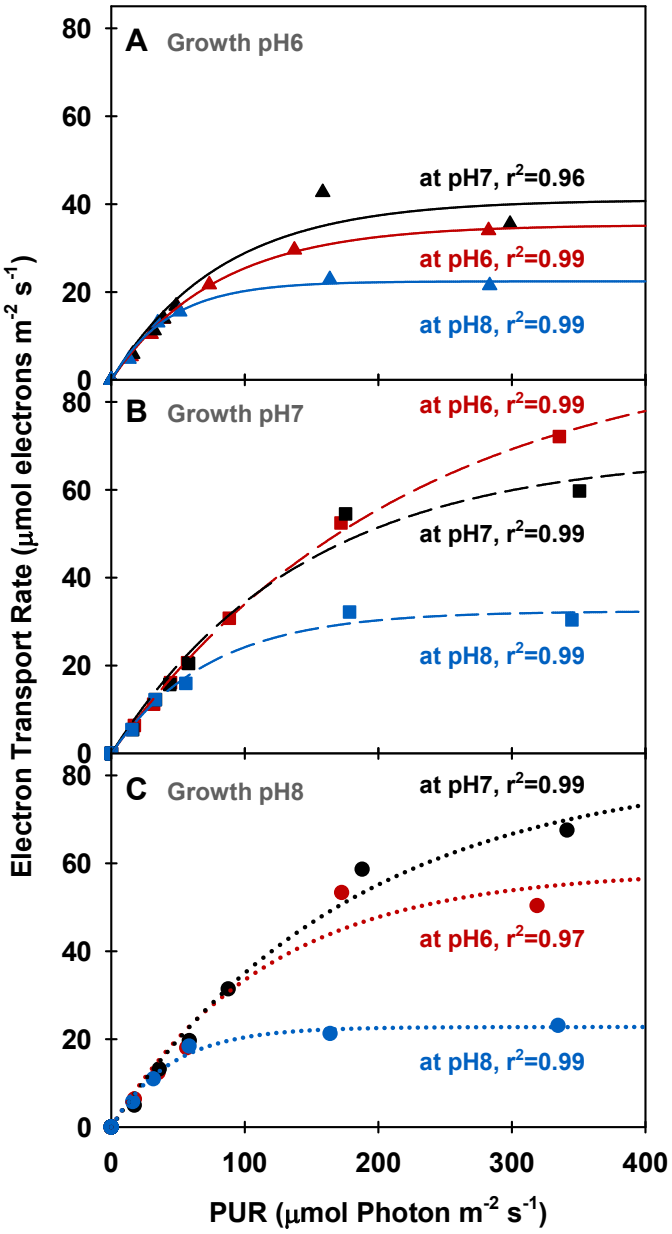

Figure 20. Electron transport rates of eelgrass leaves as a function of absorbed irradiance. PAM measurements were performed at different pH levels (red: pH6, black: pH7 and blue: pH8) using leaves grown at pH6 (A), pH7 (B) and ambient pH (C). Curves were fit using Eq.14.

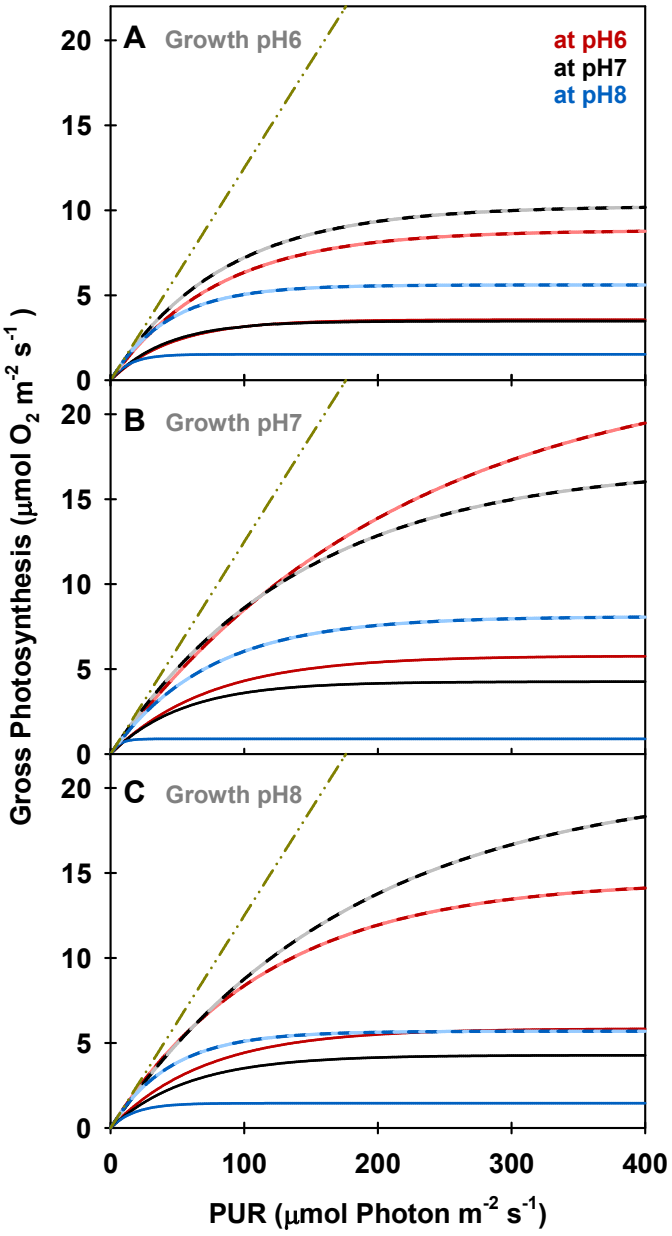

Figure 21. Modeled gross photosynthesis of eelgrass leaves as a function of absorbed irradiance. Solid lines are calculated from leaf area normalized O_2 production rates (Eq. 5) and dashed lines are estimated from ETR measurements (Eq. 15). Colors represent incubation pH levels. Green dot-dashed lines represent the theoretical O_2 production per absorbed photon under non-limiting environmental conditions.

Discussion

Long-term growth under high [CO_2] produced morphological and metabolic changes in eelgrass. Although pigment content decreased in plants grown at high CO_2, leaves increased the biomass yield resulting from increased photosynthetic carbon assimilation and decreased photorespiration. Evidence for photorespiration was the equivalent response of chlorophyll normalized O_2 production rates to increased incubation [CO_2], independent of the growth CO_2. Therefore, the instantaneous difference in O_2 production rates in CO_2-saturated vs. CO_2-limited incubation medium corresponded to the amount of O_2 consumed in the photorespiratory pathway. Thus, photosynthesis and photorespiration as a function of light for each growth condition were precisely predictable using the *P* versus *E* curves, although the responses to incubation CO_2 differed between biomass and pigment normalization due to changes in leaf morphology. Presently, models of eelgrass performance do not consider these long-term morphological and metabolic acclimation responses (Zimmerman, 2003, 2006; Zimmerman et al., 2015). Thus, the quasi-mechanistic model developed in this study permits integration of the photosynthetic and morphological acclimation due to ocean carbonation into seagrass productivity models, by adjusting the limits of the photosynthetic parameters based on substrate availability and physiological capacity.

Morphological acclimation and regulation of pigment content, rubisco activity, light capture and carbon fixation as a function of CO_2 availability have been previously observed in multiple submerged angiosperms (Madsen et al., 1996). Increasing P_g:R_D due to the enhancing impact of [CO_2] on P_E was detected even in short term (2-6 weeks) studies using tropical and temperate seagrass species without any CO_2 effect on pigment content (Zimmerman et al., 1997; Ow et al., 2015). Long term studies, moreover, concluded the significant responses of pigment content, biomass allocation, shoot survival and reproductive output in eelgrass to CO_2 availability (Chapter 2, (Palacios and Zimmerman, 2007; Zimmerman et al., 2016). Despite

decreasing pigment content and leaf absorptance, plants grown at high CO_2 were able to keep higher P_g:R_D ratio than ambient grown plants at their respective growth conditions; indicating the coupling between the regulation of photosynthetic structure and metabolic carbon demands. Such a coupling between photosynthetic regulation and growth might be poor for organisms that undergo photodamage because photosynthesis might accommodate the biochemical costs associated with protection and recovery rather than fueling the energy towards growth (Barra et al., 2014). On the other hand, eelgrass plants show no sign of photodamage even when photosynthesis is carbon limited but light saturated.

When incubated at low [CO_2], plants from the ambient CO_2 aquaria had the same photosynthetic O_2 production as the plants grown at high [CO_2]. These same photosynthetic rates highlighted no enhanced DIC uptake mechanisms in ambient eelgrass plants to begin with, as opposed to marine algae and cyanobacteria that usually upregulate their carbon concentrating mechanisms when CO_2 availability is limited in their growth environment (Björk et al., 1993; Raghavendra, 2000; Falkowski and Raven, 2007). This is also consistent with our inability to reduce photosynthesis of eelgrass from the Chesapeake region with an inhibitor of external carbonic anhydrase (McPherson et al., 2015) and Celebi - unpublished data). Seagrasses living in intertidal estuarine environments, like Chesapeake Bay eelgrass used in this study, are subject to highly variable CO_2/pH levels daily and seasonally, which might explain the unresponsiveness of CCMs for ambient plants (Duarte et al., 2013; Ruesink et al., 2015). Similarly, all plants had the same $P_{E\ (Chl)}$ when measured at saturating [CO_2] due to minimized P_R, indicating all plants approached the same physiological oxygen production capacity per available photosynthetic machinery (i.e. $P_{m\ (Chl)}$ was constant across all treatments). Therefore the difference in P_E:R_D at high incubation [CO_2] among the plants resulted from the downregulation of photosynthetic machinery in high CO_2 grown plants (i.e. chloroplast and rubisco content; also consistent with reduced N content – pers comm with Jinuntuya M.).

Despite phenotypic acclimation across the CO_2 gradient, the maximum photosynthetic efficiency (Φ_{max}) remained constant for all plants (~0.08 mol O_2 mol^{-1} absorbed photon) but photosynthesis-saturating light levels (E_k) increased, as was predicted by the model of McPherson et al. (2015). Photosynthetic efficiency within and among seagrass species vary with efficiency of light absorption and efficiency of light to carbon conversion (Ralph et al., 2007). Although the observed α values in this study were in agreement with previous estimates for eelgrass (Frost-Christensen and Sand-Jensen, 1992), constant α across different CO_2 regimes is different than common literature values observed for terrestrial C3 plants (0.082 and 0.052 mol CO_2 mol^{-1} absorbed photon at high and low [CO_2], respectively (Raghavendra, 2000). This difference might be due to acclimation to submerged environment where water stress is not coupled to CO_2 response as in terrestrial plants. The increased E_k and P_E values for high CO_2 acclimated plants will decrease the estimates of H_{sat} (i.e. average daily period of P_E) required to maintain positive carbon balance for the whole plant. H_{sat} requirement is a useful modeling tool in predicting the depth distribution of eelgrass in variable light environments (Zimmerman et al., 1991; Zimmerman et al., 1995).

A strong correlation between NPQ (i.e. xanthophyll cycle) and high light exposure has been confirmed for eelgrass (Ralph et al., 2002). A previous study found that high light acclimated eelgrass leaves had higher NPQ activity, and higher photosynthetic capacity, than low light acclimated leaves (Ralph and Gademann, 2005). This study demonstrated a similar effect on NPQ activity by [CO_2] availability. Under ambient CO_2 concentrations photosynthesis became carbon limited at lower E_k so that the excess photon absorption was diverted to NPQ, likely using the xanthophyll cycle. The high CO_2 incubations reduced this carbon limitation and increased the E_k, consequently reducing the NPQ. Due to increased E_k, the same light environment becomes less damaging at high CO_2, which may explain the reduction in both photosynthetic and photoprotective pigments observed in response to growth CO_2. This also

highlights the importance of photoprotective mechanisms in ambient grown plants to prevent photoinhibition in eelgrass, which would be costly to repair. Thus, by reducing CO_2 limitation of Rubisco, ocean carbonation should also reduce the vulnerability of eelgrass to excess reactive oxygen species (ROS) and therefore the need for photoprotection.

Furthermore, the simultaneous measurements of variable fluorescence, and O_2 flux performed here yielded quantitative estimates of changes in photoprotective pathways of eelgrass acclimated to different CO_2 environments. The difference between the theoretical O_2 evolution (i.e. the linear increase of O_2 with light) and the ETR estimates of gross photosynthesis ($P_{g\text{-}ETR}$) accounts for the absorbed photons (energy) that did not contribute to the electron transport pathway (not exciting electrons at PSII). This difference can be explained by quenching pathways, such as fluorescence and NPQ, which would reduce the photochemical quenching measured as Φ_{PSII} and integrated into $P_{g\text{-}ETR}$. This difference was most pronounced for plants grown at high CO_2 related to their significantly lower ETR values. This trend was consistent with their lower area based O_2 production rates at high CO_2 incubations when compared to pH7 and ambient pH grown plants. These plants downregulated their pigment content but increased the light-dependent NPQ at lower irradiances even at high incubation [CO_2]. This may indicate that phenotypic acclimation to ocean carbonation by downregulation of photosynthetic machinery (i.e. less pigment per area) reduced the role of photorespiration but increased the role of NPQ in photoprotection.

On the other hand, the difference between the ETR estimated gross photosynthesis ($P_{g\text{-}ETR}$) and the gross photosynthesis measured by oxygen production (P_g) may result from inaccurate assumptions of F_{ii} and/or τ (Eq.15). In theory, 8 photons absorbed equivalently both by PSI and PSII (F_{ii}= 0.5) excites total of 4 electrons producing 1 mole of O_2 (τ =0.25). This equilibrium of linear electron flow is valid when there is no limitation of resources such as CO_2 and/or accumulation of byproducts such as reducing equivalents and ROS (Scheibe et al., 2005; Dietz

and Pfannschmidt, 2011; Pfannschmidt and Yang, 2012). Under limiting conditions, this balance shifts towards pathways that ensure the optimal redox state of the chloroplast resulting in altered photon: electron: O_2 ratios (Foyer et al., 2012). Fluorescence measurements may account for the number of absorbed photons used in electron excitation but not necessarily towards the rates of oxygen production/consumption or carbon assimilation, especially at high irradiances when alternative electron sinks are available (Beer et al., 1998). Therefore, either more than four electrons are processed during production of one mole of oxygen ($\tau<0.25$) or less than half of the photons are directed to PSII (i.e. $F_{II}<0.5$). Both of these outcomes highlight deviation from simple linear electron flow.

Following the linear assumption that 4 electrons produce 1 O_2 ($\tau=0.25$) resulted in overestimation of the PG_{ETR}. Since the molecular chemistry of water splitting at PSII is well-known, τ can only be reduced in an apparent sense. This apparent ratio can result from the excitation of four electrons (as detected with PAM) either without producing O_2 or consumption of O_2 in the chloroplast that would remain undetected by the gas exchange method. The former process will indicate cyclic electron flow around PSII, which was suggested to explain the higher electron flow than the O_2 production under continuous light in intact Chlorella cells (Prasil et al., 1996) but not studied in seagrasses yet. On the other hand, two possible pathways to explain a reduction in τ due to O_2 consumption are (i) the Mehler reaction and (ii) photorespiration. The Mehler reaction increases the pH gradient resulting in ATP buildup without NADPH production that is necessary for CO_2 assimilation (Demmig-Adams and Adams, 1992). Additionally, this pH gradient may induce NPQ (Demmig-Adams and Adams III, 1996; Kanazawa and Kramer, 2002). However, in this study NPQ induction did not happen until EQY values fell below 0.6 while O_2 yield continuously decreased. Therefore, the observed nonlinearity between quantum yield of fluorescence and quantum yield of oxygen most likely resulted from O_2 consumption via photorespiration, which probably represents the primary pathway to remove excess O_2 buildup

and use the ATP energy from light reactions for this purpose. NPQ is then triggered when ATP consumption by photorespiration is unable to lower the pH gradient forming across lumen at very high irradiances.

Other pathways that keep the electron flow continuous without contributing to CO_2 assimilation are cyclic electron flow and the malate valve. Besides preventing ROS formation and accumulation of reduced species, cyclic electron flow is important in triggering NPQ via generating a pH gradient (Munekage et al., 2004; Johnson, 2005). If cyclic electron flow plays an important role, then the assumption of half of the absorbed photons going to PSII (e.g. F_{ii}=0.5) would be inaccurate. Although PAM is easily applicable in field conditions and provide non-intrusive information about the photoprotection of eelgrass through NPQ, the fluorescence measurements with PAM do overestimate the $P_{g\text{-}ETR}$ and therefore are not equivalent to true carbon assimilation. Still, by quantifying the ratio of Φ_{PSII} to Φ_{O2} as a function of light and carbon availability, the alternative electron pathways can be accounted and corrected for in the estimation of photosynthesis in eelgrass.

In conclusion, photorespiration likely serves as an important clutch to protect the photochemical pathway in CO_2-limited eelgrass even though it has often been viewed as an inefficient residue of the evolution of Rubisco. Thus, the dual function of Rubisco maintains electron flow preventing the inhibitory damage to photosystems due to light saturation when carbon assimilation is limited by CO_2 supply, and prevents accumulation of reactive oxygen species. Photorespiration could be more beneficial than carbon concentrating mechanisms as it serves multiple purposes via connecting different metabolic pathways and allows instantaneous energy and reductant removal under fluctuating environmental conditions. Indeed, photorespiration might provide a carbon concentrating mechanism via recycling of photorespired CO_2 and removing excess intracellular O_2. Therefore, even though photosynthesis is mainly carbon limited, seagrasses might require high light to keep the

photosynthetic machinery running to produce ATP to support photorespiration. This becomes more important for permanently rooted marine plants in highly variable estuarine environments, where high water column productivity causes [O_2] to rise and [CO_2] to fall, as opposed to marine algae growing under more stable oceanic conditions and phytoplankton that can drift away vertically and horizontally. The metabolic pathway connectivity that results in more than one outcome and regulated by a variety of clues might have allowed survival of eelgrass under changing climate conditions even without exploitation of HCO_3^- via CCM.

CHAPTER IV

REGULATION OF PHOTOSYNTHETIC CONTROL IN EELGRASS IN RESPONSE TO CHANGING PHOTORESPIRATORY CONDITIONS DUE TO OCEAN ACIDIFICATION

Introduction

Understanding and quantifying the photosynthetic control in eelgrass, as a model organism for C3 aquatic vascular plants, is important to predict the impacts of climate change on coastal benthic primary productivity. Increasing CO_2 and temperature are fundamentally linked in their effects on photorespiration, enzyme systems and carbon assimilation (Koch et al., 2013). Increasing temperature, decreases the solubility of CO_2 more rapidly than that of O_2 in seawater, and stimulates the oxygenation reaction relative to carboxylation due to changes in enzymatic properties of Rubisco, therefore strongly favoring photorespiration over carbon fixation (Foyer et al., 2009). Chapters 2 and 3 focused on the acclimation of eelgrass (*Zostera marina* L.) to ocean carbonation (aka ocean acidification), quantified its positive impacts on the balance between photosynthesis, photorespiration and dark respiration, and identified the distinguishing functions of photosynthetic machinery under varying environmental conditions. Although the main function of the photosynthetic apparatus is to convert sunlight to cellular energy and sugar needed to drive metabolism and growth; it must also be capable of dissipating excess absorbed sunlight safely and participate in regulating the ratio of reductants required to satisfy various metabolic demands (Foyer et al., 2012).

These functions are regulated through photosynthetic electron transport (PET) control mechanisms that operate via linear, cyclic and pseudocyclic (a.k.a. Mehler) electron pathways, non-photochemical quenching (NPQ) and photorespiration. All electron flow pathways through the PET chain creates a pH gradient across the thylakoid membrane to generate the ATP.

Linear electron transport also generates the NADPH necessary to complete the C3 cycle in stroma. Even so, linear electron transport alone cannot meet the basic ratio of 3ATP/2NADPH that is required for CO_2 fixation (Osmond, 1981; Noctor and Foyer, 1998; Foyer et al., 2012). Photorespiration, under severe carbon limitation, increases this ratio even more. Therefore, cyclic electron flow and the Mehler pathway may become important to satisfy the increased ATP demand by generating a pH gradient but no additional NADPH. This pH gradient also plays an important role in the formation and modulation of NPQ (Kanazawa and Kramer, 2002; Makino et al., 2002). The flexibility to shift between the linear and cyclic electron transport, that share the same cellular machinery permits fine tuning of the chloroplast redox state in response to rapid changes in environment conditions. Such flexibility could allow seagrasses to tolerate large daily fluctuations in irradiance, $[CO_2]$ and $[O_2]$ in shallow coastal waters.

Although cyclic electron flow and the Mehler pathway can represent important photosynthetic control switches each one is considered to divert no more than 10% of the linear flux in C3 plants (Badger et al., 2000; Foyer et al., 2012). However, these estimates might increase under stress conditions induced by high irradiance or CO_2 limitation. Longstaff et al. (2002) estimated that these alternative electron transports might account for 40% of the electron transport in the marine macroalga *Ulva lactuca,* resulting in discrepancies between photosynthetic O_2 fluxes and PAM based electron transport rates (ETR) measured under light saturation. Thus, these photosynthetic control mechanisms have significant implications for estimating quantum requirements and assimilatory quotients (Tolbert, 1997; Foyer et al., 2009). For example, photorespiration significantly lowers the quantum efficiency estimates of higher plants using the C3 pathway, macroalgae and submersed angiosperms from the theoretical upper limit of 0.125 mol O_2 mol^{-1} photon to as low as 0.03 (Osmond, 1981; Frost-Christensen and Sand-Jensen, 1992). Burris (1981) explained the lowered photosynthetic quotient values

(O_2/CO_2) in marine algae with photorespiration based on the stoichiometry that predicts 3 O_2 are consumed per CO_2 evolved during a photorespiratory cycle.

Another indication of photorespiration in C3 plants is the higher CO_2 compensation point (~60 ppm), defined as, the CO_2 concentration of the medium at which the net photosynthesis becomes zero (i.e. no net CO_2 exchange at saturating irradiance) (Atwell et al., 1999). Plants that evolved mechanisms to reduce the photorespiration, such as C4 plants, are therefore able to sustain net photosynthesis even at low external [CO_2] (i.e. CO_2 compensation point ~5 ppm) (Raghavendra, 2000). Measuring the actual rate of photorespiration via net gas exchange (either O_2 or CO_2) often produces ambiguous results due to inter – and intracellular recycling of gases and the operation of different types of oxidative reactions simultaneously in the light, resulting in no net change of measured O_2 and CO_2 flux (Raghavendra, 2000). Relative to the Mehler reaction, which can represent as much as 30% of dark respiration, photorespiration can exceed dark respiration rates by as much as 8 times (Raghavendra, 2000). Despite the imprecision, under standard atmospheric conditions (400 ppm CO_2 and 21% O_2) the rate of photorespiration in C3 plants has been approximated to be one-fourth to one-third of the photosynthetic rate.

The photosynthetic control mechanisms described above not only regulate the short-term redox requirements but also coordinate the expression of genes encoding the proteins of photosystems (Foyer et al., 2012). When eelgrass leaves were incubated at high CO_2 (or under darkness), the increased acidity inside the cytoplasm changed the membrane potential impacting the proton pump (H^+-ATPase) and sodium exclusion mechanisms, which might facilitate the DIC uptake (Fernández et al., 1999). Therefore, H^+ fluxes and pH homeostasis of marine autotrophs may be affected by acidified seawater (Taylor et al., 2012).

With knowledge of the long term redox acclimation patterns in eelgrass to ocean acidification from the previous chapters, this study focused on the regulation of photosynthetic

control mechanisms in eelgrass leaves prior to and after acclimation to ocean acidification using multiple techniques simultaneously. These techniques differ in their principle and limitations of measuring photochemical pathways. Therefore, it was assumed that the discrepancy in the estimates of photosynthetic rates from different instruments provides quantitative information on the relative rates of photochemical and photoprotective pathways under a variety of CO_2:O_2 environmental scenarios. Understanding the impact of seawater chemistry on quantum requirements and assimilatory quotients in eelgrass are important to predict the carbon sequestration efficiency of seagrasses in a changing marine environment.

Materials and Methods

The experimental facility and sampling from pH treatments

The eelgrass leaves used in this study were grown in an outdoor climate change experimental facility at the Virginia Aquarium and Marine Science Center, Virginia Beach, VA. The details of experimental design and control of manipulations for this long term project on impacts of ocean acidification on eelgrass were described in Chapter 2 and by Zimmerman et al. (2016). To summarize briefly, vegetative shoots with intact roots and rhizomes were collected in May 2013 from the South Bay sub-tidal population in Eastern Shore, VA, USA and transplanted into 20 fiberglass open top aquaria. The aquaria were continuously enriched with CO_2 gas from June 2013 to October 2014 to attain treatment levels ranging from pH 6 to ambient (~pH 7.7), with 0.5 pH intervals between the treatments. For the purpose of this study, eelgrass plants from these pH treatments were used to measure the changes in photosynthetic response of leaves after one month and 15 months of acclimation to high CO_2 environment, during July 2013 and September - October 2014, respectively. Freshly collected 2nd youngest leaves from pH 6.0, pH 6.5 and ambient pH treatments were subjected to laboratory measurements of photochemistry under fully controlled incubation conditions described below.

Incubation measurements of leaf photochemistry

For the 2013 experiments, incubation measurements were performed in water-jacketed oxygen electrode chambers. The hole in the chamber cap was enlarged to permit the entry of a fiberoptic probe for simultaneous measurement of variable fluorescence using a Mini-PAM fluorometer (Walz) as outlined in Chapter 3. The 2014 experiments were performed using a custom designed water-jacketed incubation chamber, constructed from clear polycarbonate (Appendix Figure 33). In the new setup, photosynthesis and respiration rates were measured polarographically with a Clark type mini-oxygen electrode. In both experimental setups, variable fluorescence (a measure of EQY, NPQ and ETR), and seawater pH (a proxy for dissolved inorganic carbon (DIC) uptake), were monitored using Pulse Amplitude Modulated (PAM) fluorometer (Mini PAM, Walz, Germany) and a glass pH electrode/meter (Cole-Parmer), respectively. Turbulent flow was provided by a magnetic stirrer to prevent boundary layer limitation of gas exchange along the leaf surface. Continuous analog signals from the three sensors were recorded using a 20-bit data logger and LabView software (2009 edition, National Instruments). Voltage data were post processed into metabolic rates using linear regression tools in MATLAB R2014 (The MathWorks Inc.). O_2 and pH electrode drifts were measured without leaf tissue prior to each incubation experiment and subtracted from the rates measured with leaf tissue to determine net fluxes of O_2 and CO_2. Illumination was provided by a Kodak slide projector (ELH bulb) and its intensity was adjusted with neutral density filters. Incubation irradiances were calibrated daily against a scalar radiometer (QSL, Biospherical Instruments Inc.).

The light saturated photosynthetic response to varying O_2:DIC ratios was measured using leaves, grown at pH 6, pH 6.5 and ambient pH (~7.7). Using different leaves for each incubation condition allowed independent replications along the pH gradient for curve-fitting analysis. The pH and the oxygen concentration of the incubation water were adjusted by

bubbling CO_2 and/or an O_2 + N_2 mixtures into the chamber prior to the incubation. Incubation temperature (25°C simulating conditions in the aquaria at the time of the experiments, and 30°C inducing heat stress) was controlled by a circulating water bath connected to the water jacket of the chamber. Leaves were cleaned of epiphytes by gently scraping with a razor blade, and placed in a dark, temperature-stabilized chamber for 20 minutes prior to initiating the measurements. A three cm long piece of leaf tissue, cut ~1 cm above the meristem, was consecutively used during a 10 min dark (i.e. dark respiration) and a 10 min light measurement (i.e. net photosynthesis at 310 µmol photons m^{-2} s^{-1}) during the 2013 experiments. For the 2014 incubation experiments, segments from 2 different leaves, each 6.5 cm long and cut ~1 cm above their meristems, were incubated for 16 min under darkness (i.e. dark respiration) followed by a 16 min long measurement at saturated light (i.e. net photosynthesis at 460 µmol photons m^{-2} s^{-1}). After the incubations, pigment content and optical properties of the leaf tissues were measured and analyzed as described in Chapter 2.

The incubation water was collected in May 2013 and July 2014 from Owls Creek next to the aquarium facility. These stocks, [salinity= 25 (PSS)], were filtered through 0. 2 μm Nucleopore pore filter and refrigerated in dark bottles (~5° C) prior to use. After incubations, aliquots were taken from the chamber for alkalinity titrations using an automated potentiometric titrator (Metroohm). The changes in concentrations of DIC species were calculated using CO2SYS (Ver. 2.1; Lewis and Wallace 2012) from the difference of the pH of the seawater at the beginning and end of the incubations, while assuming constant temperature, salinity and alkalinity. The TCO_2 uptake rates were derived as the sum of loss of all three DIC species (CO_{2aq}, HCO_3^- and CO_3^{2-}) from the seawater. Although CO_3^{2-} is not directly utilized by leaves, changing pH due to photosynthesis in a closed system will shift the distribution of DIC species therefore redistributing CO_3^{2-} into CO_{2aq} and HCO_3^-.

Determination of photochemical rates

Net oxygen evolution and net DIC uptake rates were normalized to biomass, leaf area and total pigment content. The effect of incubation pH on light-saturated net photosynthesis was estimated using the following Gaussian models:

$$P_{net}=P_m*e^{\left(-0.5*\left[\frac{pH_{incub}-pH_m}{b}\right]^2\right)} \quad (16)$$

where P_m was the estimate of maximum P_{net} (i.e. light, flow and CO_2 saturated net photosynthesis) and pH_m was the pH corresponding to P_m. The value of b controls the width of the bell in pH units, permitting determination of the pH at which P_{net} is reduced to ~50% of P_m. During the analysis of 2014 samples, the pH_m and P_m parameters were constrained to the estimates from 2013 because these experiments covered a wider pH range to define the shape of the bell.

Net photosynthetic rates, combined from different incubations, were also analyzed as a function of initial [CO_2] of the incubation water. The CO_2 compensation point, i.e. the CO_2 concentration of the medium at which the net photosynthesis became zero, was determined by the following exponential rise model with an offset:

$$P_{net}=P_0+P*(1-e^{\left(-a*[CO_{2(aq)}]\right)}) \quad (17)$$

where P_0 was the estimate of P_{net} at [CO_2]=0 and $P_m = P + P_0$ at saturating [CO_2].

Net photosynthetic rates were converted to gross photosynthesis by adding dark respiration. Based on these gross photosynthetic and dark respiration estimates, the photosynthetic (PQ) and the respiratory quotients (RQ) for each sample were calculated by dividing the O_2 production/consumption rate by carbon uptake/release rate. Carbon fluxes were expressed in terms of either total carbon exchange (TCO_2) or only exchange of aqueous CO_2.

Photosynthetic light use efficiency was estimated through the quantum yield of oxygen (Φ_{O2}), calculated by dividing the gross oxygen evolution rate per leaf area by absorbed photons (PUR). PUR values were calculated using the spectral output of the lamp and spectral leaf absorptance as described in Chapter 3. The theoretical limit of Φ_{O2} within the light limited region of *P* vs E_{PAR} curves is 0.125 mol O_2/mol photon (=1/8), assuming all absorbed light energy is used to drive photochemistry via linear electron flow and 8 mol photons are required to produce 1 mol O_2. Within this study, Φ_{O2} was measured at saturated light levels while varying seawater pH to explain the deviation from a linear electron flow pathway depending on DIC availability in high light environment.

Variable fluorescence measurements were analyzed as described in Chapter 3 to estimate the quantum yield of PSII (Maximum Quantum Yield of fluorescence-MQY and Effective Quantum Yield of fluorescence-EQY) and Non-photochemical Quenching (NPQ) (Raghavendra, 2000; Baker, 2008). EQY were converted into estimates of Electron Transport Rate (ETR) based on the relationship as detailed in Chapter 3. The relationship of fluorescence parameters with incubation pH was estimated using the Gaussian model with a y-offset:

$$f=Q_0+Q_m*e^{\left(-0.5*\left[\frac{pH_{incub}-pH_m}{b}\right]^2\right)} \quad (18)$$

where Q_0 was the estimate of minimum EQY or maximum NPQ and pH_m was the pH corresponding to maximum EQY or minimum NPQ calculated from Q_0+Q_m.

Statistical analysis

Photosynthesis and fluorescence models were implemented by using the non-linear regression curve fitting tools in SigmaPlot (Systat Software Inc., Version 13.0). The effects of incubation water [O_2] and growth pH (i.e. conditions) across the incubation pH gradient (i.e. covariate) were analyzed by ANCOVA. When the normality assumptions failed, significances

among the conditions were determined by ANOVA on ranks, followed by multiple comparisons using Dunn's method. The relationships between O_2 and DIC fluxes were evaluated using Model I linear regression. Pigment content and leaf optical properties were compared among the conditions by ANOVA followed by multiple comparisons using the Tukey method.

Results

The wide pH range in 2013 experiments, manipulated via CO_2 enrichment, identified for the first time the limit of positive CO_2 impact on eelgrass photosynthesis (Figure 22). From pH 9 down to pH 5, the [CO_2] of the seawater increased exponentially from 1 to 25000 μmol L^{-1}, while [HCO_3^-] barely doubled from 1100 to 1900 μmol L^{-1} (Figure 22 A). In response to increasing [CO_2], light-saturated net oxygen production increased nonlinearly 8-fold to a maximum value of 80 μmol O_2 hr^{-1} mg^{-1} Chl when pH decreased from 8.1 to 6.1, while further decrease of pH reduced O_2 production (Figure 22 B). Net photosynthesis increased exponentially until [CO_2] and [O_2] were equivalent at pH 7. At pH 6, where net photosynthesis was maximal, [CO_2] and [HCO_3^-] were equivalent. Within the experimental range, the dark respiratory oxygen consumption was not affected by incubation pH and averaged around 7.2 μmol O_2 hr^{-1} mg^{-1} Chl (Table 11). Neither the rate of change nor the pH optima of net photosynthesis were affected by the growth environment (pH 6 vs. ambient, Table 12 and Figure 22 B). Reducing [O_2] of the incubation water to half of air saturation (i.e. 122 μM O_2) did not change the observed relationship between net photosynthesis and pH, although the pH optimum decreased from pH 6.2 to pH 5.9 (Figure 22 B, Table 12). The overall response of dissolved inorganic carbon (TCO_2) uptake to seawater pH was consistent with the net O_2 production trend (Figure 22 C), except that maximum TCO_2 uptake rates at optimum pH were higher than the corresponding O_2 production rates (Table 12, coefficient P_m). The Gaussian model also predicted the optimum pH for the maximum TCO_2 uptake to be 0.3 pH units higher than the optimum pH of maximum O_2

production (coefficient pH_m). However, estimation of TCO_2 uptake from ΔpH was only accurate within the pH range of 6 to 9. At lower pH the absolute [TCO_2] was 500 fold higher than the maximum uptake rates observed at optimum pH, swamping the metabolically-derived signal. Therefore, photosynthetic carbon uptake rates for pH incubations below 6.0 were excluded from further analysis.

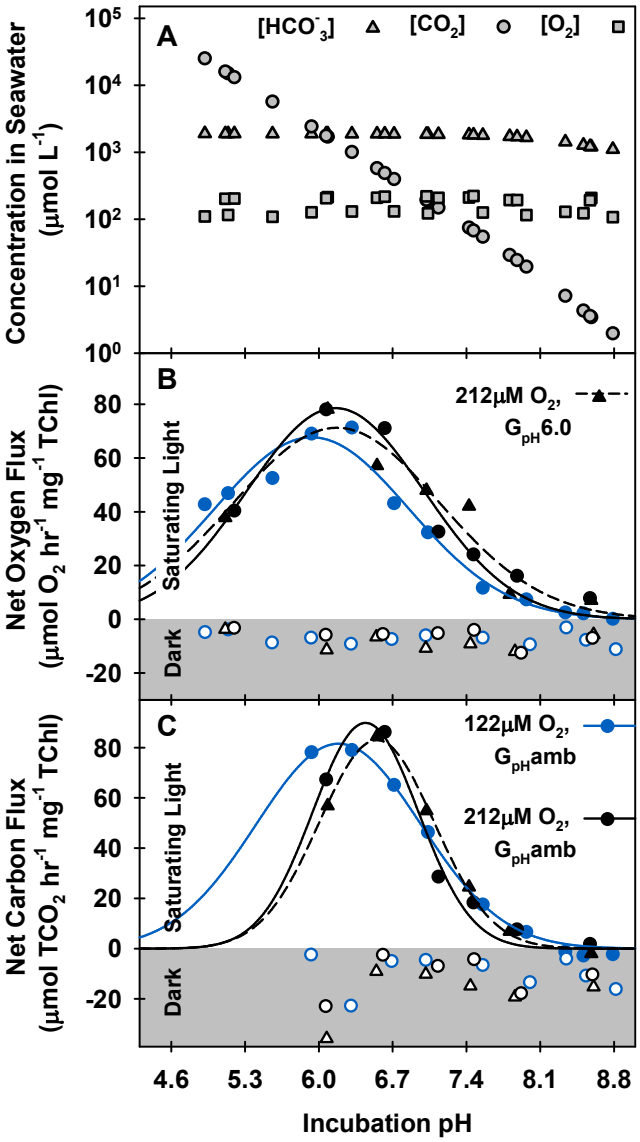

Figure 22. (A) The absolute concentrations of O_2 and dissolved inorganic carbon species (CO_2 and HCO^-_3) in the incubation seawater. All incubations were performed at 25°C. (B) Net O_2 flux and (C) Net Carbon flux of eelgrass leaves as a function of incubation pH. Plots (B) and (C): Filled symbols indicate measurements at saturating light levels (310 µmol photons m^{-2} s^{-1}) and open symbols represent the corresponding dark respiration rates. Light-saturated rates were fit to the Gaussian function (Eq.16). Different initial O_2 levels are indicated by color, where 212µM is equivalent to air saturation. Symbols represent plants grown at different pH treatments (G_{pH}).

Table 11. Dark respiration (DR) rates measured with O_2 evolution method. Rates were normalized both to Fresh Weight (FW) and Pigment content. Effects of incubation pH on DR rates among different oxygen categories were analyzed by ANCOVA.

2013 incubations		Dark Respiration (μmol O_2 hr^{-1} mg^{-1} Chl)	Dark Respiration (μmol O_2 hr^{-1} g^{-1} FW)
Conditions	n	Mean ± SEM	Mean ± SEM
122μM O_2 G_{pH}amb	12	7.09 ± 0.69	8.26 ± 1.04
212μM O_2 G_{pH}6.0	7	8.49 ± 1.20	5.95 ± 1.05
212μM O_2 G_{pH}amb	7	6.19 ± 1.15	5.62 ± 0.82

2014 incubations		Dark Respiration (μmol O_2 hr^{-1} mg^{-1} Chl)	Dark Respiration (μmol O_2 hr^{-1} g^{-1} FW)
Conditions	n	Mean ± SEM	Mean ± SEM
122μM O_2 G_{pH}6.5 25°C	9	12.96 ± 1.09	14.64 ± 1.26
212μM O_2 G_{pH}6.5 25°C	9	7.51 ± 0.95	8.38 ± 1.02
212μM O_2 G_{pH}6.5 30°C	6	10.3 ± 2.62	11.29 ± 2.81
76μM O_2 G_{pH}6.5 25°C	6	12.41 ± 1.34	13.39 ± 1.84

ANCOVA for the Equal Slopes Model: Pigment normalized

Source of Variation	df	SS	MS	F	*P*
Conditions	2	19.43	9.71	1.40	0.268
Incubation pH	1	25.10	25.10	3.61	0.071
Residual	22	152.87	6.95	--	--
Total	25	196.92	7.88	--	--

ANCOVA for the Equal Slopes Model: Pigment normalized

Source of Variation	df	SS	MS	F	*P*
Conditions	3	185.70	61.90	4.85	0.009
Incubation pH	1	91.42	91.42	7.16	0.013
Residual	25	319.20	12.77	--	--
Total	29	566.59	19.54	--	--

Table 11. *continued*

ANCOVA for the Equal Slopes Model: Biomass normalized						ANCOVA for the Equal Slopes Model: Biomass normalized					
Source of Variation	df	SS	MS	F	*P*	Source of Variation	df	SS	MS	F	*P*
Conditions	2	42.53	21.27	2.71	0.089	Conditions	3	217.82	72.61	3.96	0.019
Incubation pH	1	43.33	43.33	5.51	0.028	Incubation pH	1	67.29	67.29	3.67	0.067
Residual	22	172.94	7.86	--	--	Residual	25	458.95	18.36	--	--
Total	25	256.11	10.24	--	--	Total	29	720.47	24.84	--	--

Table 12. Results of non-linear regression analysis for pigment specific photosynthesis as a function of incubation pH measured in 2013 at different oxygen concentrations.

2013 incubations	Gaussian fit: $P_{net} = P_m*exp(-0.5*([pH_{incub} -pH_m] / b)^2)$						Analysis of Variance (Corrected for the mean of the observations)					
		Coefficient		SE	t	*P*	r^2		df	SS	MS	F	*P*
Pnet (µmol O_2 hr^{-1} mg^{-1} TChl)	122µM O_2 G_{pH}amb	P_m	67.71	3.22	21.0	<0.0001	0.97	Regression	2	7358.1	3679.0	136.3	<0.0001
		b	0.92	0.06	14.8	<0.0001		Residual	9	242.9	27.0		
		pH_m	5.93	0.05	112.0	<0.0001		Total	11	7600.9	691.0		
	212µM O_2 G_{pH}amb	P_m	78.59	5.04	15.6	<0.0001	0.96	Regression	2	4160.8	2080.4	53.5	0.0013
		b	0.84	0.06	12.98	0.0002		Residual	4	155.5	38.9		
		pH_m	6.16	0.07	93.2	<0.0001		Total	6	4316.3	719.4		
	212µM O_2 G_{pH}6.0	P_m	71.28	6.70	10.7	0.0004	0.91	Regression	2	3529.0	1764.5	21.4	0.0073
		b	0.98	0.12	7.99	0.0013		Residual	4	329.8	82.5		
		pH_m	6.17	0.12	51.3	<0.0001		Total	6	3858.8	643.1		

Table 12. *continued*

		Coefficient		SE	t	*P*	r^2		df	SS	MS	F	*P*
Pnet (μmol TCO_2 hr^{-1} mg^{-1} TChl)	122μM O_2 G_{pH}amb	P_m	81.55	1.66	49.3	<0.0001	0.997	Regression	2	9945.7	4972.9	858.8	<0.0001
		b	0.78	0.04	19.5	<0.0001		Residual	6	34.7	5.8		
		pH_m	6.19	0.04	143.6	<0.0001		Total	8	9980.5	1247.6		
	212μM O_2 G_{pH}amb	P_m	89.84	6.74	13.3	0.0009	0.98	Regression	2	5695.3	2847.6	63.6	0.0035
		b	0.50	0.05	9.9	0.0022		Residual	3	134.3	44.8		
		pH_m	6.44	0.05	140.2	<0.0001		Total	5	5829.6	1165.9		
	212μM O_2 G_{pH}6.0	P_m	82.97	2.04	40.7	<0.0001	0.997	Regression	2	5533.7	2766.9	527.1	0.0002
		b	0.55	0.02	28.8	<0.0001		Residual	3	15.7	5.2		
		pH_m	6.55	0.02	384.7	<0.0001		Total	5	5549.5	1109.9		

Maximum quantum yields of fluorescence (MQY), measured during dark respiration after acclimating to the pH range of the incubation experiments, were close to 0.8 indicating that the leaves were not stressed by the pH and O_2 manipulations (Figure 23 A). However, compared to oxygen flux measurements under saturating irradiance, the variable fluorescence method underestimated the photosynthetic response of eelgrass leaves to CO_2 enrichment (Figure 23 A). The effective quantum yield of fluorescence (EQY) measured during photosynthesis at saturating light levels increased only 2-fold from 0.3 up to 0.6 when seawater pH decreased from 8.8 to 6.1. Similar to net O_2 production and net TCO_2 uptake measurements, decreasing pH below 6.0 reduced the EQY. The mirror-image pattern exhibited by non-photochemical quenching (NPQ) with respect to pH suggests a reduction in the photoprotective utilization of xanthophyll cycle when photosynthesis was maximally released from CO_2 limitation at pH 6.0 (Figure 23 B). Contrary to the EQY, NPQ changed more drastically within the same pH range. NPQ increased 6-fold up to 1.8 when photosynthesis diminished at higher pH values. At pH 6.0, where net photosynthesis and EQY were maximum and NPQ was minimum (Table 13), dissolved aqueous CO_2 accounted for 50% of the TCO_2 in the seawater. At pH 8, however, the dissolved CO_2 was reduced to 1% of the TCO_2 (Figure 23 C). Therefore, the exponential increase in CO_2 between pH 6 and 9 increased the CO_2:O_2 molar ratio from 0.01 up to 10, corresponding to the drastic increase in net photosynthesis, likely due to increased carboxylation and reduced oxygenation reactions of Rubisco. On the other hand, due to contribution of HCO_3^-, the TCO_2:O_2 molar ratios between pH 6 and 9 were constant at 10 for air-saturated incubations and at 20 for reduced oxygen incubations. The constant molar ratio revealed a DIC pool composed of 99% HCO_3^- could not sustain the physiologically available photosynthetic capacity of eelgrass leaves.

Leaf incubation experiments were repeated in 2014 only with plants grown in the optimum CO_2 treatment (i.e. in pH 6.5 tanks), because 2013 results suggested no difference in

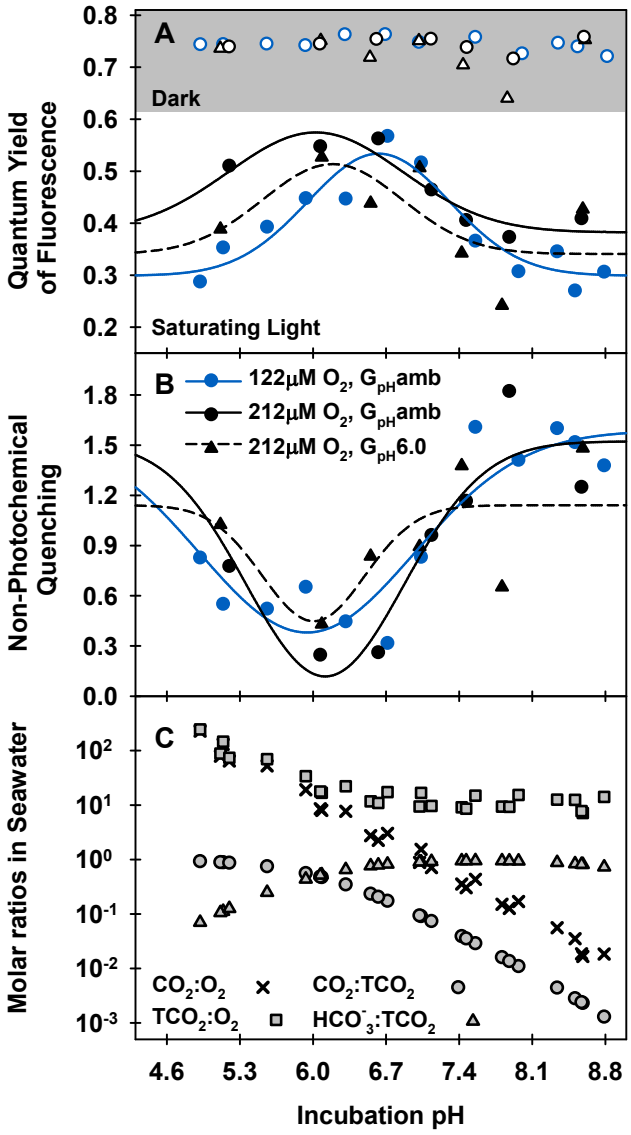

Figure 23. Fluorescence parameters of eelgrass leaves as a function of incubation pH. (A) Open symbols represent the maximum quantum yield of fluorescence (MQY) measured in darkness, while filled symbols represent the effective quantum yield of fluorescence (EQY) at saturating light levels. (B) Non-photochemical quenching (NPQ). Both EQY and NPQ were fit to the Gaussian function (Eq.18). (C) The relative importance of O_2 and DIC in the incubation seawater presented by molar ratios.

Table 13. Results of non-linear regression analysis for fluorescence parameters as a function of incubation pH measured in 2013 at different oxygen concentrations.

2013 incubations		Gaussian fit: $f = Q_0+Q_m*\exp(-0.5*([pH_{incub} -pH_m] / b)^2)$						Analysis of Variance (Corrected for the mean of the observations)					
		Coefficient		SE	t	*P*	r^2		df	SS	MS	F	*P*
EQY	122µM O_2 G_{pH}amb	Q_m	0.23	0.03	7.52	<0.0001	0.88	Regression	3	0.085	0.028	19.13	0.0005
		b	0.68	0.14	4.95	0.0011		Residual	8	0.012	0.002		
		pH_m	6.63	0.09	71.33	<0.0001		Total	11	0.096	0.009		
		Q_0	0.30	0.02	12.30	<0.0001							
	212µM O_2 G_{pH}amb	Q_m	0.19	0.04	4.97	0.0157	0.90	Regression	3	0.030	0.010	8.60	0.0553
		b	0.83	0.22	3.76	0.0328		Residual	3	0.004	0.001		
		pH_m	6.03	0.15	39.63	<0.0001		Total	6	0.033	0.006		
		Q_0	0.38	0.03	11.75	0.0013							
	212µM O_2 G_{pH}6.0	Q_m	0.17	0.11	1.57	0.2146	0.47	Regression	3	0.027	0.009	0.89	0.5354
		b	0.67	0.55	1.22	0.3109		Residual	3	0.030	0.010		
		pH_m	6.19	0.45	13.66	0.0008		Total	6	0.057	0.010		
		Q_0	0.34	0.09	4.00	0.028							

Table13. *continued*

		Coefficient		SE	t	*P*	r^2		df	SS	MS	F	*P*
NPQ	122μM O_2 G_{pH}amb	Q_m	-1.21	0.20	-6.15	0.0003	0.85	Regression	3	2.270	0.757	14.55	0.0013
		b	1.03	0.27	3.85	0.0049		Residual	8	0.416	0.052		
		pH_m	5.94	0.15	40.28	<0.0001		Total	11	2.686	0.244		
		Q_0	1.59	0.19	8.48	<0.0001							
	212μM O_2 G_{pH}amb	Q_m	-1.40	0.34	-4.17	0.0252	0.86	Regression	3	1.625	0.542	6.01	0.0875
		b	0.76	0.23	3.36	0.0437		Residual	3	0.271	0.090		
		pH_m	6.12	0.17	36.49	<0.0001		Total	6	1.896	0.316		
		Q_0	1.52	0.27	5.66	0.0109							
	212μM O_2 G_{pH}6.0	Q_m	-0.69	0.46	-1.50	0.2308	0.47	Regression	3	0.398	0.133	0.89	0.5382
		b	0.49	0.37	1.32	0.2797		Residual	3	0.448	0.149		
		pH_m	6.01	0.43	13.92	0.0008		Total	6	0.846	0.141		
		Q_0	1.14	0.23	4.92	0.0161							

photosynthetic control among the plants grown at different pH treatments. Leaves from the optimum treatment, grown for 15 months in a high CO_2 environment under natural light and temperature fluctuations, represented approximately the 6th leaf generation acclimated to ocean acidification (based on growth rates in Zimmerman et. al 2016). The 2014 experiments focused on the combined effect of oxygen and inorganic carbon concentrations on the role of photorespiration by measuring the light saturated photosynthesis more frequently at higher pH values and wider range of [O_2] to provide more levels of seawater CO_2:O_2 (Figure 24 A). Even though [HCO_3^-] decreased dramatically above pH 7.9, it exceeded [O_2] more than 7 fold at all pH levels whereas [CO_2] exceeded only below pH 7.0. Both net oxygen production and net TCO_2 uptake rates per total chlorophyll increased 8 to 9-fold between pH 8.1 and 6.5 (Figure 24 B and C), similar to the rates observed in 2013 experiments. Biomass specific dark respiration rates were constant as a function of incubation pH, but differed significantly among the O_2 and temperature incubation conditions (Table 11). Both pigment and biomass normalized dark respiration rates of high CO_2 acclimated plants increased with increasing temperature and decreasing O_2 concentration of the incubation seawater. The Gaussian model fits predicted no difference in net photosynthetic flux among the different incubation conditions (Table 14).

The MQY of dark adapted leaves at all incubation conditions were close to 0.8, indicating no physiological stress to the photosynthetic apparatus, and consistent with the 2013 experiments (Figure 25 A). The change of EQY as a function of seawater pH was again less than the change in net photosynthesis measured with O_2 and TCO_2 methods. Overall, EQY increased from 0.1 up to 0.4 as pH decreased from 8.5 to 6.5, while NPQ decreased from 2.5 to 1 (Figure 25 B, Table 15). Similar to 2013 incubations, the main changes of seawater chemistry, driving the changes in net photosynthesis and fluorescence parameters, were observed in CO_2:O_2 and CO_2:TCO_2 molar ratios (Figure 25 C).

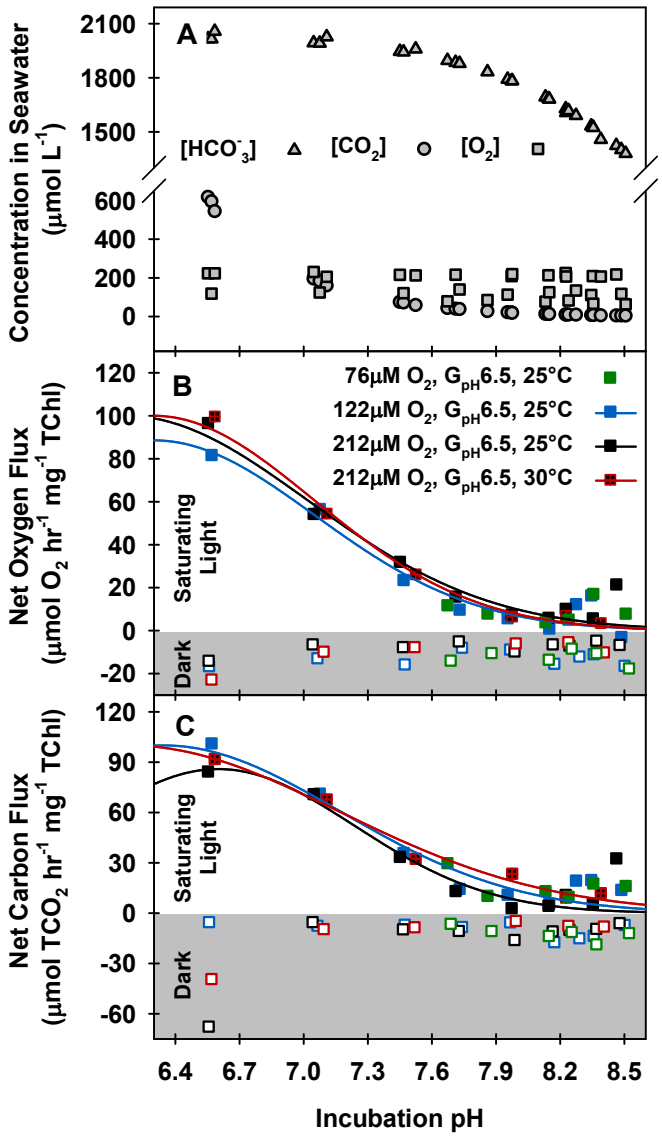

Figure 24. (A) The absolute concentrations of O_2 and dissolved inorganic carbon species (CO_2 and HCO^-_3) in the incubation seawater. (B) Net O_2 flux and (C) Net Carbon flux of eelgrass leaves as a function of incubation pH. Both plots: Filled symbols indicate measurements at saturating light levels (460 µmol photons m^{-2} s^{-1}) and open symbols represent the corresponding dark respiration rates. Light-saturated rates were fit to the Gaussian function (Eq.16). Different initial O_2 levels are indicated by color, where 212µM is equivalent to air saturation. All leaves were collected from plants grown at pH 6.5 treatments ($G_{pH}6.5$).

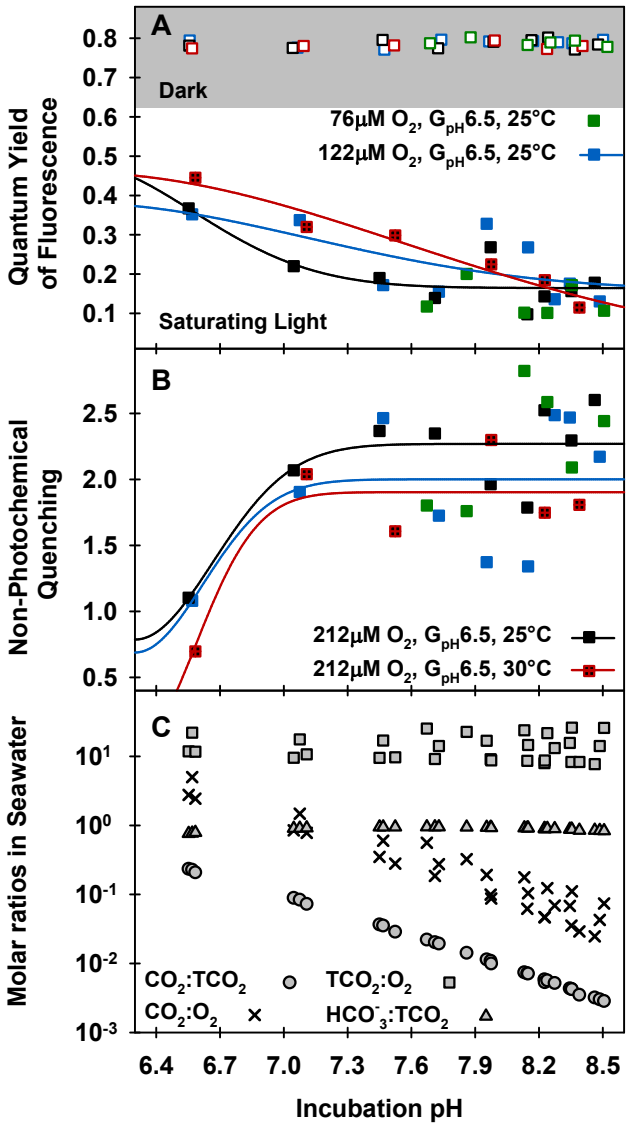

Figure 25. Fluorescence parameters of eelgrass leaves as a function of incubation pH. (A) Open symbols represent the maximal quantum yield of fluorescence (MQY) measured in darkness, while filled symbols represent the effective quantum yield of fluorescence (EQY) at saturating light levels. (B) Non-photochemical quenching (NPQ). Both EQY and NPQ were fit to the Gaussian function (Eq.18). (C) The relative importance of O_2 and DIC in the incubation seawater presented by molar ratios.

Table 14. Results of non-linear regression analysis for pigment specific photosynthesis as a function of incubation pH measured in 2014 at different oxygen concentrations.

2014 incubations		Gaussian fit: $P_{net} = P_m * \exp(-0.5 * ([pH_{incub} - pH_m] / b)^2)$					Analysis of Variance (Corrected for the mean of the observations)					
		Coefficient		SE	t	*P*	r^2		df	SS	MS	F	*P*
Pnet (µmol O_2 hr^{-1} mg^{-1} TChl)	122µM O_2 G_{pH}6.5 25°C	P_m	88.57	21.70	4.1	0.0065	0.94	Regression	2	5992.6	2996.3	47.4	0.0002
		b	-0.75	0.24	-3.1	0.0210		Residual	6	378.9	63.2		
		pH_m	6.30	0.48	13.0	<0.0001		Total	8	6371.5	796.4		
	212µM O_2 G_{pH}6.5 25°C	P_m	100.00	31.44	3.2	0.019	0.94	Regression	2	6866.4	3433.2	44.4	0.0003
		b	-0.85	0.28	-3.0	0.0241		Residual	6	463.8	77.3		
		pH_m	6.17	0.61	10.0	<0.0001		Total	8	7330.2	916.3		
	212µM O_2 G_{pH}6.5 30°C	P_m	100.00	14.35	7.0	0.0061	0.99	Regression	2	7139.1	3569.6	173.8	0.0008
		b	-0.75	0.15	-4.9	0.0161		Residual	3	61.6	20.5		
		pH_m	6.30	0.29	21.6	0.0002		Total	5	7200.7	1440.1		

Table 14. *continued*

		Coefficient		SE	t	*P*	r^2		df	SS	MS	F	*P*
Pnet (μmol TCO_2 hr^{-1} mg^{-1} TChl)	122μM O_2 G_{pH}6.5 25°C	P_m	100.00	21.16	4.7	0.0032	0.93	Regression	2	7781.3	3890.6	35.2	0.0005
		b	-0.83	0.25	-3.3	0.0169		Residual	6	662.6	110.4		
		pH_m	6.34	0.48	13.1	<0.0001		Total	8	8443.9	1055.5		
	212μM O_2 G_{pH}6.5 25°C	P_m	85.89	12.36	7.0	0.0004	0.84	Regression	2	6155.8	3077.9	16.2	0.0038
		b	-0.64	0.22	-3.0	0.0252		Residual	6	1138.8	189.8		
		pH_m	6.60	0.31	21.3	<0.0001		Total	8	7294.6	911.8		
	212μM O_2 G_{pH}6.5 30°C	P_m	100.00	19.21	5.2	0.0138	0.98	Regression	2	5425.4	2712.7	79.5	0.0025
		b	0.99	0.23	4.3	0.0232		Residual	3	102.4	34.1		
		pH_m	6.18	0.46	13.4	0.0009		Total	5	5527.8	1105.6		

Table 15. Results of non-linear regression analysis for fluorescence parameters as a function of incubation pH measured in 2014 at different oxygen concentrations.

2014 incubations		Gaussian fit: $f = Q_0+Q_m*\exp(-0.5*([pH_{incub} -pH_m] / b)^2)$					Analysis of Variance (Corrected for the mean of the observations)					
		Coefficient		SE	t	*P*	r^2		df	SS	MS	F	*P*
EQY	122µM O_2 $G_{pH}6.5$ 25°C	Q_m	0.23	0.83	0.3	0.80	0.44	Regression	3	0.030	0.010	1.3	0.36
		b	-1.11	5.03	-0.2	0.83		Residual	5	0.038	0.008		
		pH_m	6.00	7.63	0.8	0.47		Total	8	0.068	0.009		
		Q_0	0.16	0.26	0.6	0.57							
	212µM O_2 $G_{pH}6.5$ 25°C	Q_m	0.32	2.56	0.13	0.91	0.69	Regression	3	0.036	0.012	3.6	0.10
		b	-0.57	2.47	-0.23	0.83		Residual	5	0.017	0.003		
		pH_m	6.00	7.05	0.85	0.43		Total	8	0.053	0.007		
		Q_0	0.16	0.03	5.81	0.00							
	212µM O_2 $G_{pH}6.5$ 30°C	Q_m	0.46	1.00	0.46	0.69	0.95	Regression	3	0.064	0.021	12.9	0.07
		b	1.57	4.08	0.38	0.74		Residual	2	0.003	0.002		
		pH_m	6.00	3.29	1.82	0.21		Total	5	0.067	0.014		
		Q_0	0.00	0.76	0.00	1.00							

Table 15. *continued*

		Coefficient		SE	t	*P*	r^2		df	SS	MS	F	*P*
NPQ	122μM O_2 G_{pH}6.5 25°C	Q_m	-1.31	285.4	0.00	1.00	0.32	Regression	3	0.746	0.249	0.77	0.56
		b	-0.32	34.2	-0.01	0.99		Residual	5	1.609	0.322		
		pH_m	6.30	111.4	0.06	0.96		Total	8	2.355	0.294		
		Q_0	2.00	0.2	8.52	0.00							
	212μM O_2 G_{pH}6.5 25°C	Q_m	-1.48	26.10	-0.06	0.96	0.70	Regression	3	1.191	0.397	3.82	0.09
		b	-0.37	4.54	-0.08	0.94		Residual	5	0.520	0.104		
		pH_m	6.30	12.41	0.51	0.63		Total	8	1.712	0.214		
		Q_0	2.27	0.14	16.70	<0.0001							
	212μM O_2 G_{pH}6.5 30°C	Q_m	-1.90	2441	0.00	0.999	0.80	Regression	3	1.196	0.399	2.58	0.29
		b	-0.29	131.7	0.00	0.999		Residual	2	0.309	0.155		
		pH_m	6.30	501.2	0.01	0.991		Total	5	1.505	0.301		
		Q_0	1.90	0.2	8.39	0.014							

All measurements from both years with incubation pH above 5.9 (n=51) were combined to estimate the CO_2 compensation point of eelgrass leaves where net photosynthesis stopped (Figure 26). At high [CO_2], both CO_2 uptake and O_2 evolution models produced a maximum rate of net photosynthesis of 80±4 μmol hr^{-1} mg^{-1} Chl, with half saturation constants ($K_{s(CO2)}$) of 150±12 and 130±14 μmol L^{-1} CO_2, respectively. The exponential rise models with y-offset predicted the net oxygen production to be still positive (ca. 8 μmol O_2 hr^{-1} mg^{-1} Chl, Figure 26 A) while net CO_2 uptake stopped when [CO_2] reached 13 μmol L^{-1} (Figure 26 B). This suggested the contribution of other DIC species to sustain the net positive oxygen evolution at low [CO_2] since the CO_2 uptake model relied only on the changes of aqueous CO_2 concentrations during the incubation. Yet the uptake rate of HCO_3^-, which relied only on the changes of HCO_3^- concentrations during the incubation (Figure 26 C), exceeded the O_2 evolution rates highlighting the dynamic chemical equilibrium between the three DIC species in the seawater during photosynthesis. Therefore, the true net carbon uptake rates, estimated with pH electrode method, needed to be based on the changes in total DIC (i.e. TCO_2) rather than individual DIC species. The relative effects of [O_2] and [CO_2] in the seawater (Figure 27) further explained the reason for the saturation of photosynthesis once [CO_2] reached 200 μmol L^{-1} (Figure 26). At saturating light levels, when oxygenation/carboxylation reactions of Rubisco became the rate-limiting process, the gross photosynthesis increased linearly until the molar ratio of CO_2:O_2 in the seawater became 0.7 and 0.8, for oxygen production and for TCO_2 uptake, respectively (Figure 27 A and B). After this threshold, which occurred at pH 7.1, CO_{2aq} was not a limiting factor and gross photosynthesis reached its maximum when [CO_2] was twice as high as [O_2] (i.e. pH 6.5). On the other hand, incubation water chemistry could not explain the variability in electron transport rates (ETR) estimated from EQY measurements of fluorescence method (Figure 27 C).

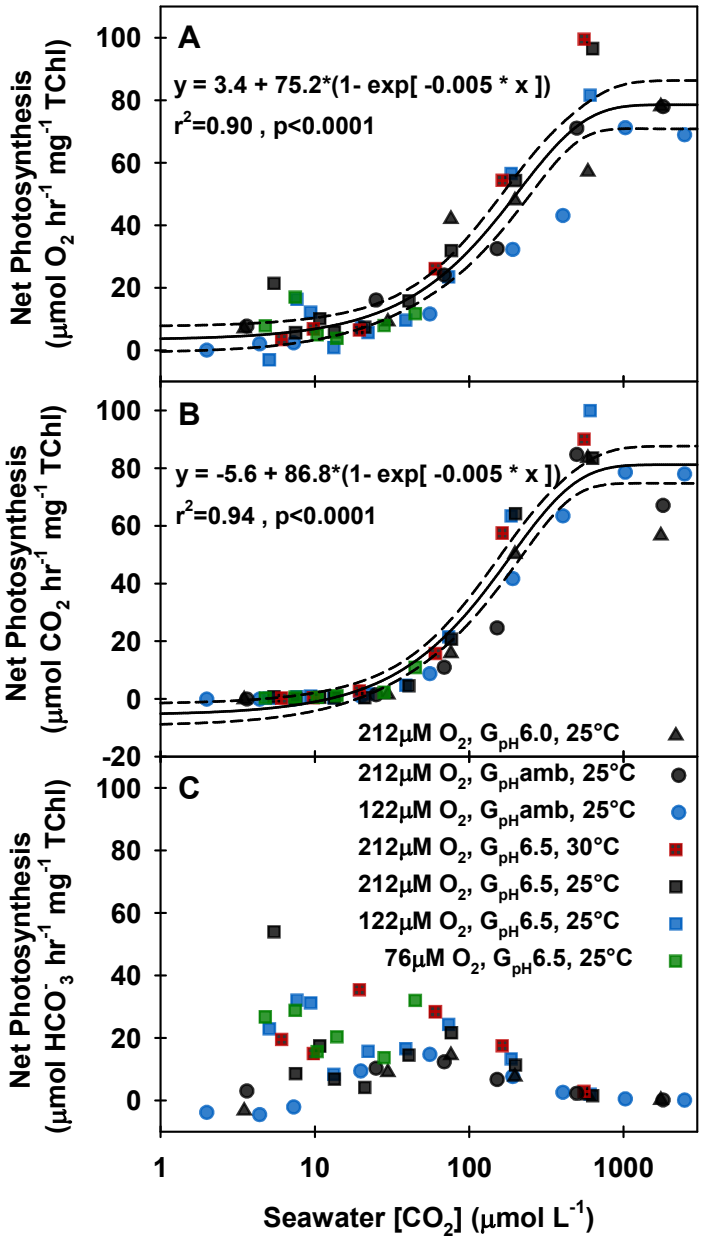

Figure 26. Net photosynthesis of eelgrass leaves as a function of aqueous [CO_2]. (A) Net O_2 flux of all samples were fit to a common exponential rise function (Eq.17). (B) Net Carbon flux derived from changes in $[CO_2]_{aq}$ only. CO_2 compensation point of eelgrass leaves was calculated from the exponential rise function. (C) Net Carbon flux derived from changes in [HCO_3^-] only.

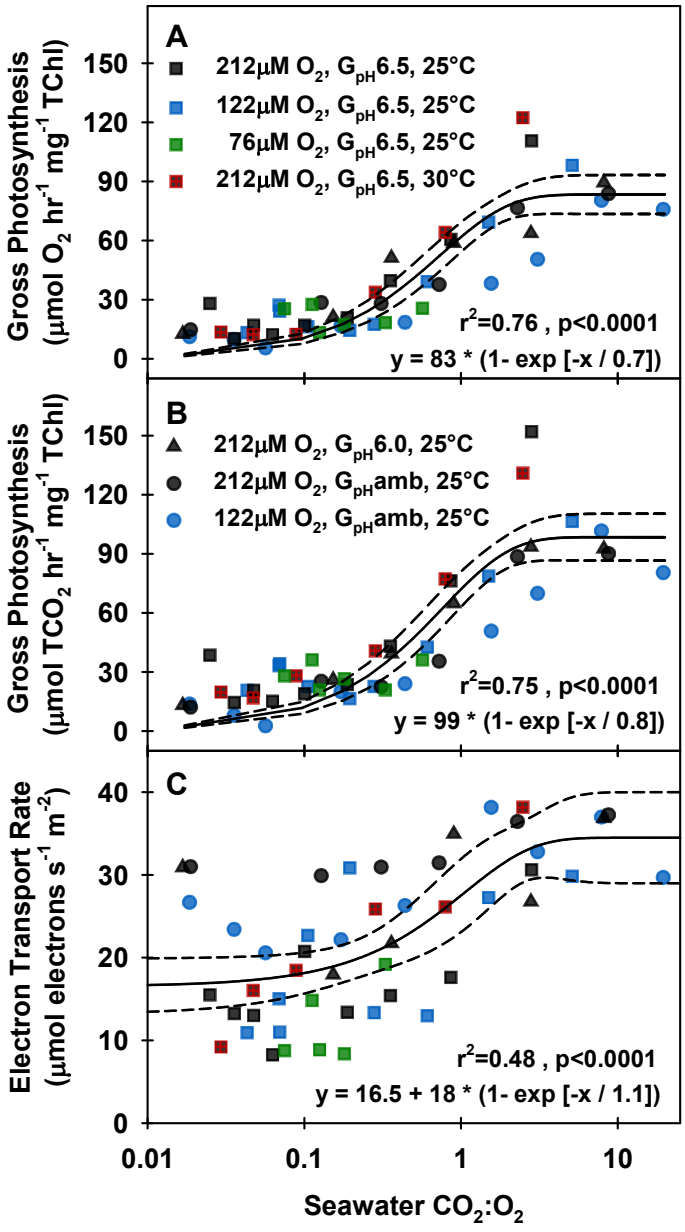

Figure 27. Gross photosynthesis of eelgrass leaves as a function of CO_2 to O_2 ratio in seawater. Net O_2 flux (A) and net total Carbon flux (B) were fit to exponential rise model. (C) Electron Transfer Rates (ETR) were derived from EQY

The linear relationship between the O_2 and CO_2 based measures of gross photosynthesis were used to estimate the photosynthetic quotient (PQ) of eelgrass leaves (Figure 28). When all samples were analyzed collectively regardless of their growth and incubation conditions, the PQs were 0.70±0.03 and 0.84±0.03, based on regression between O_2 versus CO_2 and O_2 versus TCO_2, respectively. While the O_2 vs CO_2 regression predicted an offset value of 16 μmol O_2 hr^{-1} mg^{-1} Chl though no CO_2 uptake, regression between O_2 and TCO_2 passed through the origin. These PQ values were lower than the theoretical value of 1 for ideal equilibrium between light and dark reactions of photosynthesis.

PQs derived from individual samples revealed effects of their growth conditions (Figure 29). PQ relying on the ratio of gross O_2 production to TCO_2 uptake showed no significant dependence on incubation pH but was consistently higher in plants grown at ambient CO_2 treatments (Figure 29 A, Table 16). Contrary to PQ, RQ relying on the ratio of gross O_2 consumption to TCO_2 release was significantly affected by incubation pH (Figure 29 B). In particular, the decreasing oxygen concentration in the incubation seawater significantly increased the RQ for the plants grown at high CO_2 treatment (pH 6.5) (Table 16). Analysis of PQ relying only on the aqueous CO_2 uptake permitted differentiation of the relative contribution of CO_2 and HCO_3^- to the photosynthetic demands as a function of seawater pH (Figure 29 C). At neutral pH (pH 7), when [CO_2] and [O_2] in the seawater were equivalent, the RQ approached the theoretical value of 1 (Figure 29 B and D). The strong pH dependency of the respiratory quotients showed the importance of seawater carbonate chemistry in buffering the respiratory release of CO_2.

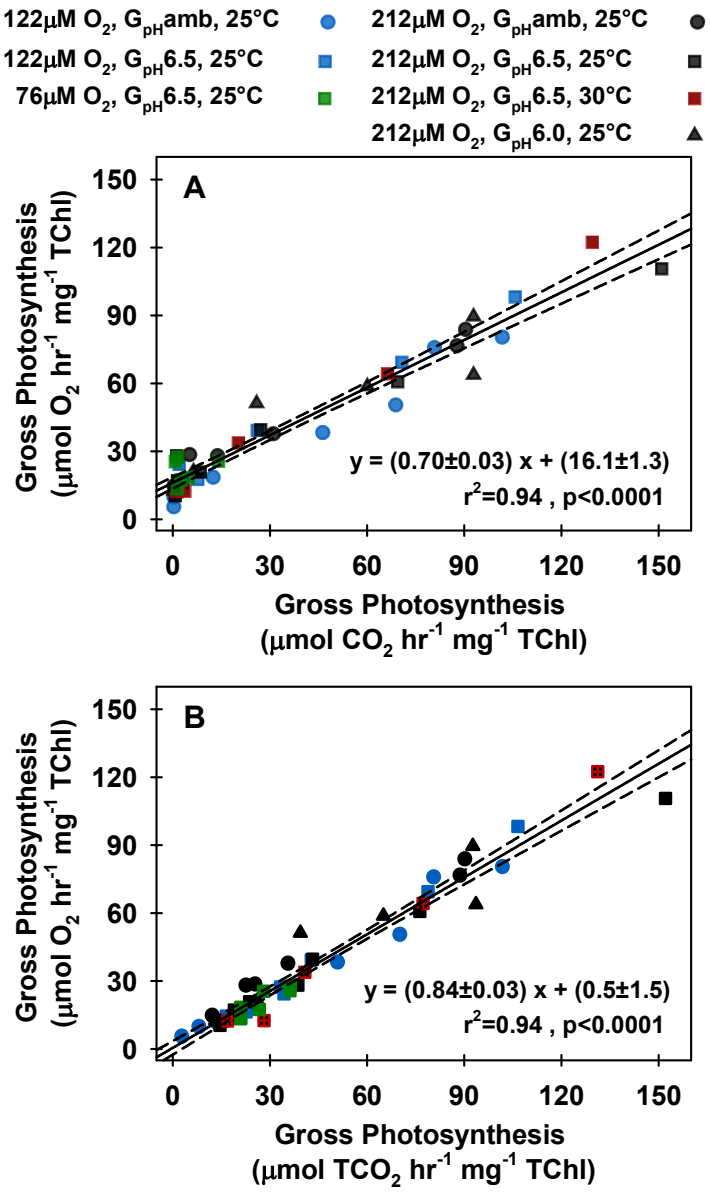

Figure 28. Relationship between oxygen production and carbon uptake supported by aqueous CO_2 only (A) and supported by total inorganic carbon pool (B). The solid line represents the linear relationship, while dashed lines are the 95% confidence intervals.

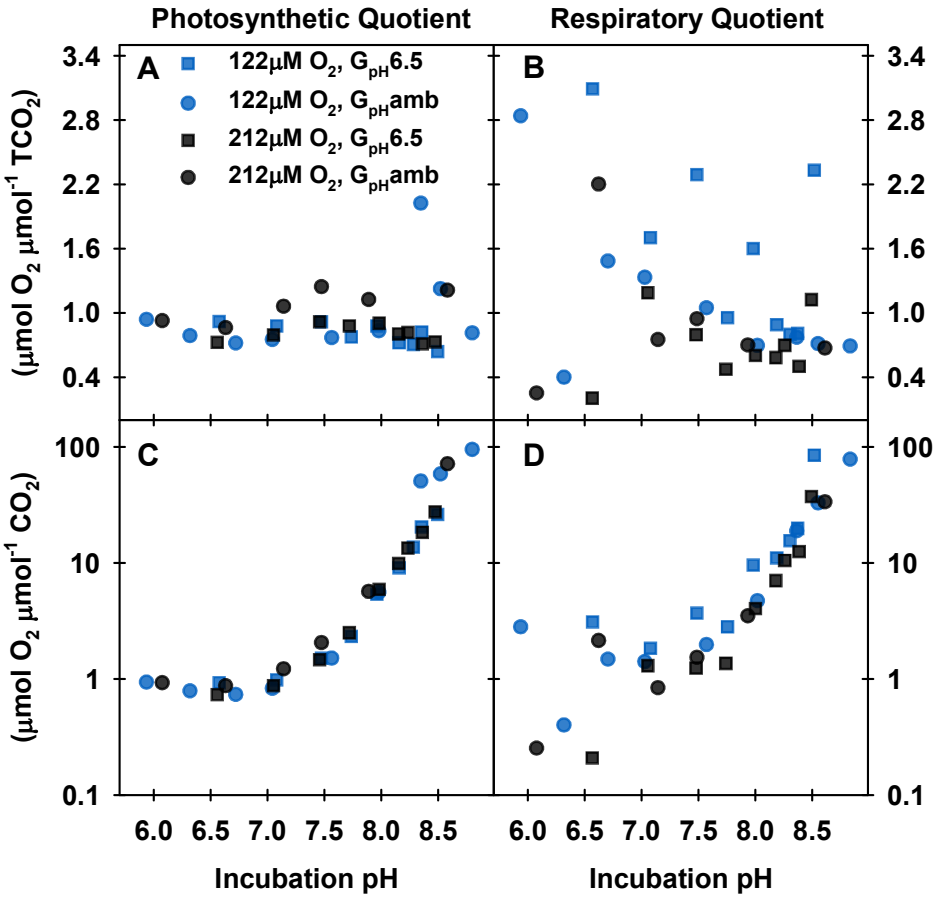

Figure 29. Photosynthetic (PQ) and Respiratory (RQ) quotients of eelgrass leaves as a function of incubation pH. PQ were calculated from gross photosynthesis measurements of individual samples, and their corresponding RQ were derived from dark respiration rates. Quotients were based on the contribution of total carbon uptake/release (A and B) and based only on aqueous CO_2 uptake/release (C and D).

Table 16. Comparison of Photosynthetic (PQ) and Respiratory (RQ) quotients of eelgrass leaves among different oxygen concentrations and different growth pH (G_{pH}). Different letters represent significant differences between the conditions determined by Dunn's Method following ANOVA on ranks analysis. Effects of incubation pH on quotients were analyzed by ANCOVA.

		PQ ($\mu mol\ O_2\ \mu mol^{-1}\ TCO_2$)		RQ ($\mu mol\ O_2\ \mu mol^{-1}\ TCO_2$)	
Conditions	n	Mean ± SEM		Mean ± SEM	
122μM O_2 G_{pH}6.5	9	0.81 ± 0.03 [a, b]		1.61 ± 0.28 [a]	
122μM O_2 G_{pH}amb	9	0.99 ± 0.14 [a, b]		1.11 ± 0.24 [a, b]	
212μM O_2 G_{pH}6.5	9	0.81 ± 0.03 [a]		0.69 ± 0.10 [b]	
212μM O_2 G_{pH}amb	6	1.08 ± 0.06 [b]		0.92 ± 0.27 [a, b]	
Analysis of Variance for the Equal Slopes Model: PQ					
Source of Variation	df	SS	MS	F	*P*
Condition	3	0.49	0.16	3.025	0.046
Incubation pH	1	0.13	0.13	2.415	0.131
Residual	28	1.52	0.05	--	--
Total	32	2.05	0.06	--	--
Analysis of Variance for the Equal Slopes Model: RQ					
Source of Variation	df	SS	MS	F	*P*
Condition	3	4.51	1.50	4.001	0.017
Incubation pH	1	2.23	2.23	5.928	0.022
Residual	28	10.52	0.38	--	--
Total	32	16.80	0.53	--	--

The molar ratio of CO_2 to O_2 in seawater explained the regulation of photochemical pathways in eelgrass under light-saturation (Figure 30). Based on solubility constants, this molar ratio is around 0.06 at 25°C in air-equilibrated seawater with salinity of 25 PSS and pH 8.1, and decreases with increasing temperature and pH, with decreasing salinity, as well as due to photosynthesis in net autotrophic ecosystems. In the incubation experiments, when $[CO_2]$:$[O_2]$ was <0.1, the quantum yield of oxygen (Φ_{O2}) was low while PQ (O_2/CO_2) and NPQ were highest. For $[CO_2]$: $[O_2]$ >0.1, CO_{2aq} specific PQ decreased to minimum of 1 and Φ_{O2} increased significantly albeit the constant saturating light (Figure 30 A and B). These changes in PQ and Φ_{O2} corresponded to the reduction of NPQ as photoprotective pathway hence absorbed photons were utilized in carbon assimilation (Figure 30 C). Φ_{O2} was similar among the different plants and incubation conditions across the entire range, whereas increasing O_2 saturation level slightly decreased the decline rate of PQ when CO_2:O_2 was <1. On the other hand, NPQ was higher in plants grown at high CO_2 treatments (pH6.5) which might be related to the differences in optical properties of the leaves, such as higher Chl *a:b* and slightly decreased optical cross section. Inducing these minute variabilities in pigment content and optical properties among the different incubation conditions were not intentional but resulted from the interactive effects of sampling season and the growth CO_2 environment of the plants (Table 17). In contrast to the fluorescence method, gas exchange measurements permitted integration of these variabilities into the photosynthetic flux measurements by normalizing the rates to appropriate leaf properties. The difference of NPQ between the growth conditions might also be related to different light levels used in 2013 and 2014 experiments (310 vs 460 µmol photons m^{-2} s^{-1}). Nevertheless, both of these PAR levels were beyond the light requirement to saturate the photosynthesis of eelgrass, based on E_k values reported in Chapter 3. As a result decreasing NPQ in all plants as CO_2:O_2 increased showed the important photoprotective role of this process when CO_2 is limiting photosynthesis

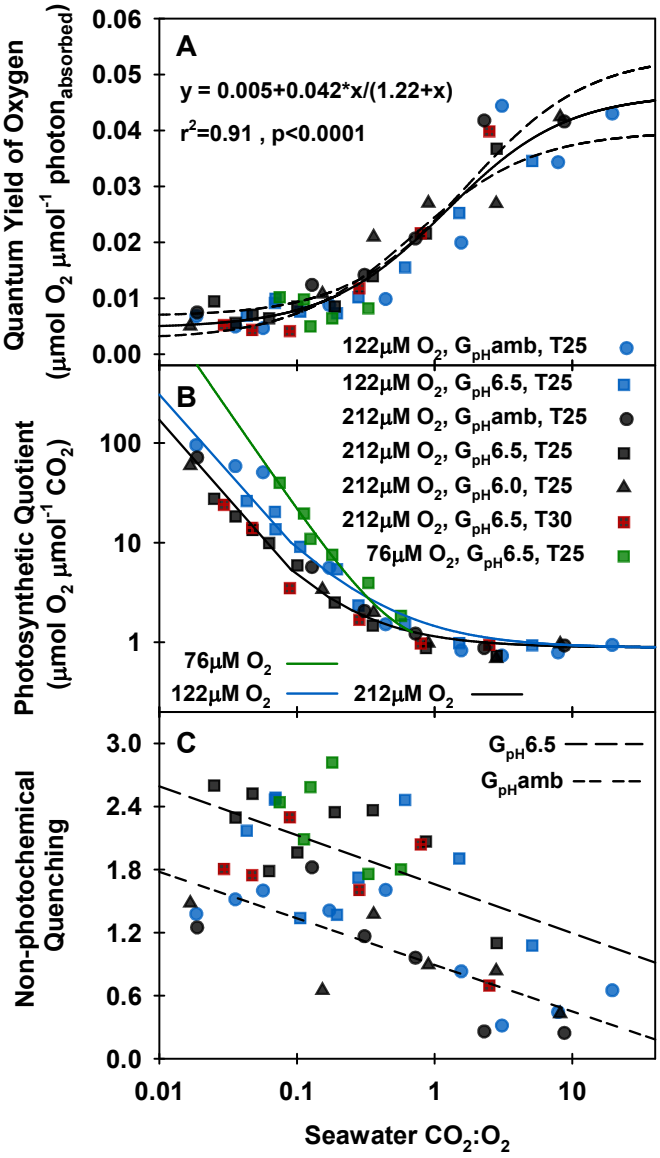

Figure 30. Photosynthetic performance and photoprotection in eelgrass as a function of CO_2 to O_2 ratio in seawater. (A) Quantum yield of oxygen estimates of all samples at saturated light levels were fit to single rectangular hyperbola function. (B) Photosynthetic quotient relying on aqueous CO_2 uptake only were fit to inverse second order polynomial functions based on the O_2 level of the incubation seawater. (C) The response of NPQ to photosynthetic substrate availability was compared between plants grown at different pH treatments.

Table 17. Pigment content and optical properties of leaves used in photosynthesis measurements. FW: Fresh Weight, LA: Leaf Area, Chl: Chlorophyll, Car: Carotenoid, a*: optical cross section at 680nm.

Growth pH	ambient	ambient	6.0	6.5	6.5	6.5	6.5
Incubation condition	212µM O_2 25°C	122µM O_2 25°C	212µM O_2 25°C	212µM O_2 25°C	212µM O_2 30°C	122µM O_2 25°C	76µM O_2 25°C
Sampling year	2013 Jul	2013 Aug	2013 Jul	2014 Sep-Oct	2014 Oct.	2014 Sep-Oct	2014 Sep.
Sample size	7	12	7	9	6	9	6
FW per LA ($mg\ cm^{-2}$)	28.1 ± 1.5 ab	26.8 ± 1.4 bc	32.5 ± 1.3 a	22.6 ± 0.9 cd	19.1 ± 0.4 d	23.1 ± 1.1 bcd	23.0 ± 1.0 bcd
Total Chl per FW ($mg\ Chl\ g^{-1}\ FW$)	0.95 ± 0.06 ab	1.17 ± 0.08 a	0.69 ± 0.04 b	1.13 ± 0.04 a	1.10 ± 0.03 a	1.14 ± 0.05 a	1.08 ± 0.07 a
Total Chl per LA ($µg\ Chl\ cm^{-2}$)	26.2 ± 0.5 ab	30.2 ± 1.2 a	22.3 ± 1.2 b	25.6 ± 1.7 ab	20.9 ± 0.5 b	26.5 ± 2.0 ab	24.5 ± 1.3 ab
Total Car per LA ($µg\ Cx\ cm^{-2}$)	-	-	-	5.74 ± 0.31 a	4.84 ± 0.12 a	5.70 ± 0.33 a	5.21 ± 0.33 a
Chl a:b	2.55 ± 0.02 a	2.63 ± 0.07 ab	2.68 ± 0.04 abc	3.11 ± 0.06 d	3.16 ± 0.06 d	3.07 ± 0.10 cd	2.94 ± 0.18 abcd
TCar:TChl	-	-	-	0.23 ± 0.01 a	0.23 ± 0.00 a	0.22 ± 0.01 a	0.21 ± 0.01 a
a*(680)	5.36 ± 0.49 ab	5.22 ± 0.44 ab	6.29 ± 0.38 a	3.73 ± 0.28 bc	4.62 ± 0.12 abc	3.64 ± 0.25 c	4.08 ± 0.22 bc

Discussion

In this study, photosynthetic performance of eelgrass leaves, quantified under fully controlled incubation conditions, followed a Gaussian function with seawater pH, having a peak centered at about 6.2. Plants may vary their photosynthetic performance depending on the external growth conditions but the efficiency of a particular biochemical process under physiological constraints and external conditions (e.g. the net photosynthesis per photosynthetic machinery per available substrate) often produces a Gaussian-type response curve. Both the physiological maximum capacity of the photosynthetic machinery and its corresponding optimum pH range were consistent among the plants grown at different CO_2 treatments (e.g. pH6, pH6.5 and ambient pH) and sampled during different seasons (e.g. summer 2013, fall 2014). Although the plants were acclimated to varying growth conditions, a common capacity of photosynthetic machinery under same incubation conditions pointed out no induction of a mechanism to increase the affinity for DIC uptake but only the instantaneous control of photorespiration, similar to the findings of Chapter 3.

The photosynthetic rates at today's oceanic pH of 8.1 and above were confirmed to be at the low-end of oxygen production and DIC uptake for eelgrass leaves. These rates corresponded to approximately 15% of the maximum capacity. The drastic increase of net photosynthesis from pH 8.1 to the optimum pH 6.2 resulted from the exponential increase of $[CO_2]$ rather than 15% increase of $[HCO_3^-]$, which was already above saturation (>1mM sensu Invers et al. (2001)). This optimum incubation pH of photosynthesis validates the observed maximum biomass production, survival and reproductive success of the plants that were cultivated at pH 6 and 6.5 treatments during a 18 month long CO_2 enrichment experiment that included two prolonged periods where temperatures exceeded the 25° C threshold for stress in eelgrass (Zimmerman et.al. 2016). Similar positive effects of CO_2 enrichment on seagrass performance have been observed both in long-term experiments and in natural volcanic CO_2

vents (Zimmerman et al., 1997; Palacios and Zimmerman, 2007; Hall-Spencer et al., 2008; Jiang et al., 2010; Campbell and Fourqurean, 2011; Ow et al., 2015).

Net photosynthesis, whether measured by gas flux (O_2 and CO_2) or by variable fluorescence both exhibited a well-behaved Gaussian response to pH with similar optimum pH range, although differed in their magnitudes of response. This deviation in parameter estimation (i.e. different amplitudes) under the same incubation conditions suggested the use of alternative electron transfer pathways that are important for the instantaneous regulation of photosynthetic control. Similar findings to this study using different seagrass species revealed the inconsistency between the two methods when photosynthesis is carbon limited and inferred the role of photorespiration (Beer and Björk, 2000; Silva and Santos, 2004; Silva et al., 2009). The estimation of electron transfer rate (ETR) based on effective quantum yield of fluorescence (EQY) assumes that the heat loss term is constant and the quenching of fluorescence is due to the linear electron flow to drive photochemistry (Baker, 2008). However, this assumption has two limitations when the PAM method is applied to measure carbon-limited photosynthesis, such as in seagrasses. Firstly, the Mehler pathway and photorespiration are not accounted for, which maintain electron flow and therefore detected as high EQY but resulting in O_2 consumption. Secondly, the heat loss via NPQ at saturating light levels plays a significant photoprotective role in seagrasses (Ralph et al., 2002; Ralph and Gademann, 2005) and cannot be assumed to be a constant process. In this study, the moderate increase of EQY with decreasing pH, as opposed to drastic increase of oxygen production and TCO_2 uptake, indicated the electron flow through PSII at high pH was maintained through alternative pathways. These included operations of the xanthophyll cycle and photorespiration, which could be monitored by the drastic changes in NPQ and net oxygen production as a function of CO_2 availability. The regulation of NPQ as a photoprotective mechanism under changing seawater chemistry showed differences among the plants grown at different CO_2 treatments.

Similar differences in NPQ response among the plants acclimated to different CO_2 environments were explained by the variability of the leaf pigment content (Chapter 3), which not only corresponds to the light environment the plants are living in but also acclimates to ocean acidification (Chapter 2). This study confirmed that the regulation of NPQ is also dependent on CO_2 availability even though the plants were incubated at the same saturating light level. This highlights that NPQ is not only active for high light protection but controls electron flow dynamically under various substrate limitations. Therefore this inconsistency between the methods has important implications for the estimation of photosynthetic production rates from ETR measurements that use a constant 0.25 O_2/ETR molar ratio (Chapter 3 and (Silva et al., 2009). Using the relationship of NPQ and quantum yield of oxygen to seawater CO_2:O_2 from this study, it is possible to have correction factors for this molar ratio at various CO_2:O_2 conditions. These correction factors will allow the conversion of the ETR measurements, which are non-invasive and easily applicable in field conditions (Silva et al., 2009), to photosynthetic production rates that accounted for the photosynthetic control mechanisms.

Within this study, one of the main assumptions to estimate the DIC uptake from the measurements of changes in pH was the conservation of alkalinity during photosynthesis and respiration. The simplistic stoichiometry of photosynthetic O_2 production relies on only CO_2 uptake, which does not change the alkalinity but removes dissolved inorganic carbon and acidity, thereof increasing pH. However, operation of a H^+ ATPases to create a low pH zone in the periplasmic space has been observed in *Zostera marina, Zostera noltii, Halophila stipulacea* and *Ruppia maritima* (Beer et al., 2002; Mercado et al., 2003). Although the active efflux of H^+ requires the expenditure of ATP, it speeds up the conversion of external HCO^-_3 to CO_2 to yield a net influx of CO_2 for carbon assimilation (Raven et al., 2014). A sensitivity analysis by assuming decreased alkalinity during photosynthesis measurements due to H^+ efflux increased the estimates of DIC uptake rate, especially at high pH ranges, but also resulted in further reduction

of Photosynthetic Quotient (PQ) estimates. So the low PQ values estimated in this study were not related to methodological inaccuracy but rather to physiological processes. Low PQ values (ranging from 0.1 to 1) in two different marine algae species were correlated to photorespiration at [O_2] greater than air saturation (Burris, 1981). While no simple relationship between PQ and seawater [O_2] was predicted to quantify the photorespiration rates for those marine algae, it was suggested that simultaneous variation of both DIC and O_2 affects PQ. A similar approach has been applied in this study to relate the PQ to pH and ultimately to the seawater CO_2:O_2.

Varying O_2 concentration and pH, via CO_2 enrichment, among the incubation experiments altered the ratio of CO_2 to O_2 in the seawater, which varied the photorespiration rates of eelgrass leaves. The variation of CO_2:O_2 ratio occurs daily and seasonally in marine environments because the solubility of these molecules in seawater depends on the temperature, pH and equilibrium with the atmosphere as well as biological processes (Mercado and Gordillo, 2011). A simple comparison of O_2 and CO_2 solubility in air equilibrated seawater indicates increasing temperature from 20°C to 30°C decreases the CO_2:O_2 ratio in acidified ocean (e.g. at pH 7.7) by 10.5% (from 0.181 to 0.162), contrary to 13.6% (from 0.066 to 0.057) at today's oceanic pH (i.e. pH 8.1). Therefore, ocean acidification and warming might have important effects on dissolved CO_2:O_2 and consequently on photorespiration in eelgrass. Since O_2 and CO_2 are competitive substrates for Rubisco, the ratio of carboxylation to oxygenation (V_c/V_o) depends both on the absolute concentrations of CO_2 and O_2 within the medium as well as on the affinity of Rubisco. The V_c/V_o ratio for C3 plants is about 3-4 fold at atmospheric equilibrium conditions of 12 μM CO_2 and 250 μM O_2 (Raghavendra, 2000). This means about 25% of the gross CO_2 fixation is lost due to the oxygenation reaction of Rubisco (Bowes, 1991). The terrestrial C3 plants have evolved Rubisco that has higher affinity for CO_2 than algae and cyanobacteria, thereof having lower half saturation constants (K_m), on average 10 μM CO_2 for isolated Rubisco (Jordan and Ogren, 1981; Falkowski and Raven, 2007). On the other hand,

submersed aquatic macrophytes have higher apparent half saturation constants (K_s, measured in vivo), ranging from 40 to 700 μM CO_2 (Bowes and Salvucci, 1989). The K_s values of 130 to 150 μM CO_2 for eelgrass from this study tied in with this range and also with the K_s values (40, 150 and 300 μM CO_2) of three different species of seagrasses (*Halophila stipulacea*, *Halodule uninervis* and *Syringodium isoetifolium*, respectively) (Madsen and Sand-Jensen, 1991). Increasing K_s estimates in aquatic environments is the outcome of external and internal resistances to CO_2 assimilation (Bowes and Salvucci, 1989). The internal resistances include the higher K_m values of Rubisco and photorespiration, while external resistances include the boundary layer formation and lower diffusion rates. The negative effect of external resistance on eelgrass photosynthesis because of boundary layer formation has been quantified as a function of flow environments by McPherson et al. (2015). But once the external resistances were eliminated, leaving photorespiration as the main internal resistance, their flow and light saturated Monod model predicted the K_s of eelgrass leaves around 194 μM CO_2 , which is in close proximity to estimates from this study that are 130 or 150 μM CO_2 when either O_2 production or CO_2 uptake method is considered, respectively. The slight difference in K_s estimates between the two studies might depend on the choice of descriptive model fit, which in this study was a negative exponential function with y-offset to estimate the CO_2 compensation point. The CO_2 compensation point ranges from 1-6 μM CO_2 for freshwater angiosperms and 0-10 μM CO_2 for aquatic macrophytes, where high values indicate the significance of photorespiration (Bowes and Salvucci, 1989; Madsen et al., 1996). This study estimated the CO_2 compensation value of eelgrass around 13 μM CO_2, towards the high end of the cited ranges therefore implying photorespiration.

While net CO_2 uptake ceased at 13 μM CO_2, net O_2 production did not level off. This positive O_2 production was assumed to be sustained via HCO_3^- uptake at high pH, since net TCO_2 uptake rates agreed more with O_2 production rates overall. Indeed, TCO_2 uptake

exceeded the O_2 production rates all the time indicating either photorespiratory consumption of O_2, meanwhile allowing recycling of photorespired CO_2, and/or internal storage of O_2 in lacunar space. The lacunar space, where O_2 is stored in gas form and therefore not detectable by an O_2 electrode, plays a significant role for transport of oxygen to belowground tissues in natural seagrass beds (Greve et al., 2003; Pedersen et al., 2004; Borum et al., 2005; Holmer et al., 2005; Sand-Jensen et al., 2005; Holmer et al., 2009). To account for the undetected O_2 loading into the phloem tissue, if the gross oxygen production rates were increased by 6%, based on the rates estimated by Bodensteiner (2006), the PQ (O_2/TCO_2) would increase from 0.84±0.03 to 0.89±0.03, still remaining lower than the theoretical value of 1. Internal storage of respired CO_2 would also explain the pH dependency of the respiratory quotient. At high pH the internally generated CO_2 that is recycled to C3 pathway under light is not released to the medium under darkness, resulting in RQ < 1. A similar closed system for CO_2 utilization in seagrasses was discussed by Beer et al. (1980). A more recent study demonstrated that terrestrial C3 plants such as rice and wheat re-assimilate both respired and photorespired CO_2, thereby boosting their photosynthesis by 10% at ambient atmospheric [CO_2] (Busch et al., 2013). Another pathway that affects net oxygen production rates but will not be detected in TCO_2 uptake, thereby resulting in lower PQ, is the Mehler reaction. While photorespiration depends on the relative ratio of CO_2:O_2 because of the encounter probability of both molecules with Rubisco, the Mehler reaction is mainly stimulated by accumulation of high O_2, which competes with ferredoxin for the electrons emitted by PSI. In this study, the PQ (O_2/CO_2) of high CO_2 acclimated plants decreased with increasing levels of O_2 saturation only when seawater CO_2:O_2 was < 1 (Figure 30). This decrease in PQ at high ambient [O_2] even though the molar ratios of CO_2:O_2 in seawater were constant, suggested the role of the Mehler reaction. Similarly, increasing [O_2] decreased PQ values in two different marine algae (Burris, 1981). Unfortunately, variable fluorescence methods are insensitive to activity of the Mehler reaction

pathway since it facilitates electron flow and generates a pH gradient, but without net oxygen production. This pH gradient is also important for modulation of NPQ to prevent photoinhibition of PSII (Rumeau et al., 2007). That might be the reason for the agreement of O_2 production with NPQ, rather than with EQY, under increasing seawater CO_2:O_2.

To conclude, the pH dependent Gaussian model was inclusive enough to accurately predict the photosynthetic performance of eelgrass plants grown at various DIC concentrations and exposed to daily fluctuating environmental conditions of light and temperature. Previous studies estimating pH dependent seagrass photosynthesis were using either linear or exponential models only within the pH range of 6 up to 9 (Invers et al., 2001; Zimmerman, 2006; Buapet et al., 2013; Campbell and Fourqurean, 2013). This study, however, determined the boundary conditions of the pH effect on photosynthesis, therefore the limit of positive CO_2 effect, rather than leaving open-ended increase with pH. By quantifying the control of photochemistry per available photosynthetic machinery as a function of seawater chemistry in this study, and as a function of light availability in Chapter 3, and also knowing the acclimation of photosynthetic machinery to changes in environmental conditions (Chapter 2), it is possible to integrate a photosynthetic control module to the existing seagrass productivity model, *GrassLight* (Zimmerman et al., 2015), to allow the photoprotection and photoacclimation processes to dynamically adjust the carbon assimilation in response to fluctuating coastal environments and climate change. Since these photosynthetic control mechanisms do not only regulate the carbon assimilation but also other metabolic pathways, for example the negative feedback of inhibited photorespiration on nitrogen metabolism (Raghavendra, 2000; Rachmilevitch et al., 2004), future studies of seagrasses can explore the cross talk between C and N metabolic pathways for the utilized sunlight energy.

CHAPTER V

CONCLUSION

Climate change in terms of increased CO_2 and temperature impacts aquatic photosynthetic organisms due to changes in the biogeochemistry of seawater (Andersson et al., 2015). At today's oceanic pH, photosynthesis of seagrasses is carbon limited due to low activity of carbon concentrating mechanisms, yet seagrasses account for approximately 10% of the ocean's total carbon storage (Fourqurean et al., 2012; Koch et al., 2013). Therefore, increasing atmospheric CO_2 concentration, which results in ocean acidification/carbonation, is predicted to have a positive impact on seagrass productivity that may facilitate more CO_2 sequestration. Previous studies have confirmed the positive influence of increasing CO_2 on photosynthesis and growth of the temperate eelgrass *Zostera marina* L., even enhancing survival under heat stress (Palacios and Zimmerman, 2007; Zimmerman et al., 2016), however the acclimation of photoprotective mechanisms was not well characterized. This study aimed to quantify the long-term impacts of ocean acidification on photochemical control mechanisms in eelgrass.

Acclimation of leaf optical properties and photochemistry were compared using eelgrass plants grown in controlled outdoor aquaria at different aqueous CO_2 concentrations ranging from 50 to 2000 µmol/kgSW (equivalent to pH 8 to 6) from May 2013 until October 2014. Long-term growth under high [CO_2] produced morphological and metabolic changes in eelgrass. Plants grown in a high CO_2 environment decreased the pigment content and increased the biomass yield, in addition to showing seasonal trends- especially responding to temperature changes. Increased chlorophyll-a specific absorption coefficient with [CO_2] reduced self-shading of pigments (i.e. package effect) within a leaf. These long-term acclimations of light harvesting efficiency due to increasing CO_2 resembled the high light adaptation of plants. Therefore, the photosynthetic machinery performs an important sensory function for

environmental cues, in addition to harvesting sun energy, which further explains the interdependent regulation of pigment composition and optical properties of eelgrass leaves by CO_2, temperature and light. Such a signaling system have been found under the control of photosynthetic redox state that depends on the continuity of the electron transport under various limiting conditions (Pfannschmidt, 2003; Pfannschmidt and Yang, 2012).

Laboratory incubation experiments resolved this mutual regulation of redox state via carbon and light availability, by measuring O_2 production, total CO_2 uptake and fluorescence of the acclimated leaves simultaneously at various pH, O_2 and light levels. At saturated light levels, increasing CO_2 between pH 8 to 6 instantaneously increased chlorophyll specific photosynthesis nonlinearly up to 8 fold, regardless of the aquarium growth conditioning. Therefore, the instantaneous difference in O_2 production rates in CO_2-saturated vs. CO_2-limited incubation medium corresponded to the amount of O_2 consumed in the photorespiratory pathway. Thus, photosynthesis and photorespiration for each growth condition were predictable using the *P* versus *E* curves, although the response to incubation CO_2 differed between biomass and pigment normalization due to changes in leaf morphology. Presently, models of eelgrass performance do not consider these long-term morphological and metabolic acclimation responses (Zimmerman, 2003, 2006; Zimmerman et al., 2015). Thus, the quasi-mechanistic model developed in this study will allow the photosynthetic and morphological acclimations resulting from ocean carbonation to be integrated into seagrass productivity models, by adjusting the limits of the photosynthetic parameters based on substrate availability and physiological capacity.

Furthermore, photosynthetic performance of eelgrass leaves followed a Gaussian function of seawater pH, with a peak centered at about 6.2. Previous studies estimating pH dependent seagrass photosynthesis were using either linear or exponential models only within the pH range of 6 up to 9 (Invers et al., 2001; Zimmerman, 2006; Buapet et al., 2013; Campbell and

Fourqurean, 2013). This study, however, determined the boundary conditions of pH effect on photosynthesis, providing the limit of positive CO_2 effect. Both the physiological maximum capacity of the photosynthetic machinery and its corresponding optimum pH range were consistent among the plants grown at different CO_2 treatments and sampled during different seasons. Although the plants were acclimated to varying growth conditions, a common capacity of photosynthetic machinery under same incubation conditions pointed out no induction of a mechanism to increase the affinity for DIC uptake but only the instantaneous control of photorespiration.

When photosynthesis was relieved from CO_2 limitation, non-photochemical quenching, a photoprotective pathway to dissipate excess light energy as heat, was reduced as well. Due to the alternative electron pathways (i.e. photorespiration and NPQ), however, fluorescence measurements overestimated gross photosynthesis ($P_{g\text{-}ETR}$) and therefore were not equivalent to true carbon assimilation in eelgrass. Still, the fluorescence measurements with PAM provided non-intrusive information about the photoprotection of eelgrass through NPQ and are easily applicable in field conditions. Therefore, quantifying the ratio of Φ_{PSII} to Φ_{O2}, as a function of light and carbon availability in this study, may allow to account for the alternative electron pathways and correct estimation of photosynthesis in eelgrass using the PAM method.

More importantly, understanding the impact of seawater chemistry on quantum requirements and assimilatory quotients in eelgrass is important to predict the carbon sequestration efficiency of seagrasses in a changing marine environment. With this study, by quantifying the control of photochemistry per available photosynthetic machinery 1) as a function of seawater chemistry (Chapter 4) and 2) as a function of light availability (Chapter 3), and 3) the acclimation of photosynthetic machinery to changes in environmental conditions (Chapter 2), it is possible to integrate a photosynthetic control module to the existing seagrass productivity model to allow the photoprotection and photoacclimation processes dynamically

adjust the carbon assimilation in response to fluctuating coastal environments and climate change (Figure 31). Such a mechanistic understanding of the balance between photosynthesis, photoprotection and growth under changing environmental conditions may help to predict whether seagrasses can maintain their successful ecological performance in future climatic conditions.

In conclusion, this 18 month long CO_2 enrichment experiment demonstrated that efficient utilization of absorbed light energy for photosynthetic carbon assimilation reduced the susceptibility to light-induced damage, therefore, the need for photoprotection of photosynthetic apparatus via NPQ and alternative electron pathways. Under constant high CO_2 and high light environment, the maintenance of balanced redox state without the need for these safety valves to dissipate excess photons and electrons triggered long-term acclimation process for downregulation of pigment biosynthesis. In contrast, under low CO_2 and high light environment, resulting in long period of light-saturated photosynthesis, these rapidly inducible dissipation pathways allow eelgrass to cope with diurnal fluctuations and to survive in highly dynamic coastal ecosystems. Likewise, the dual function of Rubisco maintains electron flow, thereby preventing the inhibitory damage to photosystems due to light saturation when carbon assimilation is limited by CO_2 supply, and preventing the accumulation of reactive oxygen species. Therefore, photorespiration likely serves as an important clutch to protect the photochemical pathway in CO_2-limited eelgrass even though it has often been viewed as an inefficient residue of the evolution of Rubisco. Indeed, photorespiration might provide a carbon concentrating mechanism via recycling of photorespired CO_2 and removing excess intracellular O_2. Therefore, high light requirements of seagrasses, even though photosynthesis is mainly carbon limited, might be needed to keep the photosynthetic machinery running to produce ATP to support photorespiration. These alternative pathways become more important for permanently rooted marine plants in highly variable estuarine environments, where high water

column productivity causes [O_2] to rise and [CO_2] to fall and alters light quantity/quality. In terrestrial plants, these photosynthetic control mechanisms not only regulate the carbon assimilation but are also linked to other metabolic pathways, for example inhibition of photorespiration initiates negative feedback on nitrogen metabolism (Raghavendra, 2000; Rachmilevitch et al., 2004). Therefore, future studies of seagrasses can explore the cross talk between photochemistry and nitrogen metabolism for the utilized sunlight energy in response to ocean carbonation.

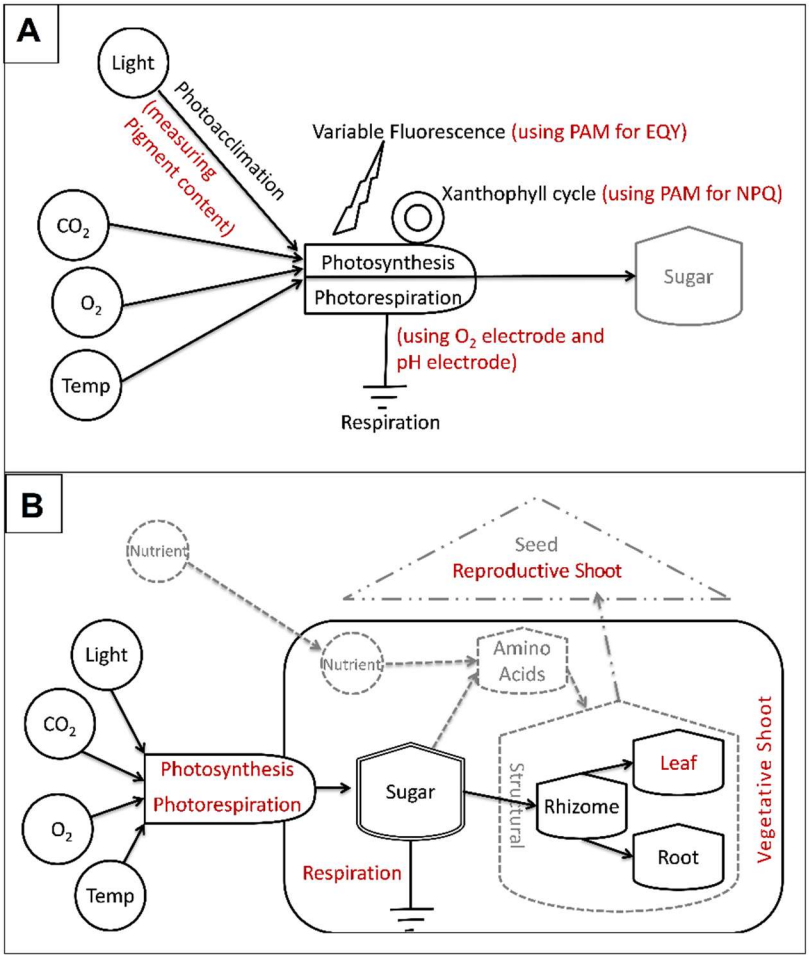

Figure 31. Conceptual diagram integrating photoacclimation, photosynthesis, photorespiration and growth in eelgrass in response to environmental parameters. (A) Photochemical processes were measured using methods highlighted with red by varying multiple environmental parameters. (B) Impact of acclimating photochemistry on whole plant metabolism were monitored throughout the 18 month long CO_2 enrichment experiment by measuring parameters highlighted with red. Gray shaded parameters, measured during the CO_2 enrichment experiment and discussed in Zimmerman et al. (2016), were not within the scope of this study.

LITERATURE CITED

Agustí S, Enríquez S, Frost-Christensen H, Sand-Jensen K, Duarte CM (1994) Light Harvesting Among Photosynthetic Organisms. Functional Ecology **8:** 273-279

Aizawa K, Miyachi S (1986) Carbonic anhydrase and CO_2 concentrating mechanisms in microalgae and cyanobacteria. FEMS Microbiology Letters **39:** 215-233

Alcoverro T, Zimmerman RC, Kohrs DG, Alberte RS (1999) Resource allocation and sucrose mobilization in light-limited eelgrass *Zostera marina*. Marine Ecology Progress Series **187:** 121-131

Anderson J, Chow W, Park Y-I (1995) The grand design of photosynthesis: Acclimation of the photosynthetic apparatus to environmental cues. Photosynthesis Research **46:** 129-139

Andersson AJ, Kline DI, Edmunds PJ, Archer SD, Bednaršek N, Carpenter RC, Chadsey M, Goldstein P, Grottoli AG, Hurst TP, King AL, Kübler JE, Kuffner IB, Mackey KRM, Menge BA, Paytan A, Riebesell U, Schnetzer A, Warner ME, Zimmerman RC (2015) Understanding ocean acidification impacts on organismal to ecological scales. Oceanography **28:** 16-27

Andrews TJ, Abel KM (1979) Photosynthetic Carbon Metabolism in Seagrasses ^{14}C-Labeling Evidence for the C3 Pathway. Plant Physiology **63:** 650-656

Andrews TJ, Lorimer GH (1978) Photorespiration -- still unavoidable? FEBS Letters **90:** 1-9

Atwell BJ, Kriedemann PE, Turnbull CGN (1999) Plants in Action: Adaptation in Nature, Performance in Cultivation. Macmillan Education Australia

Backhausen JE, Scheibe R (1999) Adaptation of tobacco plants to elevated CO_2: influence of leaf age on changes in physiology, redox states and NADP-malate dehydrogenase activity. Journal of Experimental Botany **50:** 665-675

Badger MR, Price GD (1994) The Role of Carbonic Anhydrase in Photosynthesis. Annual Review of Plant Physiology and Plant Molecular Biology **45:** 369-392

Badger MR, Susanne von C, Ruuska S, Nakano H (2000) Electron Flow to Oxygen in Higher Plants and Algae: Rates and Control of Direct Photoreduction (Mehler Reaction) and Rubisco Oxygenase. Philosophical Transactions: Biological Sciences **355:** 1433-1446

Baker NR (2008) Chlorophyll Fluorescence: A Probe of Photosynthesis In Vivo. Annual Review of Plant Biology **59:** 89-113

Barra L, Chandrasekaran R, Corato F, Brunet C (2014) The Challenge of Ecophysiological Biodiversity for Biotechnological Applications of Marine Microalgae. Marine Drugs **12:** 1641

Batiuk RA, Bergstrom P, Kemp M, Carter V, Gallegos C, Karrh L, Wilcox D, Ailstock S, Teichberg M (2000) Chesapeake Bay Submerged Aquatic Vegetation Water Quality and Habitat-Based Requirements and Restoration Targets: A Second Technical Synthesis. *In*, Vol EPA/903/R-00/014. U.S. Environmental Protection Agency, Annapolis, MD

Bauwe H (2011) Chapter 6 Photorespiration: The Bridge to C4 Photosynthesis. *In* AS Raghavendra, RF Sage, eds, C4 Photosynthesis and Related CO_2 Concentrating Mechanisms, Vol 32. Springer Netherlands, pp 81-108

Beardall J (1989) Photosynthesis and photorespiration in marine phytoplankton. Aquatic Botany **34:** 105-130

Beardall J, Giordano M (2002) Ecological implications of microalgal and cyanobacterial CO_2 concentrating mechanisms, and their regulation. Functional Plant Biology **29:** 335-347

Beer S (1989) Photosynthesis and photorespiration of marine angiosperms. Aquatic Botany **34:** 153-166

Beer S (1996) Photosynthetic utilisation of inorganic carbon in *Ulva*. Scientia Marina **60:** 125-128

Beer S, Björk M (2000) Measuring rates of photosynthesis of two tropical seagrasses by pulse amplitude modulated (PAM) fluorometry. Aquatic Botany **66:** 69-76

Beer S, Bjork M, Hellblom F, Axelsson L (2002) Inorganic carbon utilization in marine angiosperms (seagrasses). Functional Plant Biology **29:** 349-354

Beer S, Koch E (1996) Photosynthesis of marine macroalgae and seagrasses in globally changing CO_2 environments. Marine Ecology Progress Series **141:** 199-204

Beer S, Sand-Jensen K, Madsen TV, Nielsen SL (1991) The carboxylase activity of Rubisco and the photosynthetic performance in aquatic plants. Oecologia **87:** 429-434

Beer S, Shomer-Ilan A, Waisel Y (1980) Carbon Metabolism in Seagrasses: II. Patterns of photosynthetic CO_2 incorporation. Journal of Experimental Botany **31:** 1019-1026

Beer S, Vilenkin B, Weil A, Veste M, Susel L, Eshel A (1998) Measuring photosynthetic rates in seagrasses by pulse amplitude modulated (PAM) fluorometry. Marine Ecology-Progress Series **174:** 293-300

Beer S, Wetzel RG (1982) Photosynthetic carbon fixation pathways in *Zostera marina* and three Florida seagrasses. Aquatic Botany **13:** 141-146

Behrenfeld MJ, Prasil O, Babin M, Bruyant F (2004) In search of a physiological basis for covariations in light-limited and light-saturated photosynthesis. Journal of Phycology **40:** 4-25

Bidwell RGS, McLachlan J (1985) Carbon nutrition of seaweeds: Photosynthesis, photorespiration and respiration. Journal of Experimental Marine Biology and Ecology **86:** 15-46

Björk M, Haglund K, Ramazanov Z, Pedersén M (1993) Inducible mechanisms for HCO_3^- utilization and repression of photorespiration in protoplasts and thalli of three species of *Ulva* (chlorophyta). Journal of Phycology **29:** 166-173

Björk M, Weil A, Semesi S, Beer S (1997) Photosynthetic utilisation of inorganic carbon by seagrasses from Zanzibar, East Africa. Marine Biology **129:** 363-366

Black C, Burris J, Everson R (1976) Influence of Oxygen Concentration on Photosynthesis in Marine Plants. Functional Plant Biology **3:** 81-86

Bodensteiner LE (2006) The impact of light availability on benthic oxygen release by seagrasses. San Jose State University

Borum J, Pedersen O, Greve TM, Frankovich TA, Zieman JC, Fourqurean JW, Madden CJ (2005) The potential role of plant oxygen and sulphide dynamics in die-off events of the tropical seagrass, *Thalassia testudinum*. Journal of Ecology **93:** 148-158

Borum J, Sand-Jensen K, Binzer T, Pedersen O, Greve T (2006) Oxygen Movement in Seagrasses. *In* Seagrasses: biology, ecologyand conservation. Springer Netherlands, pp 255-270

Boston HL, Adams MS, Madsen JD (1989) Photosynthetic strategies and productivity in aquatic systems. Aquatic Botany **34:** 27-57

Bowes G (1991) Growth at elevated CO_2: photosynthetic responses mediated through Rubisco. Plant, Cell & Environment **14:** 795-806

Bowes G (2011) Chapter 5 Single-Cell C4 Photosynthesis in Aquatic Plants. *In* AS Raghavendra, RF Sage, eds, C4 Photosynthesis and Related CO_2 Concentrating Mechanisms, Vol 32. Springer Netherlands, pp 63-80

Bowes G, Salvucci ME (1989) Plasticity in the photosynthetic carbon metabolism of submersed aquatic macrophytes. Aquatic Botany **34:** 233-266

Buapet P, Rasmusson LM, Gullström M, Björk M (2013) Photorespiration and Carbon Limitation Determine Productivity in Temperate Seagrasses. PLoS ONE **8:** e83804

Burkholder JM, Tomasko DA, Touchette BW (2007) Seagrasses and eutrophication. Journal of Experimental Marine Biology and Ecology **350:** 46-72

Burris J, Holm-Hansen O, Black C (1976) Glycine and Serine Production in Marine Plants as a Measure of Photorespiration. Functional Plant Biology **3:** 87-92

Burris JE (1981) Effects of oxygen and inorganic carbon concentrations on the photosynthetic quotients of marine algae. Marine Biology **65:** 215-219

Busch FA, Sage TL, Cousins AB, Sage RF (2013) C3 plants enhance rates of photosynthesis by reassimilating photorespired and respired CO_2. Plant, Cell & Environment **36:** 200-212

Caemmerer S, Quick W (2004) Rubisco: Physiology in Vivo. *In* R Leegood, T Sharkey, S Caemmerer, eds, Photosynthesis, Vol 9. Springer Netherlands, pp 85-113

Campbell JE, Fourqurean JW (2011) Novel methodology for in situ carbon dioxide enrichment of benthic ecosystems. Limnology and Oceanography: Methods **9:** 97-109

Campbell JE, Fourqurean JW (2013) Mechanisms of bicarbonate use influence the photosynthetic carbon dioxide sensitivity of tropical seagrasses. Limnology and Oceanography **58:** 839-848

Cummings ME, Zimmerman RC (2003) Light harvesting and the package effect in the seagrasses *Thalassia testudinum* Banks ex König and *Zostera marina* L.: optical constraints on photoacclimation. Aquatic Botany **75:** 261-274

Demmig-Adams B, Adams III WW (1996) The role of xanthophyll cycle carotenoids in the protection of photosynthesis. Trends in Plant Science **1:** 21-26

Demmig-Adams B, Adams W, Ebbert V, Logan B (2004) Ecophysiology of the Xanthophyll Cycle. *In* H Frank, A Young, G Britton, R Cogdell, eds, The Photochemistry of Carotenoids, Vol 8. Springer Netherlands, pp 245-269

Demmig-Adams B, Adams WW (1992) Photoprotection and Other Responses of Plants to High Light Stress. Annual Review of Plant Physiology and Plant Molecular Biology **43:** 599-626

den Hartog C (1970) The sea-grasses of the world. North-Holland Pub. Co., Amsterdam

den Hartog C (1979) Seagrasses and seagrass ecosystems, an appraisal of the research approach. Aquatic Botany **7:** 105-117

Dennison WC (1987) Effects of light on seagrass photosynthesis, growth and depth distribution. Aquatic Botany **27:** 15-26

Dennison WC, Alberte RS (1982) Photosynthetic Responses of *Zostera marina* L. (Eelgrass) to in Situ Manipulations of Light Intensity. Oecologia **55:** 137-144

Dietz K-J, Pfannschmidt T (2011) Novel Regulators in Photosynthetic Redox Control of Plant Metabolism and Gene Expression. Plant Physiology **155:** 1477-1485

Doney SC, Balch WM, Fabry VJ, Feely RA (2009a) Ocean Acidification: A Critical Emerging Problem for the Ocean Sciences. Oceanography **22:** 16-25

Doney SC, Fabry VJ, Feely RA, Kleypas JA (2009b) Ocean Acidification: The Other CO_2 Problem. Annual Review of Marine Science **1:** 169-192

Douce R, Heldt H-W (2004) Photorespiration. *In* R Leegood, T Sharkey, S Caemmerer, eds, Photosynthesis, Vol 9. Springer Netherlands, pp 115-136

Downton W, Bishop D, Larkum A, Osmond C (1976) Oxygen Inhibition of Photosynthetic Oxygen Evolution in Marine Plants. Functional Plant Biology **3:** 73-79

Duarte CM (1991) Seagrass depth limits. Aquatic Botany **40:** 363-377

Duarte CM, Hendriks IE, Moore TS, Olsen YS, Steckbauer A, Ramajo L, Carstensen J, Trotter JA, McCulloch M (2013) Is Ocean Acidification an Open-Ocean Syndrome? Understanding Anthropogenic Impacts on Seawater pH. Estuaries and Coasts **36:** 221-236

Durako MJ (1993) Photosynthetic utilization of CO_2(aq) and HCO_3- in *Thalassia testudinum* (Hydrocharitaceae). Marine Biology **115:** 373-380

Eberhard S, Finazzi G, Wollman F-A (2008) The Dynamics of Photosynthesis. Annual Review of Genetics **42:** 463-515

Ellsworth DS, Crous KY, Lambers H, Cooke J (2015) Phosphorus recycling in photorespiration maintains high photosynthetic capacity in woody species. Plant, Cell & Environment **38:** 1142-1156

Emerson S, Hedges J (2008) Chemical Oceanography and the Marine Carbon Cycle. Cambridge University Press

Enríquez S (2005) Light absorption efficiency and the package effect in the leaves of the seagrass *Thalassia testudinum*. Marine Ecology Progress Series **289:** 141-150

Evans AS, Webb KL, Penhale PA (1986) Photosynthetic temperature acclimation in two coexisting seagrasses, *Zostera marina* L. and *Ruppia maritima* L. Aquatic Botany **24:** 185-197

Falkowski PG, Raven JA (2007) Aquatic photosynthesis. Princeton University Press

Fernández JA, García-Sánchez MJ, Felle HH (1999) Physiological evidence for a proton pump and sodium exclusion mechanisms at the plasma membrane of the marine angiosperm *Zostera marina* L. Journal of Experimental Botany **50:** 1763-1768

Figueroa F, Conde-Álvarez R, Gómez I (2003) Relations between electron transport rates determined by pulse amplitude modulated chlorophyll fluorescence and oxygen

evolution in macroalgae under different light conditions. Photosynthesis Research **75:** 259-275

Fourqurean JW, Duarte CM, Kennedy H, Marba N, Holmer M, Mateo MA, Apostolaki ET, Kendrick GA, Krause-Jensen D, McGlathery KJ, Serrano O (2012) Seagrass ecosystems as a globally significant carbon stock. Nature Geoscience **5:** 505-509

Foyer CH, Bloom AJ, Queval G, Noctor G (2009) Photorespiratory Metabolism: Genes, Mutants, Energetics, and Redox Signaling. Annual Review of Plant Biology **60:** 455-484

Foyer CH, Neukermans J, Queval G, Noctor G, Harbinson J (2012) Photosynthetic control of electron transport and the regulation of gene expression. Journal of Experimental Botany **63:** 1637-1661

Frost-Christensen H, Sand-Jensen K (1992) The quantum efficiency of photosynthesis in macroalgae and submerged angiosperms. Oecologia **91:** 377-384

Gieskes JM, Rogers WC (1973) Alkalinity determination in interstitial waters of marine sediments. Journal of Sedimentary Research **43:** 272-277

Greve TM, Borum J, Pedersen O (2003) Meristematic Oxygen Variability in Eelgrass (*Zostera marina*). Limnology and Oceanography **48:** 210-216

Hall-Spencer JM, Rodolfo-Metalpa R, Martin S, Ransome E, Fine M, Turner SM, Rowley SJ, Tedesco D, Buia M-C (2008) Volcanic carbon dioxide vents show ecosystem effects of ocean acidification. Nature **454:** 96-99

Hanke GT, Holtgrefe S, König N, Strodtkötter I, Voss I, Scheibe R (2009) Chapter 8 Use of Transgenic Plants to Uncover Strategies for Maintenance of Redox Homeostasis During Photosynthesis. *In* J Jean-Pierre, ed, Advances in Botanical Research, Vol Volume 52. Academic Press, pp 207-251

Heber U, Krause GH (1980) What is the physiological role of photorespiration? Trends in Biochemical Sciences **5:** 32-34

Hellblom F, Björk M (1999) Photosynthetic responses in *Zostera marina* to decreasing salinity, inorganic carbon content and osmolality. Aquatic Botany **65:** 97-104

Hemminga MA, Duarte CM (2000) Seagrass ecology. Cambridge University Press

Holmer M, Frederiksen MS, Møllegaard H (2005) Sulfur accumulation in eelgrass (*Zostera marina*) and effect of sulfur on eelgrass growth. Aquatic Botany **81:** 367-379

Holmer M, Pedersen O, Krause-Jensen D, Olesen B, Hedegård Petersen M, Schopmeyer S, Koch M, Lomstein BA, Jensen HS (2009) Sulfide intrusion in the tropical seagrasses *Thalassia testudinum* and *Syringodium filiforme*. Estuarine, Coastal and Shelf Science **85:** 319-326

Hough AR, Wetzel RG (1977) Photosynthetic pathways of some aquatic plants. Aquatic Botany **3:** 297-313

Hough RA (1974) Photorespiration and Productivity in Submersed Aquatic Vascular Plants. Limnology and Oceanography **19:** 912-927

Huner N, Dahal K, Hollis L, Bode R, Rosso D, Krol M, Ivanov AG (2012) Chloroplast Redox Imbalance Governs Phenotypic Plasticity: the “Grand Design of Photosynthesis” Revisited. Frontiers in Plant Science **3:** 1-12

Igamberdiev AU, Bykova NV, Lea PJ, Gardestrom P (2001) The role of photorespiration in redox and energy balance of photosynthetic plant cells: A study with a barley mutant deficient in glycine decarboxylase. Physiol Plant **111:** 427-438

Invers O, Zimmerman RC, Alberte RS, Pérez M, Romero J (2001) Inorganic carbon sources for seagrass photosynthesis: an experimental evaluation of bicarbonate use in species inhabiting temperate waters. Journal of Experimental Marine Biology and Ecology **265:** 203-217

Jeffrey SW, Humphrey GF (1975) New spectrophotometric equations for determining chlorophylls a, b, c1, c2 in higher plants, algae, and natural phytoplankton. Biochem. Physiolo. Pflanzen **167:** 191-194

Jiang ZJ, Huang X-P, Zhang J-P (2010) Effects of CO_2 Enrichment on Photosynthesis, Growth, and Biochemical Composition of Seagrass *Thalassia hemprichii* (Ehrenb.) Aschers. Journal of Integrative Plant Biology **52:** 904-913

Johnson GN (2005) Cyclic electron transport in C3 plants: fact or artefact? Journal of Experimental Botany **56:** 407-416

Jones R, Ougham H, Thomas H, Waaland S (2012) The Molecular Life of Plants. Wiley

Jordan DB, Ogren WL (1981) Species variation in the specificity of ribulose biphosphate carboxylase/oxygenase. Nature **291:** 513-515

Kalaji HM, Schansker G, Ladle RJ, Goltsev V, Bosa K, Allakhverdiev SI, Brestic M, Bussotti F, Calatayud A, Dąbrowski P, Elsheery NI, Ferroni L, Guidi L, Hogewoning SW, Jajoo A, Misra AN, Nebauer SG, Pancaldi S, Penella C, Poli D, Pollastrini M, Romanowska-Duda ZB, Rutkowska B, Serôdio J, Suresh K, Szulc W, Tambussi E, Yanniccari M, Zivcak M (2014) Frequently asked questions about in vivo chlorophyll fluorescence: practical issues. Photosynthesis Research **122:** 121-158

Kanazawa A, Kramer DM (2002) In vivo modulation of nonphotochemical exciton quenching (NPQ) by regulation of the chloroplast ATP synthase. Proceedings of the National Academy of Sciences **99:** 12789-12794

Kirk JTO (1994) Light and photosynthesis in aquatic ecosystems. Cambridge University Press

Koch EW, Barbier EB, Silliman BR, Reed DJ, Perillo GME, Hacker SD, Granek EF, Primavera JH, Muthiga N, Polasky S, Halpern BS, Kennedy CJ, Kappel CV, Wolanski E (2009) Non-linearity in ecosystem services: temporal and spatial variability in coastal protection. Frontiers in Ecology and the Environment **7:** 29-37

Koch M, Bowes G, Ross C, Zhang X-H (2013) Climate change and ocean acidification effects on seagrasses and marine macroalgae. Global Change Biology **19:** 103-132

Krause-Jensen D, Carstensen J, Nielsen S, Dalsgaard T, Christensen P, Fossing H, Rasmussen M (2011) Sea bottom characteristics affect depth limits of eelgrass *Zostera marina*. Marine Ecology Progress Series **425:** 91-102

Kuypers MMM, Pancost RD, Damste JSS (1999) A large and abrupt fall in atmospheric CO_2 concentration during Cretaceous times. Nature **399:** 342-345

Larkum AD, Drew E, Ralph P (2006a) Photosynthesis and Metabolism in Seagrasses at the Cellular Level. *In* Seagrasses: biology, ecologyand conservation. Springer Netherlands, pp 323-345

Larkum AWD, Orth RJ, Duarte CM, eds (2006b) Seagrasses : biology, ecology, and conservation. Springer, Dordrecht

Lee K-S, Park SR, Kim YK (2007) Effects of irradiance, temperature, and nutrients on growth dynamics of seagrasses: A review. Journal of Experimental Marine Biology and Ecology **350:** 144-175

Lichtenthaler HK, Wellburn AR (1983) Determinations of total carotenoids and chlorophylls a and b of leaf extracts in different solvents. Biochemical Society Transactions **11:** 591-592

Longstaff BJ, Dennison WC (1999) Seagrass survival during pulsed turbidity events: the effects of light deprivation on the seagrasses Halodule pinifolia and Halophila ovalis. Aquatic Botany **65:** 105-121

Longstaff BJ, Kildea T, Runcie JW, Cheshire A, Dennison WC, Hurd C, Kana T, Raven JA, Larkum AW (2002) An in situ study of photosynthetic oxygen exchange and electron transport rate in the marine macroalga *Ulva lactuca* (Chlorophyta). Photosynth Res **74:** 281-293

Madsen TV, Maberly SC, Bowes G (1996) Photosynthetic acclimation of submersed angiosperms to CO_2 and HCO^-_3. Aquatic Botany **53:** 15-30

Madsen TV, Sand-Jensen K (1991) Photosynthetic carbon assimilation in aquatic macrophytes. Aquatic Botany **41:** 5-40

Madsen TV, Sand-Jensen K, Beer S (1993) Comparison of photosynthetic performance and carboxylation capacity in a range of aquatic macrophytes of different growth forms. Aquatic Botany **44:** 373-384

Makino A, Miyake C, Yokota A (2002) Physiological Functions of the Water–Water Cycle (Mehler Reaction) and the Cyclic Electron Flow around PSI in Rice Leaves. Plant and Cell Physiology **43:** 1017-1026

Maurino VG, Peterhansel C (2010) Photorespiration: current status and approaches for metabolic engineering. Current Opinion in Plant Biology **13:** 248-255

McPherson ML, Zimmerman RC, Hill VJ (2015) Predicting carbon isotope discrimination in Eelgrass (*Zostera marina* L.) from the environmental parameters—light, flow, and [DIC]. Limnology and Oceanography **60:** 1875-1889

Mercado JM, Gordillo FJL (2011) Inorganic carbon acquisition in algal communities: are the laboratory data relevant to the natural ecosystems? Photosynthesis Research **109:** 257-267

Mercado JM, Niell FX, Silva J, Santos R (2003) Use of light and inorganic carbon acquisition by two morphotypes of *Zostera noltii* Hornem. Journal of Experimental Marine Biology and Ecology **297:** 71-84

Moore KA, Jarvis JC (2008) Environmental Factors Affecting Recent Summertime Eelgrass Diebacks in the Lower Chesapeake Bay: Implications for Long-term Persistence. Journal of Coastal Research **SI:** 135-147

Moore KA, Shields EC, Parrish DB, Orth RJ (2012) Eelgrass survival in two contrasting systems: role of turbidity and summer water temperatures. Marine Ecology Progress Series **448:** 247-258

Munekage Y, Hashimoto M, Miyake C, Tomizawa K-I, Endo T, Tasaka M, Shikanai T (2004) Cyclic electron flow around photosystem I is essential for photosynthesis. Nature **429:** 579-582

Niyogi KK (2000) Safety valves for photosynthesis. Curr Opin Plant Biol **3:** 455-460

Noctor G, Foyer CH (1998) A re-evaluation of the ATP :NADPH budget during C3 photosynthesis: a contribution from nitrate assimilation and its associated respiratory activity? Journal of Experimental Botany **49:** 1895-1908

Ogren WL (1984) Photorespiration: Pathways, Regulation, and Modification. Annual Review of Plant Physiology **35:** 415-442

Ogren WL (2003) Affixing the O to Rubisco: discovering the source of photorespiratory glycolate and its regulation. Photosynthesis Research **76:** 53-63

Ort DR, Baker NR (2002) A photoprotective role for O_2 as an alternative electron sink in photosynthesis? Current Opinion in Plant Biology **5:** 193-198

Orth R, Williams M, Marion S, Wilcox D, Carruthers TB, Moore K, Kemp WM, Dennison W, Rybicki N, Bergstrom P, Batiuk R (2010) Long-Term Trends in Submersed Aquatic Vegetation (SAV) in Chesapeake Bay, USA, Related to Water Quality. Estuaries and Coasts **33:** 1144-1163

Orth RJ, Carruthers TJB, Dennison WC, Duarte CM, Fourqurean JW, Heck KL, Hughes AR, Kendrick GA, Kenworthy WJ, Olyarnik S, Short FT, Waycott M, Williams SL (2006a) A Global Crisis for Seagrass Ecosystems. BioScience **56:** 987-996

Orth RJ, Luckenbach ML, Marion SR, Moore KA, Wilcox DJ (2006b) Seagrass recovery in the Delmarva Coastal Bays, USA. Aquatic Botany **84:** 26-36

Osmond B, Badger M, Maxwell K, Björkman O, Leegood R (1997) Too many photons: photorespiration, photoinhibition and photooxidation. Trends in Plant Science **2:** 119-121

Osmond CB (1981) Photorespiration and photoinhibition : Some implications for the energetics of photosynthesis. Biochimica et Biophysica Acta (BBA) - Reviews on Bioenergetics **639:** 77-98

Ow YX, Collier CJ, Uthicke S (2015) Responses of three tropical seagrass species to CO_2 enrichment. Marine Biology **162:** 1005-1017

Palacios S, Zimmerman R (2007) Response of eelgrass *Zostera marina* to CO_2 enrichment: possible impacts of climate change and potential for remediation of coastal habitats. Marine Ecology Progress Series **344:** 1-13

Pedersen O, Binzer T, Borum J (2004) Sulphide intrusion in eelgrass (*Zostera marina* L.). Plant, Cell & Environment **27:** 595-602

Pfannschmidt T (2003) Chloroplast redox signals: how photosynthesis controls its own genes. Trends in Plant Science **8:** 33-41

Pfannschmidt T, Yang C (2012) The hidden function of photosynthesis: a sensing system for environmental conditions that regulates plant acclimation responses. Protoplasma **249:** 125-136

Prasil O, Kolber Z, Berry J, Falkowski P (1996) Cyclic electron flow around Photosystem II in vivo. Photosynthesis Research **48:** 395-410

Rachmilevitch S, Cousins AB, Bloom AJ (2004) Nitrate assimilation in plant shoots depends on photorespiration. Proceedings of the National Academy of Sciences of the United States of America **101:** 11506-11510

Raghavendra AS (2000) Photosynthesis: A Comprehensive Treatise. Cambridge University Press

Ralph PJ, Durako MJ, Enríquez S, Collier CJ, Doblin MA (2007) Impact of light limitation on seagrasses. Journal of Experimental Marine Biology and Ecology **350:** 176-193

Ralph PJ, Gademann R (2005) Rapid light curves: A powerful tool to assess photosynthetic activity. Aquatic Botany **82:** 222-237

Ralph PJ, Polk SM, Moore KA, Orth RJ, Smith WO (2002) Operation of the xanthophyll cycle in the seagrass *Zostera marina* in response to variable irradiance. Journal of Experimental Marine Biology and Ecology **271:** 189-207

Raven J, Beardall J (2003) Carbon Acquisition Mechanisms of Algae: Carbon Dioxide Diffusion and Carbon Dioxide Concentrating Mechanisms. *In* AD Larkum, S Douglas, J Raven, eds, Photosynthesis in Algae, Vol 14. Springer Netherlands, pp 225-244

Raven JA (1984) Energetics and transport in aquatic plants. A.R. Liss

Raven JA (1991) Plant responses to high O_2 concentrations: relevance to previous high O_2 episodes. Palaeogeography, Palaeoclimatology, Palaeoecology **97:** 19-38

Raven JA, Beardall J (2014) CO_2 concentrating mechanisms and environmental change. Aquatic Botany **118:** 24-37

Raven JA, Beardall J, Giordano M (2014) Energy costs of carbon dioxide concentrating mechanisms in aquatic organisms. Photosynth Res **121:** 111-124

Raven JA, Cockell CS, De La Rocha CL (2008) The evolution of inorganic carbon concentrating mechanisms in photosynthesis. Philosophical Transactions of the Royal Society B: Biological Sciences **363:** 2641-2650

Raven JA, Giordano M, Beardall J, Maberly SC (2011) Algal and aquatic plant carbon concentrating mechanisms in relation to environmental change. Photosynth Res **109:** 281-296

Raven JA, Johnston AM (1991) Mechanisms of Inorganic-Carbon Acquisition in Marine Phytoplankton and Their Implications for the Use of Other Resources. Limnology and Oceanography **36:** 1701-1714

Raven JA, Johnston AM, Kubler JE, Korb R, McInroy SG, Handley LL, Scrimgeour CM, Walker DI, Beardall J, Vanderklift M, Fredriksen S, Dunton KH (2002) Mechanistic interpretation of carbon isotope discrimination by marine macroalgae and seagrasses. Functional Plant Biology **29:** 355-378

Reinfelder JR (2011) Carbon Concentrating Mechanisms in Eukaryotic Marine Phytoplankton. Annual Review of Marine Science **3:** 291-315

Ruesink JL, Yang S, Trimble AC (2015) Variability in Carbon Availability and Eelgrass (*Zostera marina*) Biometrics Along an Estuarine Gradient in Willapa Bay, WA, USA. Estuaries and Coasts **38:** 1908-1917

Rumeau D, Peltier G, Cournac L (2007) Chlororespiration and cyclic electron flow around PSI during photosynthesis and plant stress response. Plant Cell Environ **30:** 1041-1051

Sand-Jensen K, Pedersen O, Binzer T, Borum J (2005) Contrasting Oxygen Dynamics in the Freshwater Isoetid Lobelia dortmanna and the Marine Seagrass *Zostera marina*. Annals of Botany **96:** 613-623

Scheibe R, Backhausen JE, Emmerlich V, Holtgrefe S (2005) Strategies to maintain redox homeostasis during photosynthesis under changing conditions. Journal of Experimental Botany **56:** 1481-1489

Sharkey TD (1988) Estimating the rate of photorespiration in leaves. Physiologia Plantarum **73:** 147-152

Short FT, Neckles HA (1999) The effects of global climate change on seagrasses. Aquatic Botany **63:** 169-196

Silva J, Santos R (2004) Can chlorophyll fluorescence be used to estimate photosynthetic production in the seagrass *Zostera noltii*? Journal of Experimental Marine Biology and Ecology **307:** 207-216

Silva J, Y S, R S, S B (2009) Measuring seagrass photosynthesis: methods and applications. Aquatic Biology **7:** 127-141

Sisson GM, Shen J, Reay WG, Miles EJ, Kuo AY-s, Wang HV (2010) The development of a management tool to assess bacterial impacts in Rudee Inlet, Virginia Beach. Virginia Institute of Marine Science, Dept. of Physical Sciences, Gloucester Point, Va.

Smith RD, Pregnall AM, Alberte RS (1988) Effects of anaerobiosis on root metabolism of *Zostera marina*; (eelgrass): implications for survival in reducing sediments. Marine Biology **98:** 131-141

Somerville CR (2001) An Early *Arabidopsis* Demonstration. Resolving a Few Issues concerning Photorespiration. Plant Physiology **125:** 20-24

Spreitzer RJ, Salvucci ME (2002) RUBISCO: Structure, Regulatory Interactions, and Possibilities for a Better Enzyme. Annual Review of Plant Biology **53:** 449-475

Taylor AR, Brownlee C, Wheeler GL (2012) Proton channels in algae: reasons to be excited. Trends in Plant Science **17:** 675-684

Tcherkez GGB, Farquhar GD, Andrews TJ (2006) Despite slow catalysis and confused substrate specificity, all ribulose bisphosphate carboxylases may be nearly perfectly optimized. Proceedings of the National Academy of Sciences **103:** 7246-7251

Tolbert NE (1997) The C2 oxidative photosynthetic carbon cycle. Annual Review of Plant Physiology and Plant Molecular Biology **48:** 1-25

Tolbert NE, Osmond CB, Great Barrier Reef Photorespiration expedition (1976) Photorespiration in marine plants. CSIRO

Touchette BW, Burkholder JM (2000) Overview of the physiological ecology of carbon metabolism in seagrasses. Journal of Experimental Marine Biology and Ecology **250:** 169-205

van Heuven S, Pierrot D, Rae JWB, Lewis E, Wallace DWR (2011) MATLAB Program Developed for CO_2 System Calculations. *In*, Ed ORNL/CDIAC-105b. Department of Energy, Oak Ridge, Tennessee, Carbon Dioxide Information Analysis Center, Oak Ridge National Laboratory, U.S.

Vaudrey JMP, Kremer JN, Branco BF, Short FT (2010) Eelgrass recovery after nutrient enrichment reversal. Aquatic Botany **93:** 237-243

Vogelman TC, Nishio JN, Smith WK (1996) Leaves and light capture: Light propagation and gradients of carbon fixation within leaves. Trends in Plant Science **1:** 65-70

Voss I, Sunil B, Scheibe R, Raghavendra AS (2013) Emerging concept for the role of photorespiration as an important part of abiotic stress response. Plant Biology **15:** 713-722

Waldbusser GG, Salisbury JE (2014) Ocean acidification in the coastal zone from an organism's perspective: multiple system parameters, frequency domains, and habitats. Ann Rev Mar Sci **6:** 221-247

Walters RG (2005) Towards an understanding of photosynthetic acclimation. J Exp Bot **56:** 435-447

Webb W, Newton M, Starr D (1974) Carbon dioxide exchange of *Alnus rubra*. Oecologia **17:** 281-291

Woodward FI (2002) Potential impacts of global elevated CO_2 concentrations on plants. Current Opinion in Plant Biology **5:** 207-211

Xin C-P, Tholen D, Devloo V, Zhu X-G (2015) The Benefits of Photorespiratory Bypasses: How Can They Work? Plant Physiology **167:** 574-585

Yin ZH, Johnson GN (2000) Photosynthetic acclimation of higher plants to growth in fluctuating light environments. Photosynth Res **63:** 97-107

Zeebe RE (2012) History of Seawater Carbonate Chemistry, Atmospheric CO_2, and Ocean Acidification. Annual Review of Earth and Planetary Sciences **40:** 141-165

Zhu X-G, Long SP, Ort DR (2008) What is the maximum efficiency with which photosynthesis can convert solar energy into biomass? Current Opinion in Biotechnology **19:** 153-159

Zimmerman RC (2003) A Biooptical Model of Irradiance Distribution and Photosynthesis in Seagrass Canopies. Limnology and Oceanography **48:** 568-585

Zimmerman RC (2006) Light and Photosynthesis in Seagrass Meadows. *In* AWD Larkum, RJ Orth, CM Duarte, eds, Seagrasses: Biology, Ecology and Conservation. Springer Netherlands, Dordrecht, pp 303-321

Zimmerman RC, Hill VJ, Gallegos CL (2015) Predicting effects of ocean warming, acidification, and water quality on Chesapeake region eelgrass. Limnology and Oceanography **60:** 1781-1804

Zimmerman RC, Hill VJ, Jinuntuya M, Celebi B, Ruble D, Smith M, Cedeno T, Swingle WM (2016) Experimental Impacts of Climate Warming and Ocean Carbonation on Eelgrass (*Zostera marina* L.). Marine Ecology Progress Series **Submitted**

Zimmerman RC, Kohrs DG, Steller DL, Alberte RS (1997) Impacts of CO_2 Enrichment on Productivity and Light Requirements of Eelgrass. Plant Physiology **115:** 599-607

Zimmerman RC, Reguzzoni JL, Alberte RS (1995) Eelgrass (*Zostera marina* L.) transplants in San Francisco Bay: Role of light availability on metabolism, growth and survival. Aquatic Botany **51:** 67-86

Zimmerman RC, Reguzzoni JL, Wyllie-Echeverria S, Josselyn M, Alberte RS (1991) Assessment of environmental suitability for growth of *Zostera marina* L. (eelgrass) in San Francisco Bay. Aquatic Botany **39:** 353-366

Zimmerman RC, Smith RD, Alberte RS (1987) Is growth of eelgrass nitrogen limited? A numerical simulation of the effects of light and nitrogen on the growth dynamics of *Zostera marina*. Marine Ecology Progress Series **41:** 167-176

Zimmerman RC, Smith RD, Alberte RS (1989) Thermal acclimation and whole-plant carbon balance in *Zostera marina* L. (eelgrass). Journal of Experimental Marine Biology and Ecology **130:** 93-109

APPENDIX

Table 18. Multiple linear regression model results for general effects of environmental parameters on leaf optical properties without grouping into separate pH treatments. Only the standardized coefficients were reported to highlight the relative importance of the significant predictors.

Dependent Variable	Predictors: Constant, Daily Average Temperature (C°), Daily Average log[CO2] (umol/kgSW), Daily Total PAR [Shade corrected] (M/d). These parameters were averaged over 2-week period prior to sampling date.							
FW per LA (mg/cm^2)	ANOVA	df	Mean Square	F	Sig.	Standardized Coefficients	Beta	Sig.
Adjusted R Square	Regression	3	3289.9	139.7	<0.001	Daily Average log[CO_2]	0.456	<0.001
0.599	Residual	276	23.55			Daily Total PAR	-0.103	0.039
	Total	279				Daily Average Temp	0.731	<0.001
Total Chl per LA (µg Chl/cm^2)	ANOVA	df	Mean Square	F	Sig.	Standardized Coefficients	Beta	Sig.
Adjusted R Square	Regression	3	12.93.1	47.5	<0.001	Daily Average log[CO_2]	-0.467	<0.001
0.333	Residual	276	27.23			Daily Total PAR	-0.184	0.004
	Total	279				Daily Average Temp	0.397	<0.001
Total Car per LA (µg Cx/cm^2)	ANOVA	df	Mean Square	F	Sig.	Standardized Coefficients	Beta	Sig.
Adjusted R Square	Regression	3	49.01	41.66	<0.001	Daily Average log[CO_2]	-0.487	<0.001
0.304	Residual	276	1.18			Daily Total PAR	-0.342	<0.001
	Total	279				Daily Average Temp	0.148	0.024
Chl a:b	ANOVA	df	Mean Square	F	Sig.	Standardized Coefficients	Beta	Sig.
Adjusted R Square	Regression	3	35.21	173.8	<0.001	Daily Average log[CO_2]	0.035	0.332
0.650	Residual	276	0.203			Daily Total PAR	-0.154	0.001
	Total	279				Daily Average Temp	-0.697	<0.001

Table 18. *continued*

Tcar:TChl	ANOVA	df	Mean Square	F	Sig.	Standardized Coefficients	Beta	Sig.
Adjusted R Square	Regression	3	0.067	73.48	<0.001	Daily Average log[CO_2]	0.180	<0.001
0.438	Residual	276	0.001			Daily Total PAR	-0.119	0.044
	Total	279				Daily Average Temp	-0.544	<0.001
a^*_L430 (m^2/g Chl-*a*)	ANOVA	df	Mean Square	F	Sig.	Standardized Coefficients	Beta	Sig.
Adjusted R Square	Regression	3	389.31	49.86	<0.001	Daily Average log[CO_2]	0.448	<0.001
0.344	Residual	276	7.81			Daily Total PAR	0.124	0.052
	Total	279				Daily Average Temp	-0.417	<0.001
A677 (%)	ANOVA	df	Mean Square	F	Sig.	Standardized Coefficients	Beta	Sig.
Adjusted R Square	Regression	3	0.131	19.91	<0.001	Daily Average log[CO_2]	-0.151	0.006
0.169	Residual	276	0.007			Daily Total PAR	-0.209	0.004
	Total	279				Daily Average Temp	-0.236	0.001

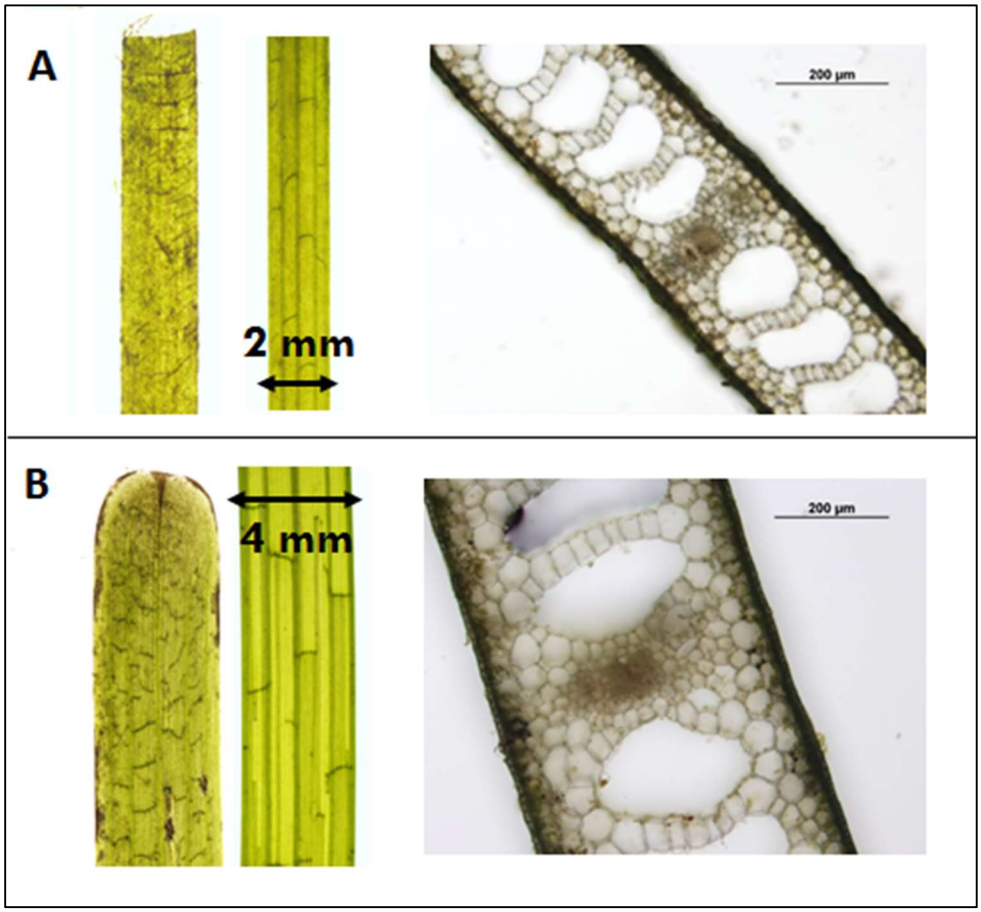

Figure 32. Micrographs of eelgrass leaves sampled in September 2013 from ambient treatment (A) and from pH 6.1 treatment (B). Micrographs of leaf surface and cross-sectional view were provided courtesy of Dr. Fred Dobbs.

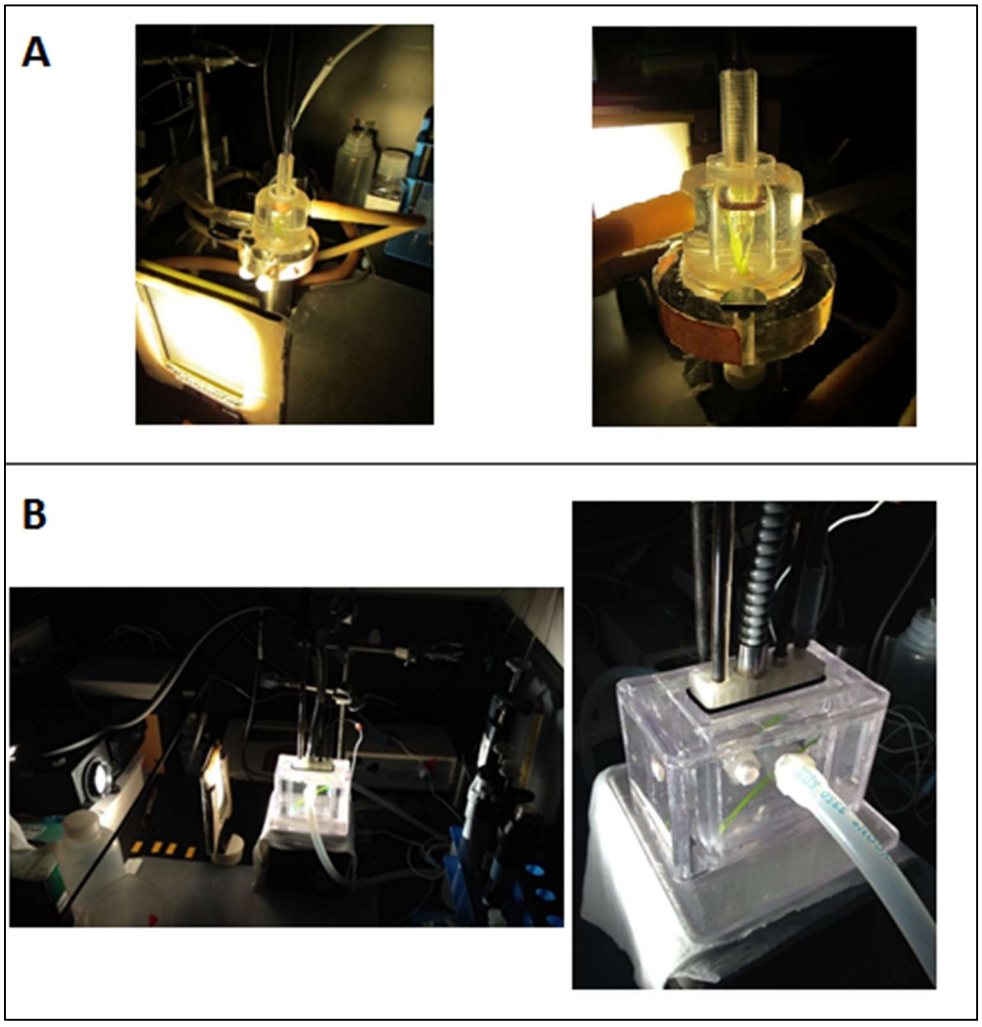

Figure 33. Experimental setup used during photosynthesis measurements in Chapter III (A) and in Chapter IV (B). Leaf samples were incubated in sealed and temperature controlled chambers which were fitted with sensors for measuring O_2 production, fluorescence and pH drift simultenously.

Table 19. Results of non-linear regression analysis for pigment specific photosynthesis versus E_{PUR} curves. P_E: Light saturated Gross Photosynthesis (µmol O_2 hr^{-1} mg^{-1} Chlorophyll), $E_{k\ (PUR)}$: photosynthesis-saturating irradiance calculated using photosynthetically usable irradiance (µmol absorbed photon s^{-1} m^{-2}), R_D: Dark respiration (µmol O_2 hr^{-1} mg^{-1} Chlorophyll).

Model parameters								Analysis of Variance (Corrected for the mean of the observations)					
Growth pH	Measurement pH		Coefficient	SE	t	p	r^2		DF	SS	MS	F	p
6	6.0	P_E	70.2	4.3	16.4	<0.0001	0.974	Regression	2.0	9701.4	4850.7	209.2	<0.0001
		$E_{k\ (PUR)}$	47.5	7.0	6.8	<0.0001		Residual	11.0	255.0	23.2		
		R_D	8.7	1.8	4.9	0.001		Total	13.0	9956.4	765.9		
	7.0	P_E	55.2	3.7	15.0	<0.0001	0.970	Regression	2.0	5681.2	2840.6	146.3	<0.0001
		$E_{k\ (PUR)}$	36.4	6.0	6.1	0.000		Residual	9.0	174.7	19.4		
		R_D	8.5	1.8	4.8	0.001		Total	11.0	5855.9	532.4		
	8.0	P_E	24.5	2.1	11.4	<0.0001	0.956	Regression	2.0	1269.6	634.8	76.1	<0.0001
		$E_{k\ (PUR)}$	14.5	4.9	3.0	0.020		Residual	7.0	58.4	8.3		
		R_D	11.5	1.3	8.9	<0.0001		Total	9.0	1327.9	147.5		
7	6.0	P_E	68.0	3.2	21.0	<0.0001	0.984	Regression	2.0	8533.8	4266.9	343.0	<0.0001
		$E_{k\ (PUR)}$	64.2	7.4	8.7	<0.0001		Residual	11.0	136.8	12.4		
		R_D	6.5	1.3	5.0	0.000		Total	13.0	8670.7	667.0		

Table 19. *continued*

Growth pH	Measurement pH		Coefficient	SE	t	p	r^2		DF	SS	MS	F	p
7	7.0	P_E	49.3	3.1	15.9	<0.0001	0.973	Regression	2.0	4417.7	2208.9	162.8	<0.0001
		$E_{k\ (PUR)}$	43.9	6.9	6.4	0.000		Residual	9.0	122.1	13.6		
		R_D	6.7	1.5	4.5	0.001		Total	11.0	4539.9	412.7		
	8.0	P_E	12.5	3.1	4.0	0.005	0.723	Regression	2.0	382.1	191.1	9.1	0.011
		$E_{k\ (PUR)}$	4.7	15.8	0.3	0.775		Residual	7.0	146.6	20.9		
		R_D	5.2	2.0	2.6	0.038		Total	9.0	528.7	58.7		
8	6.0	P_E	62.6	2.4	26.1	<0.0001	0.992	Regression	2.0	5457.9	2729.0	458.5	<0.0001
		$E_{k\ (PUR)}$	68.6	7.2	9.5	<0.0001		Residual	7.0	41.7	6.0		
		R_D	5.0	1.1	4.7	0.002		Total	9.0	5499.6	611.1		
	7.0	P_E	44.9	4.0	11.3	<0.0001	0.952	Regression	2.0	3681.4	1840.7	89.4	<0.0001
		$E_{k\ (PUR)}$	57.1	13.3	4.3	0.002		Residual	9.0	185.4	20.6		
		R_D	4.9	1.8	2.7	0.025		Total	11.0	3866.8	351.5		
	8.0	P_E	20.3	2.4	8.4	<0.0001	0.922	Regression	2.0	846.2	423.1	41.5	0.000
		$E_{k\ (PUR)}$	17.4	7.1	2.4	0.045		Residual	7.0	71.3	10.2		
		R_D	7.8	1.4	5.5	0.001		Total	9.0	917.5	101.9		

Table 20. Results of non-linear regression analysis for biomass specific photosynthesis versus E_{PAR} curves. P_E: Light saturated Gross Photosynthesis (µmol O_2 hr^{-1} g^{-1} Fresh weight), $E_{k\ (PAR)}$: photosynthesis-saturating irradiance calculated using photosynthetically active irradiance (µmol photon s^{-1} m^{-2}), R_D: Dark respiration (µmol O_2 hr^{-1} g^{-1} Fresh weight).

Model parameters								Analysis of Variance (Corrected for the mean of the observations)					
Growth pH	Measurement pH		Coefficient	SE	t	p	r^2		DF	SS	MS	F	p
6	6.0	P_E	33.5	2.8	12.1	<0.0001	0.950	Regression	2.0	2642.4	1321.2	103.6	<0.0001
		$E_{k\ (PAR)}$	65.0	14.5	4.5	0.001		Residual	11.0	140.3	12.8		
		R_D	4.7	1.3	3.5	0.005		Total	13.0	2782.7	214.1		
	7.0	P_E	40.0	2.5	15.8	<0.0001	0.973	Regression	2.0	2690.4	1345.2	163.7	<0.0001
		$E_{k\ (PAR)}$	94.7	14.8	6.4	0.000		Residual	9.0	74.0	8.2		
		R_D	5.5	1.2	4.8	0.001		Total	11.0	2764.4	251.3		
	8.0	P_E	12.9	1.1	12.0	<0.0001	0.961	Regression	2.0	350.9	175.5	87.0	<0.0001
		$E_{k\ (PAR)}$	28.4	8.6	3.3	0.013		Residual	7.0	14.1	2.0		
		R_D	5.9	0.6	9.3	<0.0001		Total	9.0	365.0	40.6		
7	6.0	P_E	67.4	7.1	9.5	<0.0001	0.925	Regression	2.0	9127.2	4563.6	67.4	<0.0001
		$E_{k\ (PAR)}$	94.0	24.2	3.9	0.003		Residual	11.0	744.6	67.7		
		R_D	6.9	3.1	2.3	0.045		Total	13.0	9871.8	759.4		

Table 20. *continued*

Growth pH	Measurement pH		Coefficient	SE	t	p	r^2		DF	SS	MS	F	p
7	7.0	P_E	54.3	6.5	8.4	<0.0001	0.911	Regression	2.0	5168.3	2584.1	45.9	<0.0001
		$E_{k\ (PAR)}$	85.3	25.1	3.4	0.008		Residual	9.0	506.9	56.3		
		R_D	7.1	3.0	2.3	0.044		Total	11.0	5675.2	515.9		
	8.0	P_E	12.1	2.9	4.2	0.004	0.741	Regression	2.0	352.1	176.0	10.0	0.009
		$E_{k\ (PAR)}$	11.6	23.5	0.5	0.637		Residual	7.0	123.1	17.6		
		R_D	5.0	1.9	2.7	0.031		Total	9.0	475.2	52.8		
8	6.0	P_E	86.8	4.7	18.5	<0.0001	0.985	Regression	2.0	10376.8	5188.4	231.2	<0.0001
		$E_{k\ (PAR)}$	124.9	18.6	6.7	0.000		Residual	7.0	157.1	22.4		
		R_D	6.8	2.1	3.3	0.013		Total	9.0	10533.9	1170.4		
	7.0	P_E	62.1	4.6	13.5	<0.0001	0.965	Regression	2.0	7411.8	3705.9	124.5	<0.0001
		$E_{k\ (PAR)}$	83.9	16.9	5.0	0.001		Residual	9.0	267.9	29.8		
		R_D	6.7	2.2	3.1	0.014		Total	11.0	7679.8	698.2		
	8.0	P_E	17.2	1.7	10.3	<0.0001	0.947	Regression	2.0	681.0	340.5	62.1	<0.0001
		$E_{k\ (PAR)}$	18.3	8.7	2.1	0.073		Residual	7.0	38.4	5.5		
		R_D	7.3	1.0	7.0	0.000		Total	9.0	719.3	79.9		

Table 21. Results of non-linear regression analysis for leaf area specific photosynthesis versus E_{PUR} curves. P_E: Light saturated Gross Photosynthesis (µmol O_2 s^{-1} m^{-2}), $E_{k\ (PUR)}$: photosynthesis-saturating irradiance calculated using photosynthetically usable irradiance (µmol absorbed photon s^{-1} m^{-2}), R_D: Dark respiration (µmol O_2 s^{-1} m^{-2}).

Model parameters								Analysis of Variance (Corrected for the mean of the observations)					
Growth pH	Measurement pH		Coefficient	SE	t	p	r^2		DF	SS	MS	F	p
6	6.0	P_E	3.6	0.2	14.5	<0.0001	0.967	Regression	2.0	25.4	12.7	161.0	<0.0001
		$E_{k\ (PUR)}$	46.0	7.8	5.9	0.000		Residual	11.0	0.9	0.1		
		R_D	0.4	0.1	4.3	0.001		Total	13.0	26.2	2.0		
	7.0	P_E	3.5	0.2	20.8	<0.0001	0.984	Regression	2.0	21.4	10.7	279.1	<0.0001
		$E_{k\ (PUR)}$	41.6	4.9	8.5	<0.0001		Residual	9.0	0.3	0.0		
		R_D	0.5	0.1	6.5	0.000		Total	11.0	21.8	2.0		
	8.0	P_E	1.5	0.1	13.1	<0.0001	0.966	Regression	2.0	5.0	2.5	99.2	<0.0001
		$E_{k\ (PUR)}$	14.2	4.2	3.4	0.012		Residual	7.0	0.2	0.0		
		R_D	0.7	0.1	9.8	<0.0001		Total	9.0	5.1	0.6		
7	6.0	P_E	5.8	0.3	18.7	<0.0001	0.981	Regression	2.0	57.6	28.8	287.5	<0.0001
		$E_{k\ (PUR)}$	73.2	9.3	7.9	<0.0001		Residual	11.0	1.1	0.1		
		R_D	0.5	0.1	4.4	0.001		Total	13.0	58.7	4.5		

Table 21. *continued*

Growth pH	Measurement pH		Coefficient	SE	t	p	r^2		DF	SS	MS	F	p
7	7.0	P_E	4.3	0.5	8.7	<0.0001	0.916	Regression	2.0	30.5	15.2	49.2	<0.0001
		$E_{k\ (PUR)}$	53.7	15.3	3.5	0.007		Residual	9.0	2.8	0.3		
		R_D	0.5	0.2	2.4	0.043		Total	11.0	33.3	3.0		
	8.0	P_E	0.9	0.2	4.7	0.002	0.781	Regression	2.0	1.9	1.0	12.5	0.005
		$E_{k\ (PUR)}$	6.2	10.5	0.6	0.575		Residual	7.0	0.5	0.1		
		R_D	0.4	0.1	3.0	0.020		Total	9.0	2.5	0.3		
8	6.0	P_E	5.8	0.2	37.5	<0.0001	0.996	Regression	2.0	47.1	23.5	964.2	<0.0001
		$E_{k\ (PUR)}$	70.8	5.2	13.6	<0.0001		Residual	7.0	0.2	0.0		
		R_D	0.5	0.1	6.8	0.000		Total	9.0	47.2	5.2		
	7.0	P_E	4.3	0.3	13.9	<0.0001	0.968	Regression	2.0	33.2	16.6	135.5	<0.0001
		$E_{k\ (PUR)}$	58.1	11.0	5.3	0.001		Residual	9.0	1.1	0.1		
		R_D	0.5	0.1	3.3	0.009		Total	11.0	34.3	3.1		
	8.0	P_E	1.5	0.2	8.3	<0.0001	0.921	Regression	2.0	4.3	2.2	41.0	0.000
		$E_{k\ (PUR)}$	18.0	7.3	2.5	0.043		Residual	7.0	0.4	0.1		
		R_D	0.6	0.1	5.5	0.001		Total	9.0	4.7	0.5		

Table 22. Results of non-linear regression analysis for electron transfer rate versus E_{PUR} curves. ETR_{max}: Maximum electron transfer rate (µmol electrons s^{-1} m^{-2}), α_{max}: efficiency of electron transport rate (µmol electron $µmol^{-1}$ absorbed photon).

Model parameters								Analysis of Variance (Corrected for the mean of the observations)					
Growth pH	Measurement pH		Coefficient	SE	t	p	r^2		DF	SS	MS	F	p
6	6.0	ETR_{max}	35.3	0.4	87.0	<0.0001	0.999	Regression	1.0	1871.0	1871.0	14383.3	<0.0001
		α_{max}	0.4	0.0	59.9	<0.0001		Residual	12.0	1.6	0.1		
								Total	13.0	1872.6	144.0		
	7.0	ETR_{max}	41.0	3.3	12.6	<0.0001	0.963	Regression	1.0	2304.4	2304.4	258.7	<0.0001
		α_{max}	0.5	0.1	7.3	<0.0001		Residual	10.0	89.1	8.9		
								Total	11.0	2393.4	217.6		
	8.0	ETR_{max}	22.4	0.5	43.9	<0.0001	0.996	Regression	1.0	811.9	811.9	1857.1	<0.0001
		α_{max}	0.5	0.0	17.9	<0.0001		Residual	8.0	3.5	0.4		
								Total	9.0	815.4	90.6		
7	6.0	ETR_{max}	93.1	2.6	35.8	<0.0001	0.999	Regression	1.0	6602.7	6602.7	10308.1	<0.0001
		α_{max}	0.4	0.0	45.9	<0.0001		Residual	12.0	7.7	0.6		
								Total	13.0	6610.4	508.5		

Table 22. *continued*

Growth pH	Measurement pH		Coefficient	SE	t	p	r^2		DF	SS	MS	F	p
7	7.0	ETR_{max}	68.3	4.2	16.1	<0.0001	0.987	Regression	1.0	4969.9	4969.9	781.7	<0.0001
		α_{max}	0.5	0.0	11.9	<0.0001		Residual	10.0	63.6	6.4		
								Total	11.0	5033.5	457.6		
	8.0	ETR_{max}	32.4	1.1	28.2	<0.0001	0.992	Regression	1.0	1455.1	1455.1	950.5	<0.0001
		α_{max}	0.4	0.0	12.6	<0.0001		Residual	8.0	12.2	1.5		
								Total	9.0	1467.3	163.0		
8	6.0	ETR_{max}	58.4	5.8	10.0	<0.0001	0.970	Regression	1.0	3810.3	3810.3	261.3	<0.0001
		α_{max}	0.5	0.1	6.3	0.000		Residual	8.0	116.7	14.6		
								Total	9.0	3927.0	436.3		
	7.0	ETR_{max}	82.2	5.5	14.8	<0.0001	0.992	Regression	1.0	6334.7	6334.7	1175.7	<0.0001
		α_{max}	0.5	0.0	14.6	<0.0001		Residual	10.0	53.9	5.4		
								Total	11.0	6388.6	580.8		
	8.0	ETR_{max}	22.8	0.7	34.8	<0.0001	0.993	Regression	1.0	839.6	839.6	1162.5	<0.0001
		α_{max}	0.5	0.0	14.1	<0.0001		Residual	8.0	5.8	0.7		
								Total	9.0	845.4	93.9		

VITA

BILLUR CELEBI
Department of Ocean, Earth and Atmospheric Sciences
Old Dominion University 4600 Elkhorn Ave, Norfolk, VA 23259
Email: celebibillur@gmail.com
www.researchgate.net/profile/Billur_Celebi

EDUCATION

Ph.D. Oceanography, Old Dominion University, Norfolk, VA, USA. 2016. Dissertation Title: "Potential Impacts of Climate Change on Photochemistry of *Zostera marina* L.". (Dr. Richard C. Zimmerman, Supervisor)

M.S. Marine Biology and Fisheries, Institute of Marine Sciences, Middle East Technical University (METU), Mersin, Turkey. 2007. Thesis Title: **"**A Study on *Posidonia oceanica* (L.) Delile, 1813, Seagrass Meadows in the Levant Sea". (Dr. Ali C. Gucu, Supervisor) (GPA: 3.79/4)

B.S. Biological Sciences, METU, Ankara, Turkey. 2004. (GPA: 3.30/4)

RESEARCH INTERESTS

Climate change, Ocean Acidification, Aquatic photosynthesis, Aquatic optics, Ecology and physiology of marine plants.

POSITIONS HELD

2015- 2016	Teaching Assistant, Dept. Ocean, Earth and Atmospheric Sciences, Old Dominion University (ODU),VA, USA
2011-2014	Research Assistant, Dept. Ocean, Earth and Atmospheric Sciences, ODU
2010-2011	Teaching Assistant, Dept. Ocean, Earth and Atmospheric Sciences, ODU
2008-2010	Research Assistant, Dept. Ocean, Earth and Atmospheric Sciences, ODU
2004-2008	Research Assistant, Institute of Marine Sciences, Middle East Technical University, Turkey

AWARDS

2015	Dorothy Brown Smith Scholarship (to attend to the 4th Mediterranean Seagrass Workshop in Sardinia, ITALY)
2014	Dorothy Brown Smith Scholarship (to attend to Aquatic Sciences Meeting in Honolulu, HI, USA)
2012-2014	Virginia Sea Grant Graduate Research Fellowship, NOAA – PhD study at ODU
2010	Dorothy Brown Smith Scholarship (to attend to BioMechanics Summer Course at Friday Harbor Labs at UW)
2008-2010	Dominion Scholarship – PhD study at ODU
2006	M.S. Fellowship – M.S. study at METU-IMS funded by TUBITAK (The Scientific and Technological Research Council of Turkey)
2006	Sponsorship for Mediterranean Seagrass Workshop – funded by European Commission – DG Joint Research Centre Institute for Environment and Sustainability

TEACHING EXPERIENCE

2015	OEAS 551 Data Collection and Analysis in Oceanography
2011	OEAS 107 Introductory Oceanography Laboratory
2010	OEAS 440/640 Advanced Biological Oceanography Laboratory